



EMULSIFICATION WITH MICROSTRUCTURES

Koen C. van Dijke

Koen C. van Dijke 2009

EMULSIFICATION WITH MICROSTRUCTURES

EMULSIFICATION WITH MICROSTRUCTURES

KOEN C. VAN DIJKE

Thesis committee

Thesis supervisor

Prof. dr. ir. R. M. Boom

Professor of Food Process Engineering, Wageningen University

Thesis co-supervisor

Dr. ir. C.G.P.H. Schroën

Assistant professor Food Process Engineering Group, Wageningen University

Other members

Dr. I. Kobayashi

National Food Research Institute, Japan

Prof. dr. F. Mugele

University of Twente

Prof. dr. ir. W. Norde

Wageningen University

Prof. dr. ir. G. van Straten

Wageningen University

This research has been conducted under auspices of the Graduate School VLAG.

EMULSIFICATION WITH MICROSTRUCTURES

KOEN CORNELIS VAN DIJKE

Submitted in partial fulfilment of the requirements for the degree of doctor
at Wageningen University
by the authority of the Rector Magnificus
Prof. dr. M.J. Kropff,
in the presence of the
Thesis Committee appointed by the Doctorate Board
to be defended in public
on Friday 13 November 2009
at 1.30 PM in the Aula

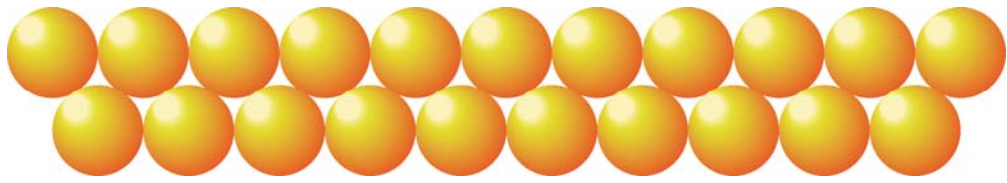
van Dijke, Koen C.
Emulsification with Microstructures
181 pages.

Thesis, Wageningen University, Wageningen, The Netherlands (2009)
With propositions, with references, with summaries in Dutch and English

ISBN: 978-90-8585-495-1

CONTENTS

1.	INTRODUCTION	1
2.	MICROCHANNEL EMULSIFICATION: FROM COMPUTATIONAL FLUID DYNAMICS TO PREDICTIVE ANALYTICAL MODEL	13
3.	EFFECT OF VISCOSITIES OF DISPERSED AND CONTINUOUS PHASES IN MICROCHANNEL OIL-IN-WATER EMULSIFICATION	39
4.	SIMULTANEOUS FORMATION OF MANY DROPLETS IN A SINGLE MICROFLUIDIC DROPLET FORMATION UNIT	59 71
5.	THE MECHANISM OF DROPLET FORMATION IN MICROFLUIDIC EDGE SYSTEMS	97
6.	PARALLELIZED EDGE-BASED DROPLET GENERATION DEVICES	115
7.	EDGE EMULSIFICATION FOR FOOD-GRADE DISPERSIONS	133
8.	DISCUSSION AND OUTLOOK	149
	REFERENCES	157
	SUMMARY	163
	SAMENVATTING	169
	DANKWOORD	175
	PUBLICATIONS	179
	CURRICULUM VITAE	181
	TRAINING ACTIVITIES	



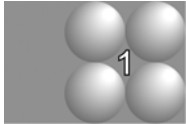
Chapter 1

INTRODUCTION



INTRODUCTION

FOOD PROCESSING



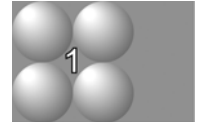
Food is a primary requirement for any living organism. In the early days, food collection and processing by humans was mainly limited to harvesting, catching (fish) or hunting (land animals), followed by cleaning or peeling, and some forms of preservation. During the development of human culture, processing raw materials in various ways to enable storage and improve the nutritional value, taste, attractiveness, convenience, digestibility, safety and variety became important and probably contributed to the unique position of humans (Wrangham, 2009). The origin of food processing goes at least all the way back to ancient Egypt. The origins of beer and bread can be traced back to Babylon and Egypt in the period from 3,000 to 5,000 BC. Examples of common food processing techniques are:

- Mixing
- Peeling
- Chopping
- Squeezing
- Evaporation
- Spray drying
- Crystallization
- Emulsification
- Drying
- Boiling
- Frying
- Steaming
- Baking
- Grilling
- Pasteurization
- Fermentation
- Chilling
- Freezing

Most of these treatments were developed or applied without any systematic knowledge of the phenomena behind them. Moreover, we still do not accurately understand many aspects of commonly used processes and observed changes during food processing, irrespective of whether we use them everyday in the kitchen at home or whether they are implemented in large-scale industrial production plants. As a consequence, several common techniques seem to be far from optimal from a technical point of view. Nicholas Kurti, one of the founding fathers of the relatively new field of Molecular Gastronomy, in which the physical and chemical processes in food during cooking are studied, is often quoted to have stated:

"I think it is a sad reflection on our civilization that while we can, and do, measure the temperature in the atmosphere of Venus we do not know what goes on inside our soufflés."

Obviously, there is still a lot of room for improvement, and for new technologies, and for this reason, food researchers, and engineers all over the world work on the ongoing understanding and development of our food, keeping in mind sustainable food production of the future. This constitutes an interesting challenge, not only due to the technological complexity of food and food processing as investigated by technologists and engineers, but also due to the combination with ethical, emotional, economic, and environmental aspects that is crucial in this worldwide development.



Next to improvement of existing processes, also completely new food products can be developed by implementing new technology and knowledge, initially often on small scale. One of the world's most famous restaurants, Ferran Adria's elBulli, has stated on their website a 'synthesis of elBulli cuisine' in which one of the terms is (www.elbulli.com):

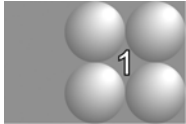
As has occurred in most fields of human evolution down the ages, new technologies are a resource for the progress of cooking.

Making unexpected structures of existing products by changing the common way of processing can result in for example a Gibbs or a Baumé. The first one is an oil-in-egg white emulsion trapped in a gel obtained by cooking the emulsion in a microwave in which the water phase expands while the proteins coagulate simultaneously. The second product is an egg which has been put in ethanol for a month, resulting in a strangely coagulated egg (This, 2006).

Mostly, developments in food technology are not this pioneering, but are aimed at improving the effectiveness and efficiency of the preparation of foods or ingredients, or improving the sensorial (taste) and nutritional (health) quality of foods, and often a combination of these. Generally speaking, foods consist of many different substances, and the quality of a product is determined not only by their molecular composition, but also by the way the constituents are present as a result of preparation. Most products are multiphase products, in which at least one phase is dispersed into another, and the morphology of the dispersion is a major determinant of the sensorial and nutritional characteristics of the product. Given the large variation in the exact formulations and preparation methods of food products, it is useful to consider dispersions as a separate

class of systems, and to study how their preparation could be improved, to obtain better products, and to improve the efficiency of the preparation.

DISPERSIONS AND EMULSIONS



A dispersion is a mixture of at least two immiscible phases. These phases may have any aggregation state. Dispersions are generally made by intensive mixing or shearing, or by mechanical disintegration, which breaks up one phase into small domains, and disperses these into another phase. Table 1 gives some examples. Most dispersions are thermodynamically unstable, which means that they tend to separate into isolated or aggregated phases. The stability of the product therefore generally depends on kinetic arrest. For the stabilization of dispersions, the interfaces between the phases need to be stabilized, such that the domains cannot aggregate or coalesce into larger ones.

From the types of dispersions mentioned in the table, we will focus mostly on emulsions, as these are by far the most common dispersion in food products. Milk, sauces, creams, mayonnaise, and dressings are examples of oil-in-water emulsions (O/W), and butter is an example of water-in-oil (W/O) emulsion.

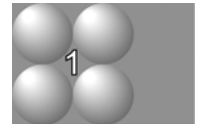
The droplet size and the droplet size distribution both are important for the product properties, and for its stability. The droplet size affects the taste and appearance of a product. For example, an O/W emulsion with smaller droplets suppresses bitterness (Nakaya *et al.*, 2006). An emulsion with larger droplets will be more opaque and whitish, while emulsions with smaller droplets will be more transparent. In the extreme case that the droplets become clearly smaller than the wavelength of visible light, the emulsion can

Table 1. Examples of dispersions.

Particle	Medium	Name	Technique
Gas	Liquid	Foam	Rotor-stator / steam injection
Liquid	Liquid	Emulsion	Homogenization / rotor-stator
Liquid	Gas	Aerosol / Fog	High pressure nozzles (atomizers, spray drying)
Solid	Liquid	Suspension	Milling, homogenization
Solid	Gas	Powder	Milling, spray drying, fluidized bed drying

even become transparent (Wooster *et al.*, 2008). The stability of the emulsion, which is its susceptibility to destabilize into two (or more) separate phases, is influenced in different ways:

- Creaming or sedimentation
- Flocculation
- Coalescence
- Ostwald ripening



In practice, two or more of these instability phenomena may operate concurrently, depending on the system (McClements, 1999). In addition, phase inversion may take place, which is the transformation of an oil-in-water emulsion into a water-in-oil emulsion or visa-versa. This usually takes place only during processing, or during consumption in the mouth. Destabilization is even more relevant for multiple emulsions such as water-in-oil-in-water (W/O/W) or oil-in-water-in-oil (O/W/O) emulsions, which both contain more interfaces, and are more unstable than single emulsions, see Figure 1, and are intrinsically hard to prepare because of these instabilities (see also next section).

It is clear that the droplet size and droplet size distribution are both important for the properties and stability of emulsion based products. However, traditional techniques to produce emulsions are far from optimal to fulfill the requirements for desired emulsion properties, but a number of new techniques have the potential to do so. We will therefore

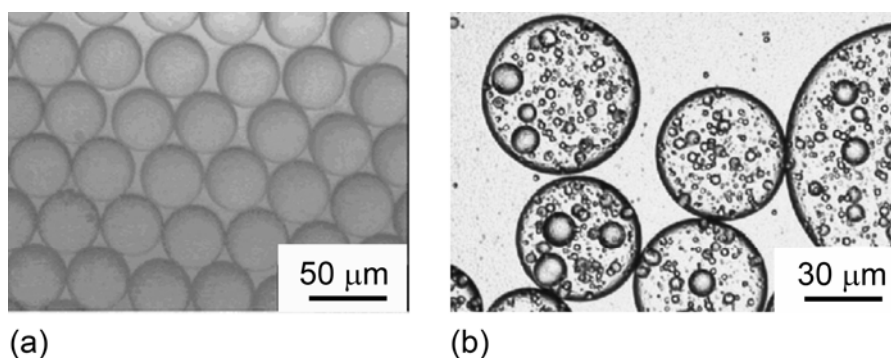
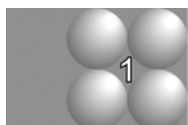


Figure 1. A microscopic picture of a monodisperse single emulsion made by microchannel emulsification (Kobayashi *et al.*, 2005b) is shown in (a). A polydisperse double emulsion made with traditional emulsification techniques (www.bayer.com).

first discuss some of the traditional emulsification techniques, and subsequently some of the newer techniques.

CONVENTIONAL EMULSIFICATION



Usually, emulsions are produced starting from a coarse pre-mix emulsion obtained by gentle mixing. The actual emulsification is performed by disrupting the pre-mix droplets in intense laminar or turbulent flow, or a combination of those, where the shear forces on the droplets have to exceed the interfacial tension forces that keep a droplet together for droplet break up. In order to facilitate the creation of an emulsion with small droplet sizes, lowering the interfacial tension by adding an emulsifier is advantageous. It should be kept in mind that not only the interfacial tension itself but also the rate at which emulsifiers adsorb to the interface is of importance. A high adsorption rate causes a newly formed droplet to quickly lower its interfacial tension, possibly leading to further disruption. Additionally, re-coalescence is prevented by quickly stabilizing the formed droplets (Walstra *et al.*, 2006).

The most commonly used devices for emulsification in the preparation of foods are schematically shown in Figure 2. The high-pressure homogenization systems (Figure 2a), rotor-stator devices (Figure 2b) and ultrasound systems (Figure 2c) all use a large amount of kinetic energy to create the emulsions and most of it is dissipated as heat in the product, therewith possibly causing heat damage. These processes can be classified as being energy inefficient (McClements, 1999): more than 90 – 99% of all energy is not used in emulsification, but dissipated in heating up the product. Another disadvantage of the present techniques is the considerable polydispersity of the obtained emulsions (Saito *et al.*, 2006).

Further, the traditional methods are too crude to be applied in the production of double emulsions, since the forces exerted in the break-up of the secondary droplets also break up the primary droplets, and thus disrupt the inner phase (Kobayashi *et al.*, 2005d). Multiple emulsions can in theory lead to a whole range of new products as they have potential for reduced calorie products and encapsulation of (healthy) components in the inner phase. A mayonnaise for example, is a concentrated emulsion of oil in egg yolk, salt, pepper,

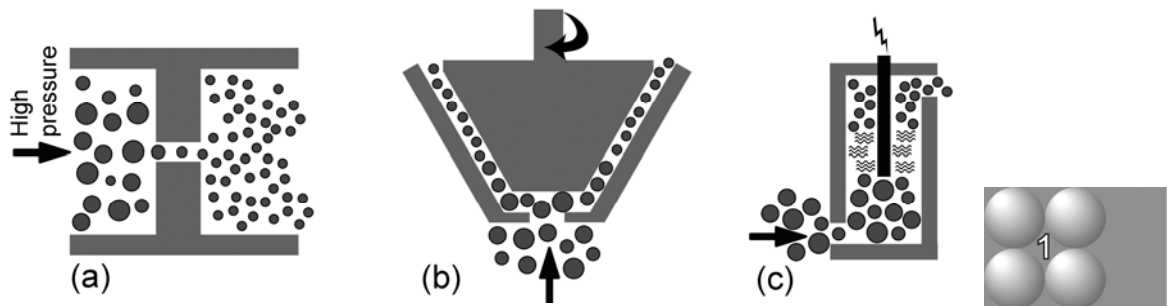
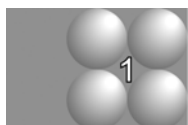


Figure 2. Schematically representation of traditional emulsification apparatus. (a) high pressure homogenizer (b) rotor-stator system (c) ultrasound device.

mustard, and vinegar (or lemon). A low-calorie mayonnaise can be obtained by filling the oil droplets with water (or a solution with the to-be-encapsulated ingredient), making use of a double emulsion structure. For these products, new microtechnological techniques hold a great advantage over traditional techniques, since they do not rely on inducing large-scale, intense force fields, but rather rely on mechanical constraining combined with localized flow to induce the formation of droplets.

EMULSIFICATION WITH MEMBRANES AND MICRO-TECHNOLOGICAL DEVICES

Almost two decades ago, Nakashima *et al.* (1991) published their first article on an alternative emulsification method, using a porous membrane. Emulsion droplets were formed by pressing the to-be-dispersed phase through the membrane pores into the cross-flowing continuous phase. The method produces droplets in a much more gentle way, and therefore, the energy efficiency is better as found by Schröder and Schubert (1999). This direct droplet formation method with membranes and the rapid development in microtechnological engineering in the electronics technology led to devices in which droplet formation could be achieved in channels in the same size range as the droplets themselves. Microfluidic devices distinguish themselves from traditional membranes by their precisely designed geometry of pores and channels, which makes them suited for the production of small and monodisperse droplets.



The emulsification mechanism in microfluidic devices is, amongst others, determined by the size of the channels and their geometric design. In so-called T-junctions, the droplets are snapped off by the shear force of the cross-flowing continuous phase (van der Graaf *et al.*, 2005; Garstecki *et al.*, 2006; De Menech *et al.*, 2008). In flow-focusing devices, the dispersed phase forms droplets due to elongation by the shear exerted through extensional flow of the continuous phase (Umbanhowar *et al.*, 2000; Utada *et al.*, 2007, Anna *et al.* 2003). Besides shear-based methods, also spontaneous droplet formation is investigated, in which the flow of the continuous phase is not needed for droplet snap off. In the spontaneous emulsification devices, which are often referred to as microchannel (MC) emulsification, the driving force for droplet detachment is the interfacial tension, which can be relatively important at the typical dimensions in microdevices.

In the shear based systems, the obtained droplet sizes are dependent both on the system geometry and on the process conditions (flow rate of continuous and dispersed phases mostly). In spontaneous emulsification or microchannel devices, the droplet size is only determined by the geometry of the system (as long as the process conditions are within a certain window), and therefore these devices show the highest potential for the production of monodisperse emulsions. Therefore this thesis focuses on these systems.

MICROCHANNEL EMULSIFICATION

If a non-wetting dispersed phase is pressed through a small channel into a continuous phase, droplets can snap-off at the outlet of such a channel if there is enough space for the continuous phase to intrude into channel. The reason for this is that the dispersed phase is first confined in the channel, but can assume a spherical shape (having a smaller interfacial area and hence less interfacial energy) when it is no longer confined. This interfacial tension induced break-up is characteristic for microchannel emulsification, leading to narrow droplet size distributions.

Generally, two configurations of microchannel emulsification systems can be distinguished in literature; their difference is mainly the orientation of the microchannels. In grooved systems, the channels are etched parallel to the surface of a substrate; in a straight-through device the channels are positioned perpendicular to the surface. The

grooved type of microchannel is more suitable for research purposes as it is possible to visualize the flow in the channels and the actual droplet formation at the outlet. The straight-through variant can be better parallelized, but can be studied only through a top-view. In Figure 3, impressions of both systems are shown.

The only energy needed for microchannel emulsification is that for pressurizing the fluids through the channels, and for overcoming the Laplace pressure of the dispersed fluid into the continuous phase. Microchannel emulsification is therefore a gentle technique which could lead to a more energy efficient way of producing narrowly dispersed single and multiple emulsions. Droplet sizes can be controlled accurately at low throughputs by adapting the size of the microchannels; increasing the oil flux through the channels at some point leads to much larger droplets, which also become polydisperse in the so-called blow-up regime. Although the phenomenon of blow-up is well-documented in literature, the underlying mechanism is far from understood, therefore, this needs to be investigated in more detail. Besides, although straight-through microchannels are in principle suited for mass-parallelization through an increase in the number of channels, this is much more complex than anticipated. Especially for droplet sizes aimed at for most food applications (0.1-10 μm), less than 1% of all channels are actively forming droplets in the monodisperse droplet formation regime (Kobayashi *et al.*, 2008). Increasing the number of active pores by increasing the applied pressure, leads to blow-up. This is probably

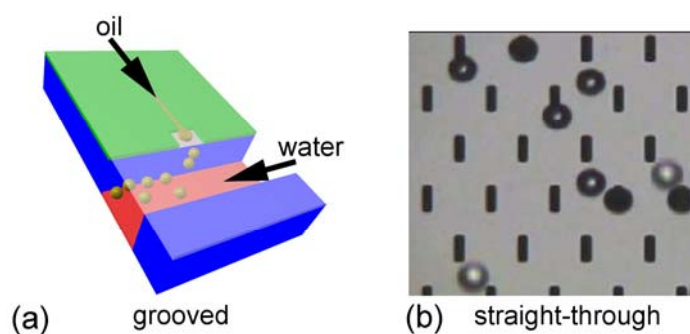
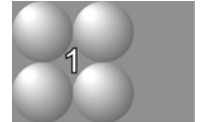
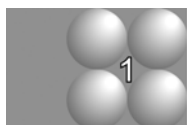


Figure 3. Microchannel emulsification systems, (a) is a grooved system, (b) is a straight-through system (Kobayashi *et al.*, 2002a).

caused by interaction between the channels, or fabrication inaccuracies, while fouling of the channels can not be ruled out; clearly, these effects are not fully understood yet.

Despite its potential, spontaneous emulsification is currently not sufficiently understood to allow scale-up. This thesis aims at elucidating those aspects of microchannel emulsification that are necessary to mature the technology further.



AIM OF THE THESIS

The goal of this research project was to gain a thorough understanding of the principles and dynamics of spontaneous droplet generation in microfluidic devices, and to use this understanding to design improved devices for the preparation of better products.

The existing microchannel devices are investigated experimentally and theoretically on their droplet formation mechanism, and its dynamics. From the mechanistic insights, new designs are proposed. Since the focus of this dissertation is on the droplet formation process itself, the stability of the produced emulsions is considered outside the scope, although some aspects of surfactant dynamics will be discussed.

OUTLINE OF THE THESIS

The first part of the thesis focuses on the fundamental mechanism of droplet formation in grooved microchannel systems.

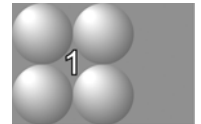
In **Chapter 2**, an analytical model for droplet formation in a single channel with a terrace structure is derived from extensive CFD simulations and experiments. The analytical model is used to predict the resulting droplet size and study the effect of several parameters on the droplet formation process.

In **Chapter 3**, the analytical model presented in the previous chapter is extended for the influence of the viscosity of the continuous phase or, more in general, the viscosity ratio of both phases used in the emulsification process. Experiments and CFD calculations are performed to elucidate the effect of the viscosities.

A new emulsification device that also uses spontaneous droplet generation is introduced in **Chapter 4**. In this Edge-based Droplet Generation (EDGE) device, droplets of the to-be-

dispersed phase are formed at the edge of a shallow but relatively wide plateau, from which multiple droplets can be generated simultaneously. In the chapter, results for a limited number of process parameters are presented.

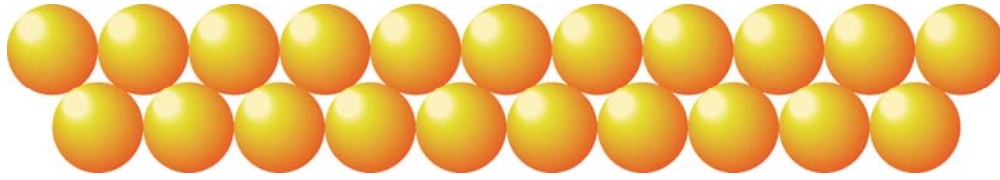
In **Chapter 5**, fundamental work on EDGE is described, considering various aspects of the droplet formation mechanism. Experiments, CFD simulations, as well as geometrical modeling are performed, in order to elucidate the essential complete filling of the plateau, and further, details on droplet formation positions, the minimal droplet size, and the influence of the viscosity ratio are discussed.



Chapter 6 shows the parallelization of EDGE units for larger-scale production and the effect of nozzle design. Various design parameters are investigated, and guidelines for the process productivity and stability are presented, including ways to scale up massively.

For food related applications, different requirements have to be met. **Chapter 7** shows the possibilities to use EDGE for food-grade dispersions such as single emulsions, double emulsions and foams. The options for scale-up of EDGE systems are discussed for the various products that were investigated.

To finalize the thesis, **Chapter 8** summarizes and discusses the research strategy followed in this research project. Furthermore, it gives a short outlook and personal view on the expected trends.



Chapter 2

MICROCHANNEL EMULSIFICATION: FROM COMPUTATIONAL FLUID DYNAMICS TO PREDICTIVE ANALYTICAL MODEL

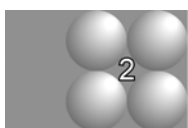
ABSTRACT

Emulsion droplet formation was investigated in terrace-based microchannel systems that generate droplets through spontaneous Laplace pressure driven snap-off. The droplet formation mechanism was investigated through high-speed imaging and computational fluid dynamics simulation, and we found good agreement in the overall shape of the phases during droplet formation. An analytical model was derived from the insights that were gained from the CFD simulations, which describes the droplet diameter as a function of applied pressure. The analytical model covers the influence of both process parameters and geometry of the terrace well and can be used for fast optimization and evaluation studies.

*This chapter has been published as: Van Dijke, K.C.; Schroën, K; Boom, R.M. Microchannel emulsification: From Computational Fluid Dynamics to Predictive Analytical Model *Langmuir* **2008**, 24, 10107*

INTRODUCTION

An emulsion is a dispersion of two (or more) immiscible fluids. They are important to several industries, such as food, cosmetics, and pharmaceuticals. Common emulsions are margarine, mayonnaise, cream liqueurs, hair and skin creams, paints and some medical, vitamin or hormone products. Furthermore, emulsions are used as the basic structure for several types of microspheres (Kobayashi *et al.*, 2001; Sugiura *et al.*, 2000; Sagis *et al.*, 2008).



The traditional preparation of emulsions is based on mechanical disruption of droplets into smaller ones, and subsequent stabilization of the newly formed interface. Frequently used industrial devices are colloid mills, high pressure homogenizers, and mixers. These machines use high shear and extensional stresses, which results in poor control over droplet size, and droplet size distribution, while they require high energy input (McClements, 1999).

In the last decade and a half, novel techniques have been developed in which small droplets are formed in one step instead of disruption of larger droplets. The trendsetter here was Nakashima *et al.* (1991) with the cross-flow membrane emulsification method. For example, for the production of an oil-in-water emulsion, the oil is pressurized through a hydrophilic membrane and the droplets are formed in the cross-flowing continuous water phase. The newest developments in this field, related to the use of microfluidic devices for the production of emulsions, can be traced back to the 1960's. The quick developments in the field of micromachining techniques to produce micro-electronic circuits are now used to create new types of structures on micron scale. These devices distinguish themselves from the traditional membranes by their precisely designed geometry of pores and channels.

Several microfluidic devices have been proposed, and it was shown that they can generate monodisperse droplets. One can roughly distinguish two types of break-up mechanisms in these devices: shear-induced (Anna *et al.*, 2003; Link *et al.*, 2004; van der Graaf *et al.*, 2005; Nisisako *et al.*, 2002; Abrahamse *et al.*, 2002) or spontaneous (Kawakatsu *et al.*,

1997; Sugiura *et al.*, 2001; Kobayashi *et al.*, 2002a). For shear-induced break-up, a flowing continuous phase is necessary to detach droplets from a channel end; for spontaneous droplet formation, the interfacial tension is the driving force for snap-off; therefore no flow of the continuous phase is needed.

In this paper, we will focus on spontaneous droplet formation, since this seems to be the most promising technique for monodisperse droplet formation. Terrace-based microchannel (MC) emulsification as proposed by Kawakatsu *et al.* (1997) gave promising results. A schematic representation of the process can be found in Figure 1. The droplet formation process is divided into an inflation and detachment process. During inflation, the dispersed phase is forced into a disk-like shape on the so-called terrace (Figure 1b&c). When the dispersed phase reaches the end of the terrace, it can spontaneously transform into a thermodynamically more favorable spherical shape (Figure 1d&e). The driving force for this is the interfacial tension, which is the dominant factor on micrometer scale (Sugiura *et al.*, 2002a).

Straight-through microchannel emulsification, STMCE (Kobayashi *et al.*, 2002a) is a variation of terrace-based microchannel emulsification. It also shows spontaneous droplet formation; the oil takes a disk-like shape inside the structure because it is confined by the channel, and once outside the structure the oil droplet can assume a spherical shape. An added benefit of straight-through techniques is that they can be scaled up, because production of an array of millions of channels on a silicon wafer is possible (see Figure 2).

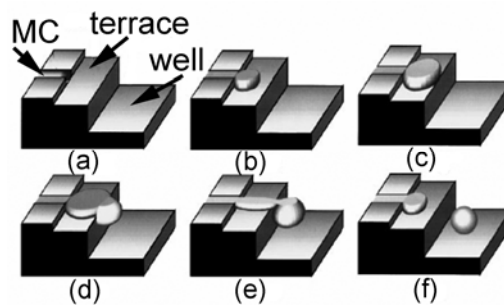
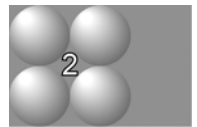


Figure 1. Droplet formation process in terrace-based microchannels (adapted from Sugiura *et al.*, 2000).

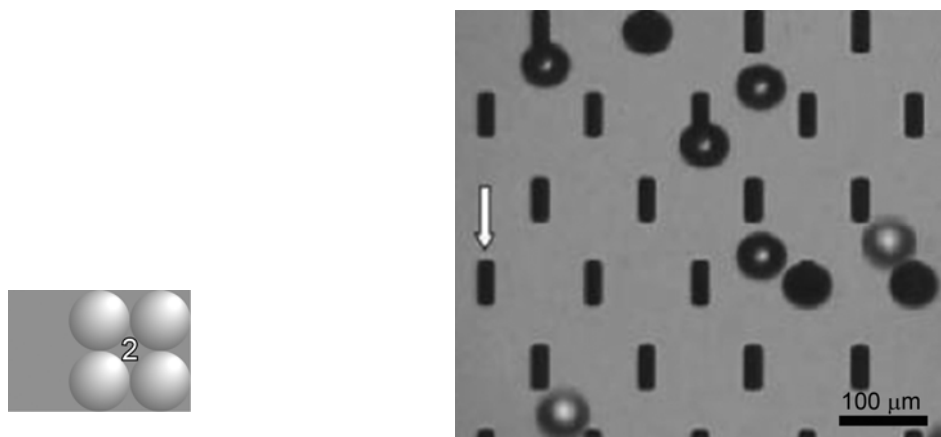


Figure 2. Straight-through microchannels (Kobayashi *et al.*, 2002a).

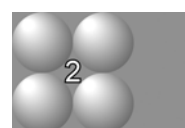
In spite of this, we here work with the terrace-based systems because these systems allow observation of the actual droplet break-up mechanism inside the structure; the scaled up systems can only be investigated from the top. However, since the basic mechanism is the same in both systems, we expect that the results can be (qualitatively) translated to STMCE.

The main issue that is touched upon in this paper is the dynamics of droplet formation in MC systems. In literature, some interesting observations have been reported regarding systems that use spontaneous droplet formation; however, detailed insight in how the droplets are formed seems lacking. For example, Sugiura and coworkers (2002b) observed that the microchannel should be narrow and long to ensure higher production rates. Besides this, they also reported that shorter terraces produce smaller droplets, and at the same time become easily unstable due to the narrow space available for the continuous phase (Sugiura *et al.*, 2000; Kawakatsu *et al.*, 2000). In some of the publications, the capillary number (Ca), which is the ratio between viscous and interfacial forces, is used to characterize the regimes of droplet formation. Above a critical value of the capillary number, the droplet size, and polydispersity, increase quite rapidly and, with further increase of Ca , even continuous outflow of the oil takes place (Sugiura *et al.*, 2002a;

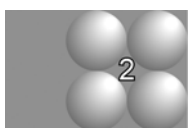
Kobayashi *et al.* 2005). In other work, Sugiura and co-workers (2002c; 2004a) tried to quantify some of the effects, deriving a relation between droplet sizes and the microchannel geometry. However, it has to be mentioned that this relation is not based on the physical processes that rule droplet break-up and that the necessary detachment length is very difficult to determine experimentally, if at all, therefore the predictive value of the equation is rather limited. In addition, the relation only covers the effects of the geometry, and not those of the process conditions, such as flow rates.

The exact role of the terrace and microchannel geometry and of the process conditions is not clear and cannot be easily optimized. It is obvious that the underlying mechanisms need to be investigated in more detail, and in this work we use Computational Fluid Dynamics for this.

In the field of emulsification, only a few researchers have modeled droplet formation through CFD. Abrahamse *et al.* (2001) simulated droplet formation out of a cylindrical pore in laminar cross-flow with the Volume of Fluids method. Van der Graaf *et al.* (2006) used a lattice Boltzmann simulation method for T-shaped microchannels (as a model for cross-flow membrane emulsification). Both Abrahamse and Van der Graaf and their coworkers modeled shear-based systems. Up-to-date only Kobayashi *et al.* (2004; 2005a; 2006) and Rayner *et al.* (2004) simulated spontaneous droplet formation for straight-through MC emulsification with the VOF method, and the Surface Evolver, respectively. The simulations of Kobayashi give insight in velocities and pressures during droplet formation. The increase in pressure difference between the neck and the growing oil droplet promotes flow of oil into the droplet. When a critical value is reached, an imbalance in flow in the neck causes break-up. The critical velocity at which the droplet detachment behavior changes drastically (at the so-called critical capillary number) is significantly influenced by the viscosity. This delays the formation of a circular neck and increases the diameter of the resulting droplet (Kobayashi *et al.*, 2006). Rayner *et al.* (2004) used the Surface Evolver, which is an interactive finite element program for the study of interfaces at rest, shaped by interfacial tension. The point of instability due to free energy could be identified and thus droplet diameter could be determined. The error of



predictions was on average only 8% for the experimental data of Kobayashi and Nakajima (2002b). Although the model could be used to predict the maximum stable volume, no fundamental insight in the complete system is obtained. The Surface Evolver simulations can only model equilibrium situations, and therefore necessarily cannot capture all dynamic effects.



In summary, considerable amounts of work have been done, both experimentally and computationally, but the link between the results seems to be missing, as is a simple model to describe the effects of various parameters that play a role during droplet formation. In this paper, we start with CFD simulations of terrace based systems (see also materials and methods section for description of the geometry). Based on the results from the extensive CFD simulations we propose an analytical model that can be used to describe the resulting droplet size. The effect of several important parameters follows directly from this model.

MATERIAL AND METHODS

Chemicals. In the experiments, n-hexadecane ($C_{16}H_{34}$) 99% for synthesis from Merck KGaA (Darmstadt, Germany) or sunflower oil from the local supermarket were used as the to-be-dispersed phase. The viscosity of sunflower oil can be different, depending on the exact composition. Here we take an average value of 30 mPa s, which is about ten times the viscosity of hexadecane. For simplicity reasons, the to-be-dispersed phase will be called the dispersed phase even before droplet formation has taken place. As the continuous phase, MilliQ ultra-pure water with or without 1% SDS was used.

Microstructures. The microchips used in the experiments are produced by Micronit Microfluidics BV (Enschede, The Netherlands). The microchip is a silicon plate (1.5 x 1.5 cm); into which the microchannels were etched with the Deep Reactive Ion Etching (DRIE) technique to ensure straight corners (round-off $< 1 \mu\text{m}$). A glass plate was bonded on top of the silicon plate to close the channels. Hydrophilic microchannels needed for oil-in-water emulsion production and suitable for visual inspection were created in this way. The emulsification systems consisted of a long dispersed phase channel (10 μm high

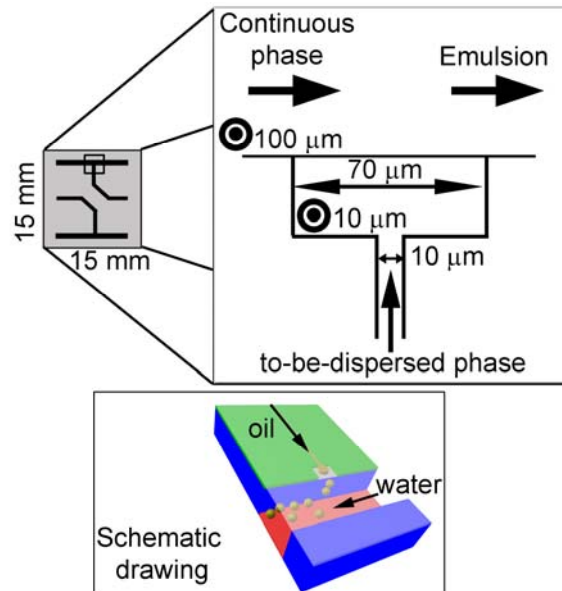


Figure 3. Typical lay-out and 3-D drawing of a microchannel system on the chips.

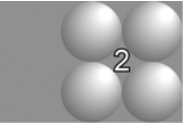
x 10 μm wide) connected to a terrace of 10 μm high (H) and varied width (W_T) and length (L_T), which ended in a much deeper continuous phase channel (150 x 100 μm). A schematic representation of a typical microchip is shown in Figure 3, as well as a 3-D drawing.

The microchip was placed in a module designed by Micronit Microfluidics BV. Both the continuous phase, and the dispersed phase were guided into the microchip through fused silica tubing (Polymicro Technologies, Phoenix, USA) connected to Hamilton gastight luer lock syringes (1700 series). The connections were Nanotight fittings and sleeves in combination with quick connect luer lock adapters, both fabricated by Upchurch Scientific. The syringes were placed into two separate Harvard syringe pumps (types PHD 2000 and 11plus).

Microscope video system. A high-speed camera (Motion Pro HS-4, Redlake MASD Inc., San Diego, USA) imaging system, up to 10.000 frames/second was connected to a microscope (Zeiss AxioPlan Upright microscope, Carl Zeiss B.V., Sliedrecht, The

Netherlands) to observe the droplet formation process in the microchip. The camera was controlled with MotionPro Central software (Redlake MASD Inc.). The module with the microchip was placed on the microscope table and illuminated (Schott KL2500) via the objectives. ImagePro plus (Media Cybernetics Inc.) was used to analyze the movies.

Simulations. We used the Volume of Fluid method incorporated in CD-Adapco's Star-CD, version 4.0, to simulate spontaneous droplet formation in terrace-based microchannels. Pre- and post-processing were done with Pro-Star. The method uses the Navier-Stokes mass and momentum conservation equations for incompressible fluid flow:



$$\nabla \cdot \mathbf{u} = 0 \quad (1)$$

$$\rho \left(\frac{\partial \mathbf{u}}{\partial t} + \mathbf{u} \nabla \mathbf{u} \right) = -\nabla p + \eta \nabla^2 \mathbf{u} + \mathbf{s}_i \quad (2)$$

where \mathbf{u} is the fluid velocity, ρ and η the fluid density and viscosity respectively, p is the pressure, t is time and \mathbf{s}_i is an additional source term. In the volume of fluid method, a scalar variable α , has the value of 0 if the cell only contains fluid 1, and a value of 1 if the cell contains only fluid 2. In cells which incorporate the fluid-fluid interface, where both fluids are present, the scalar variable has a value between 0 and 1. The volume fractions of the fluids, is determined by solving N_c-1 transport equations, where N_c is the number of components:

$$\frac{\partial \alpha_i}{\partial t} + \nabla \cdot (\alpha_i \mathbf{u}) = 0 \quad (3)$$

and

$$\sum_{i=1}^{N_c} \alpha_i = 1 \quad (4)$$

The interface is reconstructed using the High-Resolution Interface Capturing (HRIC) method. The normal force caused by the surface tension (σ) is modeled using the continuum surface force (CSF) model of Brackbill *et al.* (1992). This model introduces a volumetric source term in the momentum equation that is expressed as:

$$s_\sigma = -\sigma \nabla \left(\frac{\nabla \alpha_1}{|\nabla \alpha_1|} \right) \nabla \alpha_1 \quad (5)$$

The wall contact angle of the free surface with a solid wall is imposed as a constraint on the free-surface orientation at the contact line. Dynamic interfacial tension effects cannot be taken into account. For a detailed mathematical description of the model, we refer to the methodology manual of the software.

Half of the actual geometry of the terrace-based MC structure was modelled, since the system has a symmetry plane in the middle ($y = 0$). The dimensions of the grid in Figure 4 are such that they correspond to a MC structure with channel length, L_c , of 270 μm , and

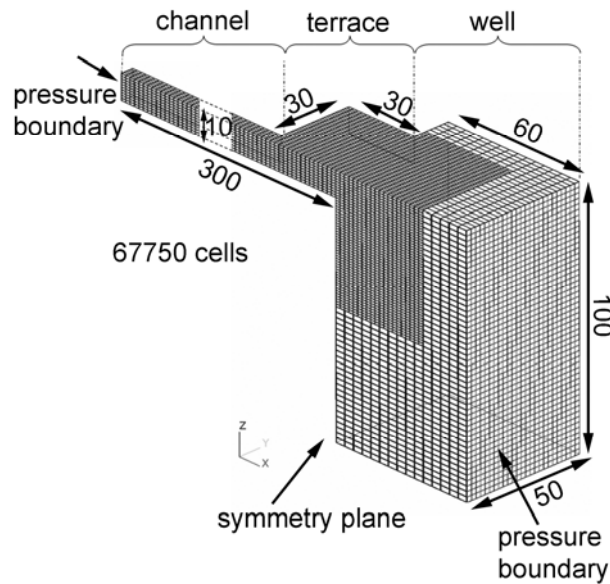
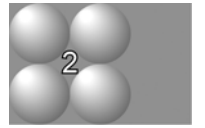
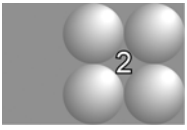


Figure 4. Computational grid of a system with $L_T = 30 \mu\text{m}$.

terrace length, L_T , of 30 μm . The height (H) of the channel and terrace was 10 μm , the width of the channel (W_c) and terrace (W_T) was 10 and 70 μm , respectively. The dimensions of the well were 60 x 100 x 100 μm ($l \times w \times h$). In this example the grid consisted of 84,750 cells. For our convenience during grid development, we positioned the channel entrance at $x = -200 \mu\text{m}$, in this way the terraces are near the origin of the coordinate system. A local grid refinement was applied near the channel and terrace exit to minimize sharp corner problems. Obviously, for other MC systems the dimensions and number of cells were slightly different.



Boundary conditions and important parameters. We applied a static inlet pressure boundary at the channel entrance at position $x = -200 \mu\text{m}$, and a reference outlet pressure-boundary of 0 Pa. In Table 1, some parameters for the simulations are listed. The contact angle, θ , was set at 30° to represent a realistic hydrophilic surface. The interfacial tension was constant; and there was no cross-flow of the continuous phase in the well. At $t = 0$ the oil-water interface is flat and at position $x = 30 \mu\text{m}$, which is chosen to let the flow fully develop before reaching the terrace.

Algorithm and analysis. The SIMPLE algorithm (Semi-Implicit Method for Pressure-Linked Equations) was used with an initial time step of 0.1 μs . Other time steps were adapted to keep the average Courant number below 0.3. The total computation time (covering about 10 ms of time simulated) was about four days when the domain was

Table 1. Relevant properties and parameters.

Property / Parameter	Phase	Value
Inlet pressures [mbar]	Hexadecane	150 - 700
Viscosities [mPa s]	Water	1.00
	Hexadecane	3.34
Densities [kg/m^3]	Water	998
	Hexadecane	773
Interfacial tension [mN/m]	Water - Hexadecane	40
Contact angle [$^\circ$]	Silicon - Hexadecane - Water	30

divided over two nodes running under Linux 2.6.8 with each two 2994 Mhz Intel® Pentium® IV XEON™ processors and a physical memory of 3044 MB.

The diameter of the resulting droplets was measured with the help of a distance-measuring tool in the post-processing software. The pressure graphs (see Figure 8) were extracted from the output files, with the use of 40 ‘sensors’ on vertices along a straight line in the middle of the channel, and part of the well. In this way, the position and time dependent pressures during the process can be visualized.

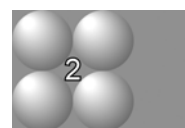
Analytical model. The equations in the analytical model are presented in the results section. For the calculations with the analytical model, we used the value of the previous time-step to solve the explicit relation in Matlab (version 7.4.0.287, The MathWorks, Inc.).

Comparison of CFD results and experiments (Figure 6): The purpose of Figure 6 is to visually compare the experiment and the simulation. The parameters that are used in the simulation are corresponding to those for the liquids used in the experiment, and we tried to stay as close to the experimental conditions as we possibly could, albeit that this is not an easy feat.

Due to the small dimensions of the channels, it is not possible to keep the flow rate constant (as this is also determined by Laplace pressure, as also followed from the simulations). Further, the applied pressure in experiments can not be measured, again due to the dimensions of the channel. An extra check was done using the time of droplet formation, which is in the same order of magnitude for experiment and simulation.

RESULTS AND DISCUSSION

Experiments and validation We use the results of our experiments mainly to validate the CFD simulations. In Figure 5 some screenshots of recorded movies from experiments with a system with terrace dimensions $L_T = 30 \mu\text{m}$ and $W_T = 70 \mu\text{m}$ and hexadecane as oil phase, as well as a system with $L_T = 30 \mu\text{m}$ and $W_T = 30 \mu\text{m}$ and sunflower oil as oil phase are depicted. The continuous phase is MilliQ ultra-pure water with 1 % SDS in both cases.



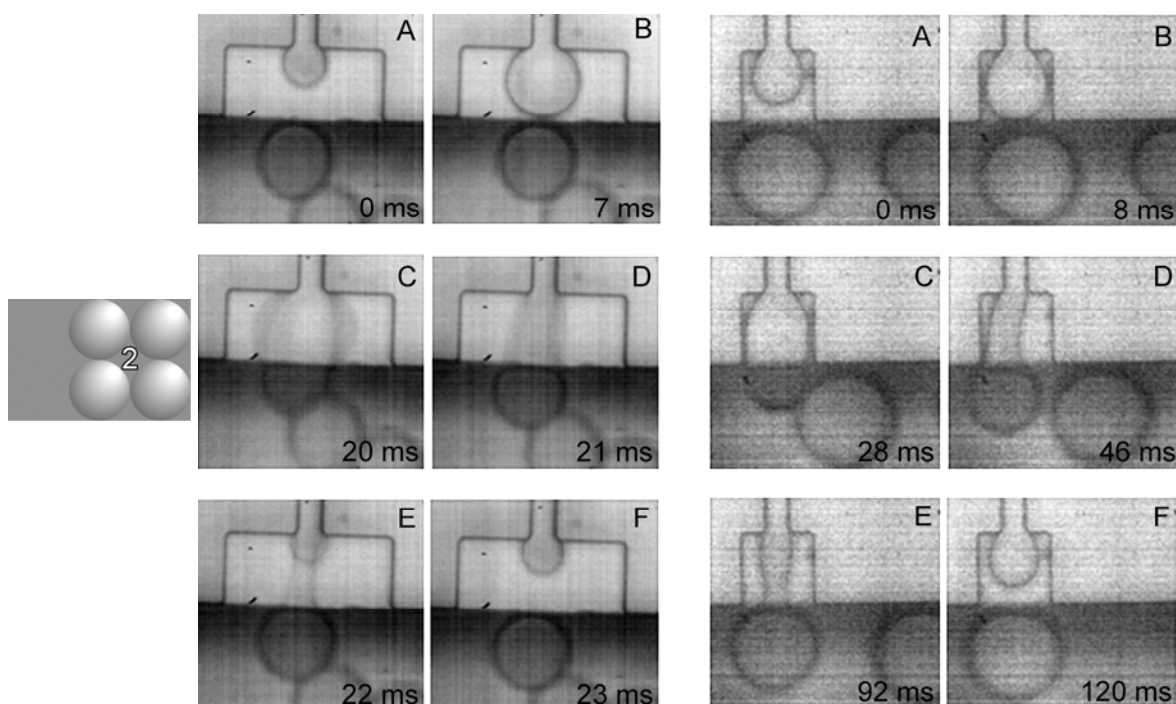


Figure 5. Screenshots of droplet formation in two different systems. On the left hand side, a large terrace ($L_T = 30 \mu\text{m}$ and $W_T = 70 \mu\text{m}$) with hexadecane is used and on the right hand side a smaller terrace ($L_T = 30 \mu\text{m}$ and $W_T = 30 \mu\text{m}$) with sunflower oil.

From the screenshots, it can be seen that hexadecane droplet formation at the larger terrace is very fast. In the sunflower oil experiments, droplet formation took around 120 ms; for hexadecane, the process goes much faster as it only takes around 23 ms. It is very difficult to conclude from the experiments which parameters cause which effect. Therefore, we used CFD simulations to elucidate the effect of the various parameters during droplet formation in microchannels, and later used these simulations to derive an analytical model which describes the effects of all the parameters individually.

We validate our CFD model quantitatively in Figure 6 (see also Materials and Methods section), in which the experimental and computational results of a system with terrace length of $30 \mu\text{m}$, and terrace width of $70 \mu\text{m}$ can be seen. Figure 6 presents photos of the droplet formation process in our microchip. Directly below these pictures, simulation

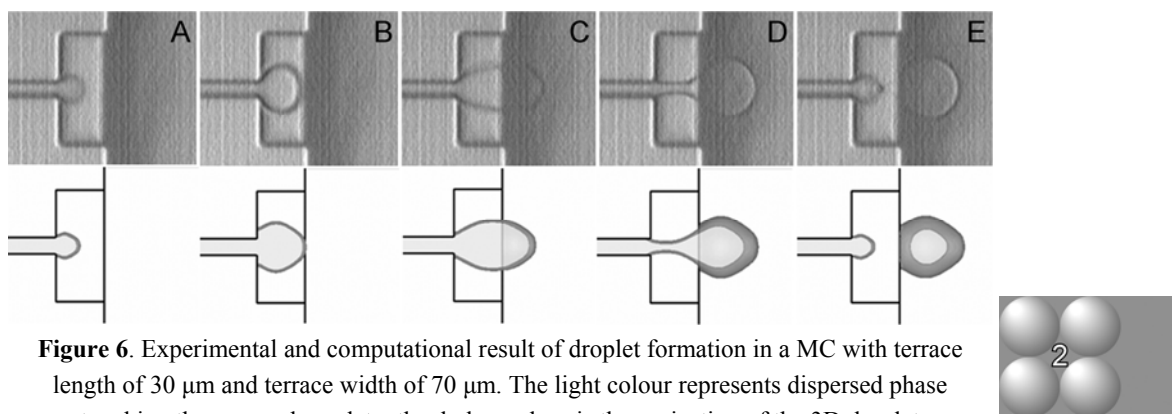


Figure 6. Experimental and computational result of droplet formation in a MC with terrace length of 30 μm and terrace width of 70 μm . The light colour represents dispersed phase touching the upper glass plate; the darker colour is the projection of the 3D droplet below the glass plate.

results are depicted, in which the interface is approximated to be at $\alpha = 0.5$. The applied pressure in the simulation was 185 mbar. Hexadecane was used as oil phase and pure water as continuous phase, and the parameters used in the simulations were in accordance (e.g. $\sigma = 40$ mN/m).

In the left picture (A), the oil enters the terrace area where it assumes the shape of a disk, which increases gradually in size till the oil reaches the end of the terrace area (B). As soon as the oil ‘rolls’ over the edge of the terrace (C), the droplet strives to assume a spherical shape in the well area. This process continues, and the neck that connects the droplet to the entrance channel become thinner (D), until finally it becomes so thin that it breaks and releases the oil droplet (E). The visual agreement between experiment and simulation is good; the observed shapes are very similar, allowing for some numerical inaccuracies due to grid size enlargement in the well area.

CFD simulations. Because microscopic observation ‘only’ allows a two-dimensional analysis of the shapes, the CFD simulations were used to also investigate the curvatures of the oil phase, in relation to the pressure inside the system. This is later used to derive the analytical model. In Figure 7, a typical result is shown, with time indicated in milliseconds. If the applied pressure is high enough, the oil will intrude the channel (7A). As soon as the oil flows out of the channel, the front of the oil starts to grow on the terrace

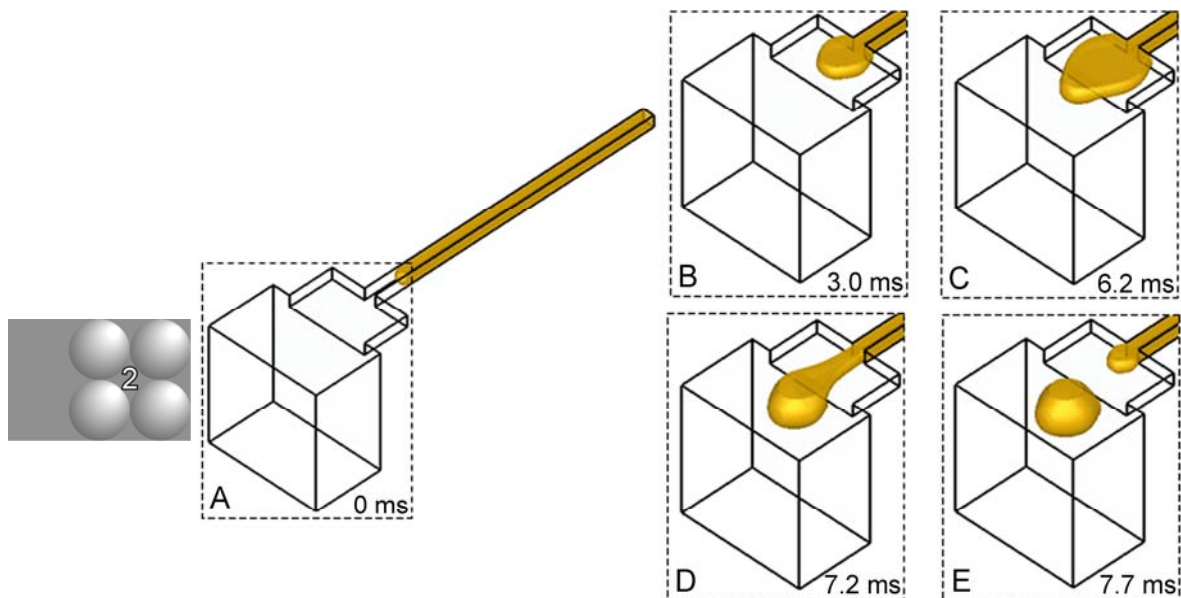


Figure 7. Typical CFD result of droplet formation in a microchannel with a terrace length of $40\ \mu\text{m}$. In A the whole channel is depicted, B until E zoom in on the channel exit area. Time is indicated in milliseconds.

(7B). In the well, the growing droplet will become spherical, eventually break-up occurs and the process repeats itself (7C-7E).

The pressure profile during droplet formation on a terrace with $L_T = 40\ \mu\text{m}$ was investigated in detail. We applied a pressure of $18.5\ \text{kPa}$ at a position of $x = -200\ \mu\text{m}$ (not visible). The pressure in the middle of the channel was plotted as a function of position along the central axis in Figures 8a-d for the oil profiles shown directly underneath. The channel was rotated and positioned in such a way that the position value of the graph is at the same level as in the picture. Please note that the oil profiles contain a symmetry plane, therefore only half of the actual simulation is shown. The oil-water interface in the middle of the channel as well as (half of) the interface against the top wall (glass plate in reality) are visible in this way. In the graphs, the minimal pressure to intrude the channel is clearly visible as the ‘jump’ in pressure (P_f) near the interface, see Figure 8a. In a cylindrical channel with radius R_c , this pressure difference at the oil front can be calculated with the

well-known Young-Laplace equation:

$$\Delta P_f = \frac{2\sigma}{R_c} \cos \theta \quad (6)$$

Here, the channel is a square-shaped and the contact angle was set at 30°. This results in a pressure jump of around 13 kPa., which is considerably lower than for a circular channel

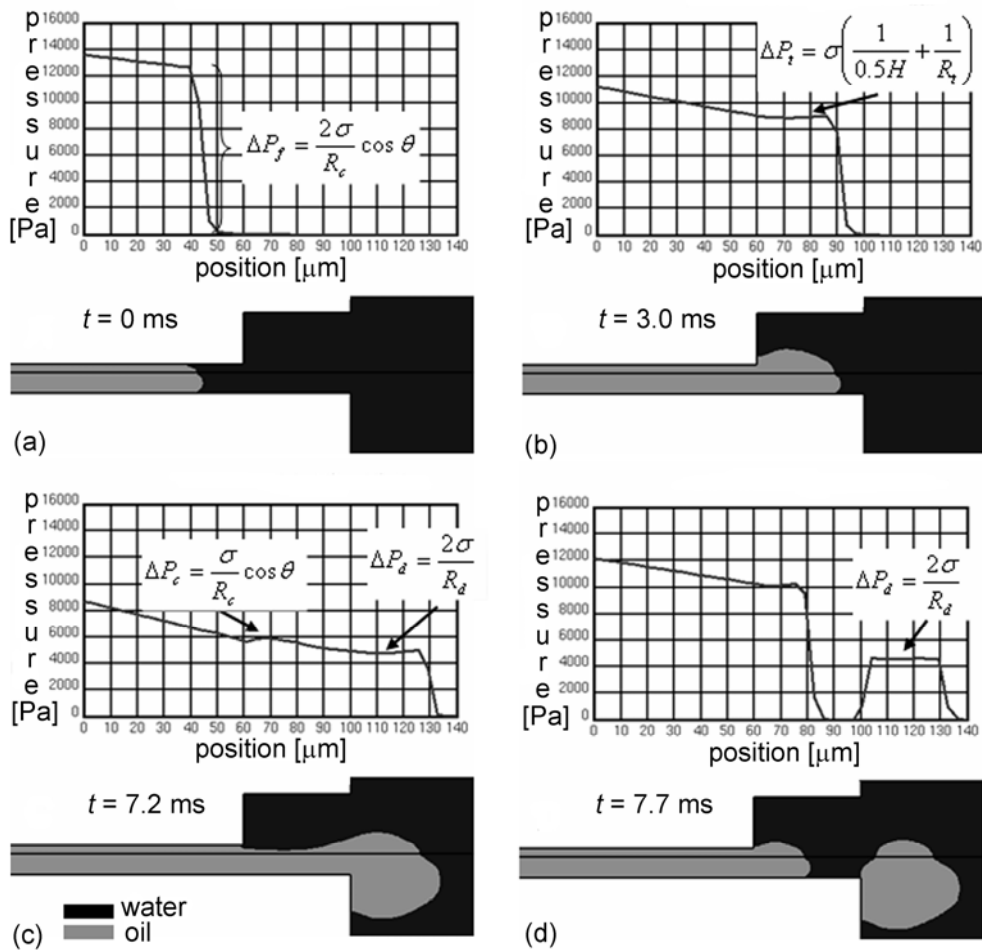
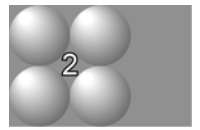
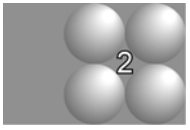


Figure 8. Pressure curves at different stages of droplet formation in a microchannel with $L_T = 40 \mu\text{m}$. The black line in the pictures represents the corner between the cross-sectional (side).

as expected (Lago and Araujo, 2003). As long as the oil is in the channel, the pressure drop over the oil remains relatively constant, due to the shape of the front (results not shown). At the channel exit, the oil will form a disk-shape, as it is not confined by the channel walls anymore (Figure 8b).

The ruling Laplace pressure is now that of the growing disk (P_t) which is determined by the radius of this disk, R_t , and the height of the terrace:



$$\Delta P_t = \sigma \left(\frac{1}{0.5H} + \frac{1}{R_t} \right) \quad (7)$$

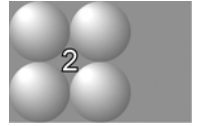
The actual values from the simulations are in agreement with this. As R_t will continuously increase, the pressure in the disk on the terrace will decrease. When the oil reaches the end of the terrace, it will flow over the edge and will grow into a spherical shape with radius R_d (Figure 8c and 8d). The Laplace pressure in this to-be-formed droplet (P_d) can be calculated with:

$$\Delta P_d = \frac{2\sigma}{R_d} \quad (8)$$

Also here, the values found with the simulations are in agreement. Due to the increase in droplet radius, the Laplace pressure will decrease and the pressure curve will become steeper, as the applied pressure ($P_{applied}$) is fixed. The oil that was in the disk-like shape will flow quite rapidly into the well and a neck will be formed on the terrace. Due to the formation of the neck, the pressure will eventually reach the minimum possible Laplace pressure of an oil column on the terrace (P_c). Since one of the curvatures in this stage is almost infinite, the value of the Laplace pressure is mainly determined by half the height of the terrace, which is equal to the radius of the channel, R_c (Figure 8c).

$$\Delta P_c = \frac{\sigma}{R_c} \cos \theta \quad (9)$$

The pressure cannot decrease further, and as a result a pressure gradient appears between P_c (on the terrace) and P_d (in the growing droplet that is still attached to the oil phase). The radius of the droplet keeps increasing, which leads to a larger pressure gradient, and consequently the larger oil flux from the terrace into the droplet. At the same time, the flow through the channel is determined by the applied pressure and the minimal possible pressure of the oil column on the terrace (Figure 8c). As soon as the oil flux supply from the inlet channel is lower than the oil flux toward the droplet, break-up will occur as shown in Figure 8d. The process repeats itself from this stage.



Analytical model. The analytical model is based on the results from the CFD simulations. The starting point of the model is the situation depicted in Figure 8c. Ideally, the whole trajectory of oil flow through the system (which is in principle also possible with this model) is covered by the model. But this would lead to description of very complex dynamic behavior, which is far beyond the scope of the model that we envision. Therefore, the situation in Figure 8c is taken as a starting point. At this point, all the oil from the maximum disk shape on the terrace minus the volume needed for the neck is in the to-be-formed droplet, but the droplet is still connected to the oil phase, and is fed with additional oil from the channel. This volume, V_{start} , corresponds to the volume of a disk with a diameter equal to the terrace length minus that of a cylinder with a diameter and a length equal to the dimensions of the terrace. The radius of this droplet can be calculated with:

$$R_{d,t=0} = \left(\frac{3V_{start}}{4\pi} \right)^{\frac{1}{3}} \quad (10)$$

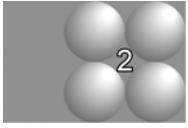
with

$$V_{start} = \frac{1}{4}\pi L_T^2 H - \frac{1}{4}\pi H^2 L_T \quad (11)$$

If at this starting point:

$$P_d \geq P_c \quad , \text{ then } \quad \frac{2\sigma}{R_d} \geq \frac{\sigma}{R_c} \cos \theta \quad (12)$$

(Please note that even if the cross-section of the neck is not always the same, the Laplace pressure will hardly be influenced, since the largest curvature of the neck hardly adds to the pressure.) First, the flux through the entire system is calculated with the familiar Hagen-Poiseuille equation:



$$\Phi_t = \frac{dV}{dt} = \frac{\pi R_c^4}{8\eta L_c} \left(P_{app} - \frac{2\sigma}{R_{d,t}} \right) \quad (13)$$

Equation 13 is valid for laminar flow in a cylindrical tube and with no-slip conditions. We use it here as a reasonable approximation. The flux will result in an increase in the droplet volume, from which the new radius can be calculated:

$$R_{d,t} = \left(\frac{3V_{drop,t}}{4\pi} \right)^{\frac{1}{3}} \quad (14)$$

At some stage, the droplet will become so large that:

$$P_d < P_c \quad , \text{ and } \quad \frac{2\sigma}{R_d} < \frac{\sigma \cos \theta}{R_c} \quad (15)$$

Now we need to define two fluxes, one through the channel (comparable to equation 13):

$$\Phi_{ch,t} = \frac{dV}{dt} = \frac{\pi R_c^4}{8\eta L_{ch}} \left(P_{app} - \frac{\sigma \cos \theta}{R_c} \right) \quad (16)$$

and one through the neck on the terrace:

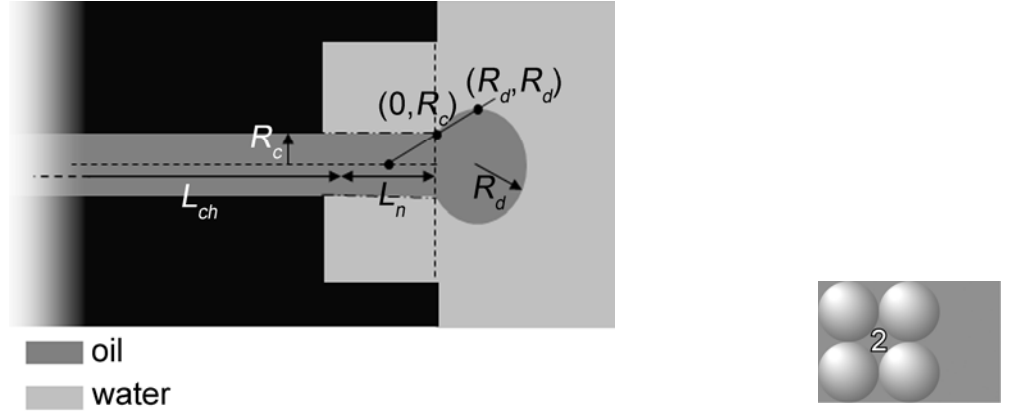


Figure 9. Schematic cross-section of a microchannel system and the definition of L_n and L_{ch} .

$$\Phi_{n,t} = \frac{dV}{dt} = \frac{\pi R_c^4}{8\eta L_n} \left(\frac{\sigma \cos \theta}{R_c} - \frac{2\sigma}{R_{d,t}} \right) \quad (17)$$

The lengths L_n and L_{ch} over which the pressure differences act, need to be defined. Here they are taken to be dependent on the droplet radius, as is observed in experiments and simulations. A straight line is constructed through points (R_d, R_d) and $(0, R_c)$, as shown in Figure 9, and intersects with the central axis of the channel at a distance $\frac{1}{2} L_n$ (the position at which the neck is expected to break) from the channel exit. From this definition follows:

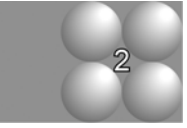
$$L_n(R_d) = 2 \frac{R_c}{\left(\frac{R_d - R_c}{R_d} \right)} \quad (18)$$

and consequently:

$$L_{ch}(R_d) = L_c - L_n(R_d) \quad (19)$$

Table 2. Dimensions of the MC plates used by Sugiura *et al.* (2002a).

MC plate	Depth [μm]	L_T [μm]	L_c [μm]
MC-2	2	15	7.7
MC-4	4	28	14
MC-8	8	57	32
MC-16	16	113	68



Using equations 18 and 19, $R_{d,t}$ is calculated in the same way as described before, see Equation 14. The droplet break-up criterion is defined as:

$$\Phi_{n,t} > \Phi_{ch,t} \quad (20)$$

The input parameters for the analytical model are dimensions of the channel and terrace, viscosity of the oil phase, surface tension, and contact angle. Only the contact angle has to be estimated, and possibly the surface tension if surfactants are present.

The results of the analytical model are compared to experimental results from Sugiura *et al.* (2002a) for four different terrace systems (see Table 2). Triolein with a viscosity of 60 mPa s was used as oil phase and the surface tension in the system was 4.5 mN/m. We

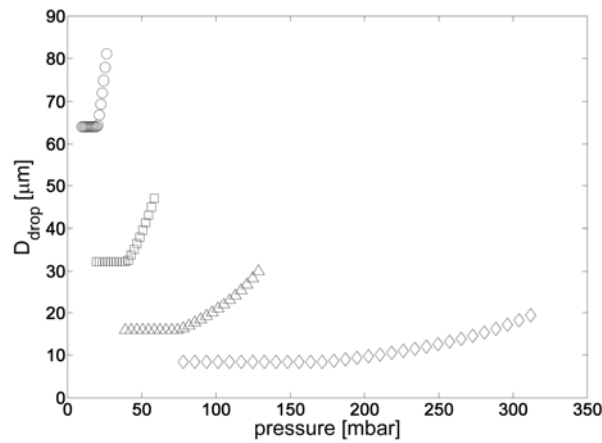


Figure 10. Predicted droplet diameter as a function applied pressure in different MC plates: MC-2 (\diamond), MC-4 (Δ), MC-8 (\square) and MC-16 (\circ).

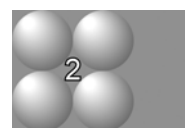
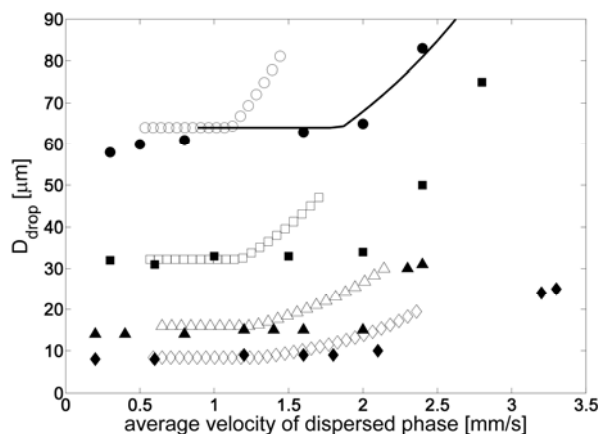


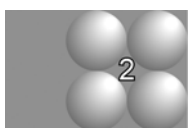
Figure 11. Measured (by Sugiura and co-workers (2002a)) and calculated droplet diameter as a function of average velocity of the oil through the channel for several MC plates: MC-2 (\diamond/\blacklozenge), MC-4 (Δ/\blacktriangle), MC-8 (\square/\blacksquare) and MC-16 (\circ/\bullet). Filled marker: data from Sugiura *et al.* (2002a), open marker: calculated data. The line represents the calculated data for MC-16 with $\sigma = 7.5$ mN/m.

assume a contact angle of 30° , which represents a hydrophilic surface. The model results are shown in Figure 10 as a function of the applied pressure.

It is obvious that less pressure is needed to form droplets with the larger channels due to the lower minimum required Laplace pressure, see Equation 6. The droplet size is stable below a certain pressure above which an increase in diameter occurs. In practice, the pressure range with constant droplet diameter is the desired regime to produce droplets with the MC system. The smaller MC plates have wider operational pressure range, albeit that higher pressure is needed to push the oil in the smaller channels. In the work of Sugiura and coworkers, the calculated average velocity of the oil in the system was used; therefore, our data were re-plotted and compared to the experimental data points in Figure 11. Please note that the actual oil velocity cannot be controlled experimentally, this is an average value.

For the smaller terraces (2, 4, and 8), the calculated and measured droplet sizes are in good agreement in the stable velocity ranges (plateau values). Only for MC-16, the model

overestimates the droplet size slightly. The difference in critical velocity, e.g. the velocity at which the diameter starts to increase, is most probably related to differences between the average velocity determined from size and frequency, as done by Sugiura and co-workers, and the average value deduced from the model. We took the calculated velocity of the oil phase in the channel, where the pressure drop is still constant because the curvature does not change here. Besides this, dynamic interfacial tension effects could play a role. There will be very rapid creation of new interface when the oil moves into the well. This will cause (at least temporarily) a higher surface tension in the system. If we use a surface tension of 7.5 mN/m, instead of 4.5 mN/m, the experimental data of MC-16, and the model results almost overlap (Figure 11). Thus, the differences between predictions and experimental observations can be explained from the assumptions made in the model (e.g., static interfacial tension), while the overall predictions are adequate.



The model can therefore be used to estimate the effect of various process parameters and geometrical dimensions (please keep in mind that these simulations only use static interfacial tensions). We defined a standard system with $L_T = 50 \mu\text{m}$, $W_T = 70 \mu\text{m}$, $H_T = 10 \mu\text{m}$, $\eta = 3.34 \text{ mPa s}$ (n-hexadecane, room temperature), $\theta = 30^\circ$, $\sigma = 40 \text{ mN/m}$, and $L_c = 250 \mu\text{m}$. The effects of variations in contact angle, interfacial tension, channel length, and terrace length, on the droplet diameter are shown in Figure 12. We choose to plot the droplet diameter as function of the applied pressure, because the average velocity is not a controllable input parameter.

In Figure 12a the effect of the terrace length is shown. For larger terraces, the amount of oil present on the terrace will result in an (attached) droplet radius which is large enough to generate immediate droplet formation. With the smaller terraces, this effect does not occur; the droplets still grow after they have first moved into the well, and the size is dependent on the applied pressure. A lower contact angle, *i.e.* a more hydrophilic surface, results in a broader working range for stable oil droplet formation. The same holds for a higher surface tension; as expected the applied pressures need to be higher. A longer channel also results in a wider pressure operation range, as was also observed experimentally by Sugiura *et al.* (2002b). At the same applied pressure, the pressure drop

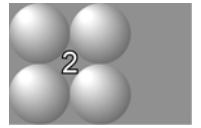
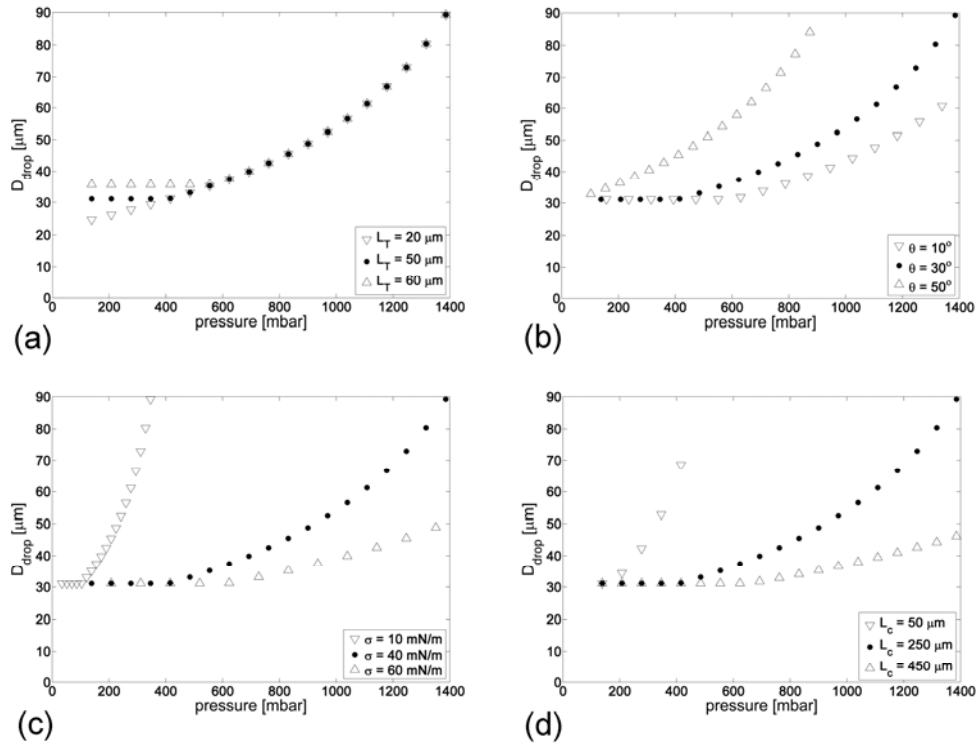


Figure 12. Influence of several parameters on droplet diameter as function of the applied pressure. In a, b, c and d, the effect of L_T , θ , σ and L_c respectively are shown. In each plot there is the standard system (\bullet), with $L_T = 50 \mu\text{m}$, $H_T = 10 \mu\text{m}$, $\eta = 3.34 \text{ mPa s}$, $\theta = 30^\circ$, $\sigma = 40 \text{ mN/m}$, and $L_c = 250 \mu\text{m}$ and a higher (Δ) and lower (∇) value shown. The results in Figure 12 c, can be used to evaluate dynamic interfacial tension effects.

over a short channel will be bigger. For droplet snap-off, a higher pressure drop will be needed between terrace and droplet, in order for the flux through the neck to become higher than the flux through the channel. Therefore, the droplets from short channels will become bigger. Besides the four parameters described in Figure 12, also, viscosity was investigated, and it was found that it does not affect the pressure-curves. The only effect is that the oil will flow faster or slower at the same pressure ranges, resulting in different droplet formation frequencies (productivity). Contrary to the work described here, which uses a pressure boundary that can be applied in practice, the study of Kobayashi and co-

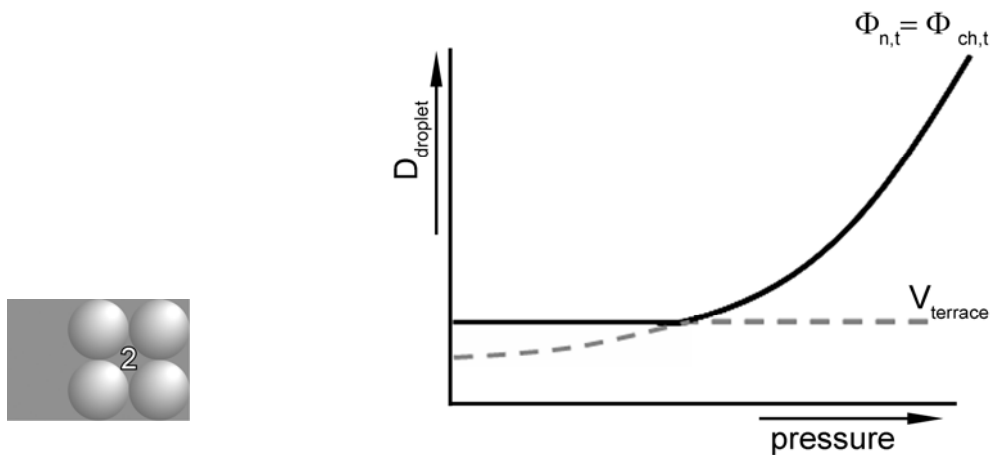


Figure 13. Generalized result for terrace based emulsification systems.

workers uses a velocity boundary (which can not be applied in experiments) and these authors have reported an effect of viscosity on the droplet size. It should be pointed out that these models are so essentially different, that it is not possible to compare the results.

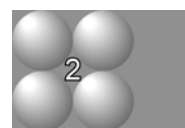
The model can also be applied to slightly different terraces with a width smaller than length. Further, the same approach will be applicable to straight-through microchannels (Kobayashi *et al.*, 2002a) and asymmetric through-holes (Kobayashi *et al.*, 2005b). The big advantage of the analytical model is that neither extensive experimentation, nor computation is necessary for a fast evaluation and possibly optimization of an emulsification system.

In summary, the analytical model predicts all effects that were noted in literature or that we observed ourselves. In Figure 13, a generalized result is shown, and the two criteria that eventually determine the droplet size are indicated. At low applied pressures, the volume on the terrace will determine the diameter of the droplet, since this volume is big enough to generate immediate droplet formation due to the pressure difference that is created between terrace and droplet. At higher pressures, the pressure difference between droplet and channel is not big enough for immediate droplet formation, and the flux criterion determines the droplet size. The droplet can grow until the flux through the neck

is higher than the flux through the channel. The actual droplet diameter is described by the solid line in Figure 13.

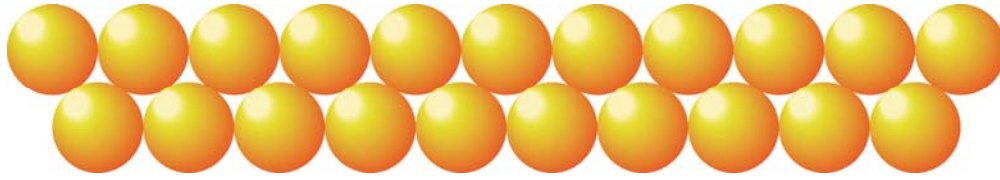
CONCLUSIONS

Computational Fluid Dynamics simulations were done on microchannel emulsification. On the basis of these results, a simple analytical model which describes the droplet diameter as function of the applied pressure was proposed. The model was able to predict all available experimental data adequately. In addition, the influence of process parameters such as dimensions of the channel, surface tension, contact angle, dispersed phase viscosity, and applied pressure on droplet formation could be predicted. Besides this, it was shown that the terrace dimensions determine the operational stability of the process. The analytical model is obviously an easy tool to use in the design of future emulsification systems, and helps in capturing the mechanistic understanding of these systems.



ACKNOWLEDGEMENT

The authors thank Cees van Rijn for communicating his initial insights in spontaneous droplet formation. Linda van Eijk, Siyu Zhao and Sophie Bartels are kindly acknowledged for performing the measurements.



Chapter 3

EFFECT OF VISCOSITIES OF DISPERSED AND CONTINUOUS PHASES IN MICROCHANNEL OIL-IN- WATER EMULSIFICATION

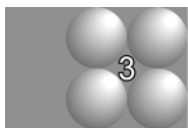
ABSTRACT

It is expected that during droplet formation in microchannel emulsification systems, the inflow of the continuous phase should be sufficiently fast for droplet formation. The ratio of the viscosities therefore influences the droplet formation process. This ratio was varied by using a range of continuous and dispersed phases. At high viscosity ratio (η_d / η_c), the droplet size is constant; the inflow of the continuous phase is fast compared to the outflow of the dispersed phase. At lower ratios, the droplet diameter increases, until a viscosity ratio is reached at which droplet formation is no longer possible (the minimal ratio). This was confirmed and elucidated through CFD simulations. The limiting value is shown to be a function of the microchannel design, and is a design parameter that needs to be adapted to the two fluids.

*This chapter has been accepted for publication as: van Dijke, K.C.; Kobayashi, I.; Schroën, K.; Uemura, K.; Nakajima, M.; Boom, R.M. Effect of viscosities of dispersed and continuous phases in microchannel oil-in-water emulsification *Microfluidics and Nanofluidics**

INTRODUCTION

Microfluidic emulsification of immiscible fluids is of interest to several different application areas because of the high monodispersity of the obtained emulsions. The gentle and controlled formation of droplets is a benefit compared to traditional techniques which use intense force fields to disrupt large, premixed droplets into smaller and relatively polydisperse droplets. Commonly used and studied microtechnological emulsification devices can be driven by transversal flow (T- and Y-junctions (Garstecki *et al.*, 2006; van der Graaf *et al.*, 2005; Steegmans *et al.*, 2009)), coflow (flow-focusing devices (Anna *et al.*, 2003; Xu and Nakajima, 2004)) or by interfacial tension (also called spontaneous droplet formation; grooved microchannels (Kawakatsu *et al.*, 1997) and straight-through microchannels (Kobayashi *et al.*, 2002a)). Several researchers explored the influence of system parameters on microemulsification processes and observed that droplet size can be varied by the design of the microfluidic device (Chapter 2; Sugiura *et al.*, 2002b; Kobayashi *et al.*, 2005b), the flow rates of both phases (Garstecki *et al.*, 2004), and the properties of the liquids and other ingredients (Saito *et al.*, 2005; Vladisavljević *et al.*, 2008).



Spontaneous droplet formation devices yield a combination of good monodispersity, relatively high throughputs (if parallelized) and robustness. The influence of many of the geometric parameters in these systems has been explored. However, the influence of the viscosity of the continuous phase is not yet clear, and is therefore explored here. During the snap-off of a droplet, the dispersed phase flowing out of the nozzle has to be replaced by an equal amount of continuous phase; otherwise the drainage of the dispersed phase out of the nozzle will be hindered and the droplet will not snap off. In grooved microchannel devices the terrace structure facilitates the inflow of the continuous phase. Kobayashi and co-workers (2004) found a minimum aspect (length/width) ratio for straight-through channels of 3-3.5 necessary to produce oil droplets. At a lower aspect ratio, the droplet will block the complete opening of the terrace, preventing inflow of the continuous phase, and thus preventing snap-off of the droplet. This was confirmed by Rayner *et al.* (2004) using static minimization of the surface area during the process. Next

to that, dynamic interfacial tension effects may occur, and if diffusion is the driving force behind surfactant transport to the interface, an effect of continuous phase viscosity is expected.

We here report on the effect of the viscosities of the phases by performing emulsification experiments with several dispersed phases into various polyethylene glycol (PEG)-water-SDS mixtures as continuous phase, supported by fluid dynamics calculations of a comparable MC-system with a single channel.

MATERIAL AND METHODS

Chemicals. In the emulsification experiments, refined soybean oil, hexadecane and several silicon oils (S200, S500, S1000 and S5000) were used as dispersed phase. Polyethylene glycol (PEG) was added in different amounts to MilliQ water with 1 wt% sodium dodecyl sulfate (SDS) to vary the viscosity (η_c) of the continuous phase. All chemicals were purchased from Wako Pure Chemical Industries, Ltd. (Osaka, Japan), except for the silicon oils which came from Shin-Etsu Chemical Co., Ltd. (Tokyo, Japan). The viscosities of the chemicals and mixtures were measured with a Vibro viscometer SV-10 (A&D Company, Ltd., Tokyo, Japan), except for the silicon oils of which the viscosities were given by the manufacturer. The density (ρ) was determined with a density meter (model DA-130N, KEM Co., Ltd., Kyoto, Japan). The static equilibrium interfacial tensions (σ^{eq}) were measured with the pendant drop method (PD-W, Kyowa Interface Science Co., Ltd., Saitama, Japan). All measurements and experiments were performed at 25°C.

In Table 1, the viscosity, density, equilibrium interfacial tension of the dispersed phases in contact with SDS solution ($\sigma^{eq,SDS}$) and the average equilibrium interfacial tensions of the oil in contact with a PEG-SDS- solution ($\sigma^{eq,PEG}$) are shown. Next to that, the viscosity and density of the water phases are given.

The addition of PEG to the water-SDS solutions results in an increased viscosity of the continuous phase; up to 68.2 mPa s for a 20 wt% PEG - 1wt% SDS - water solution. The

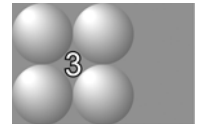


Table 1. Measured properties of phases used in the experiments at 25°C.

Dispersed phase	η_d [mPa s]	ρ_d [kg m ⁻³]	$\sigma^{eq,SDS}$ [mN m ⁻¹]	$\sigma^{eq,PEG}$ *	Continuous phase: PEG in water [wt%]**	η_c [mPa s]	ρ_c [kg m ⁻³]
Hexadecane	2.32	769	9.1	10.7	0	0.91	997
Soybean oil	48.7	916	4.7	8.1	1	1.40	1000
Silicon oil	200	965	9.7	12.5	2.5	2.10	1002
Silicon oil	500	970	10	-	5	4.83	1006
Silicon oil	1000	970	10.6	13.3	7.5	7.84	1011
Silicon oil	5000	970	15	-	10	13.9	1015
					20	68.2	1032

* average value is average for all PEG concentrations; $\sigma^{eq,PEG}$ decreased only slightly at higher wt% PEG, therefore, only one value is shown to represent all in the series. ** all solutions contain 1 wt% SDS.

equilibrium interfacial tension is influenced by the oil that is used, with the most apolar oils having the highest values. Further, addition of PEG plays a role as is reflected in SDS systematically giving lower values when in absence of PEG. The influence of the PEG concentration on the interfacial tension is however minor, and therefore these values are represented as the average of all the measurements done with different PEG concentrations for a specific oil.

Microchannel device and peripherals. In this study, we used a silicon 1.5 x 1.5 cm grooved microchannel device with 150 channels at each side of the chip; for simplicity reasons we will call this chip design 1. In Figure 1, schematic representations of the hydrophilic MC array plate with several relevant dimensions of chip design 1 are shown.

The channel depth (H) is 8 μm , the channel length (L_c) is 25.3 μm and terrace length (L_T) is 51.7 μm . The cross-section of the channel is shown in Figure 1b. The hydraulic diameter (d_{eq}), which is defined as four times the area over the perimeter, is 8 μm . Before the first experiments were carried out, the chip was subjected to plasma oxidation in a plasma reactor (PR41, Yamato Science Co.Ltd., Tokyo, Japan). After each measurement,

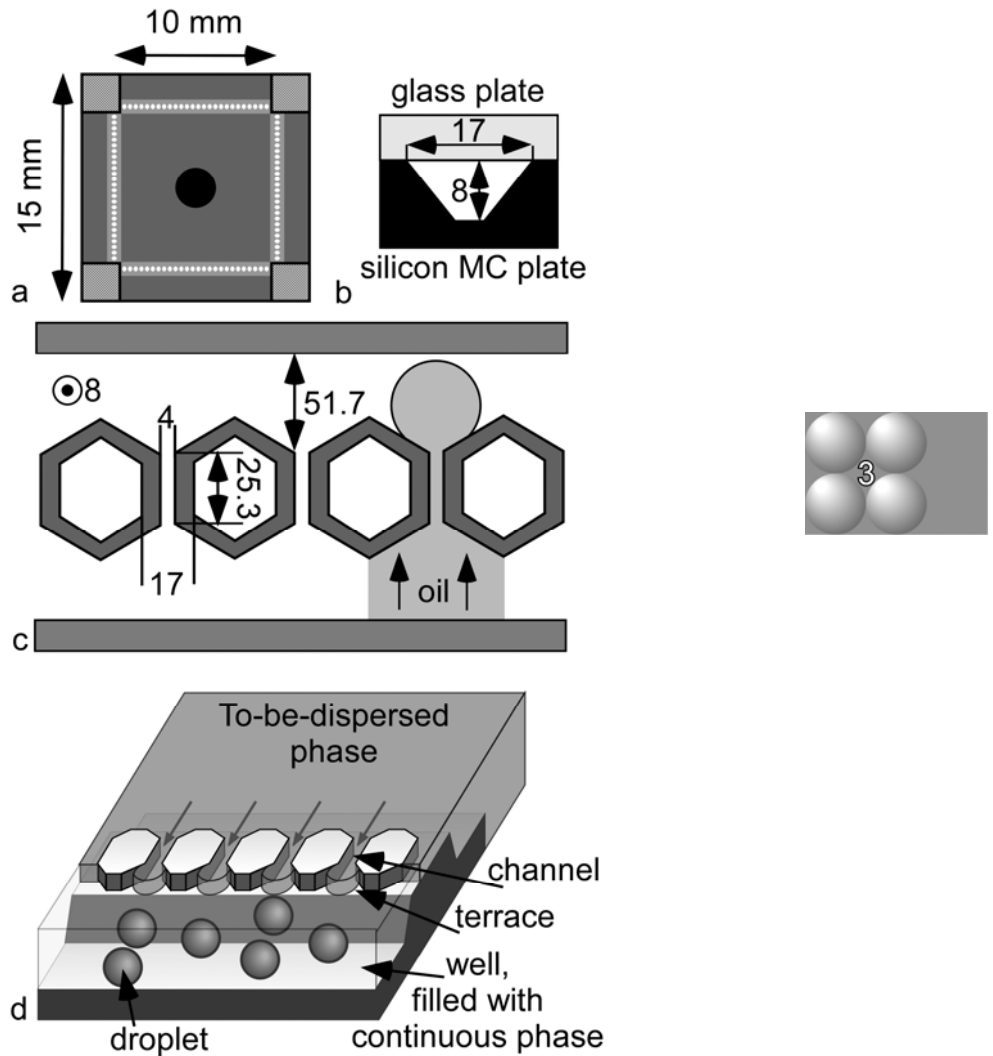


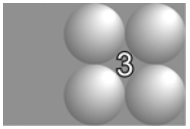
Figure 1. Schematic representation of the microchannel system. (a) chip layout (b) cross-section of a microchannel (c) top-view of three microchannels (d) three dimensional drawing of part of microchannel system producing droplets.

Dimensions are in micrometers if not mentioned.

the chip was cleaned with ethanol and a neutral detergent solution (Clean Ace Neutral) in an ultrasound water bath for 20 minutes and stored in 0.1 M nitric acid for future usage. We also used a comparable microchannel chip albeit with a longer channel ($L_{c,MCL} = 70$

μm), shorter terrace ($L_{T,MCL} = 30 \mu\text{m}$) and channel depth ($H_{MCL} = 7 \mu\text{m}$) in a few measurements; and this chip we will indicate with design 2. The MC plates were placed in the module shown in Figure 2, which was initially filled with the continuous phase; we observed droplet formation with a microscopic high-speed video system.

The to-be-dispersed phase was pressurized via hydrostatic pressure (by increasing the height of the supplying vessel) until the break-through pressure was reached and droplets start to form. (Figure 1d shows a schematic representation of four active microchannels.) The theoretical break-through pressure for a cylindrical channel with diameter D_{ch} and contact angle θ , can be calculated with Laplace's law:



$$\Delta P_{\min} = \frac{4\sigma \cos \theta}{D_{ch}}$$

(1)

This equation can be used to calculate the approximate value of the break-through pressures in the systems used in this work.

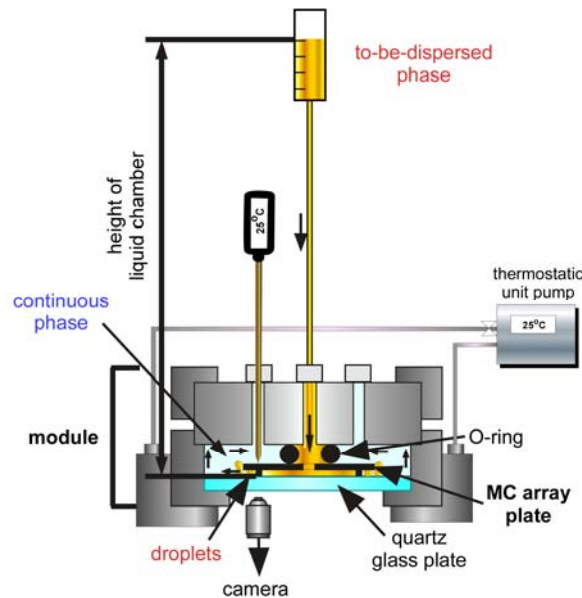


Figure 2. Schematic drawing of all peripherals for microchannel emulsification.

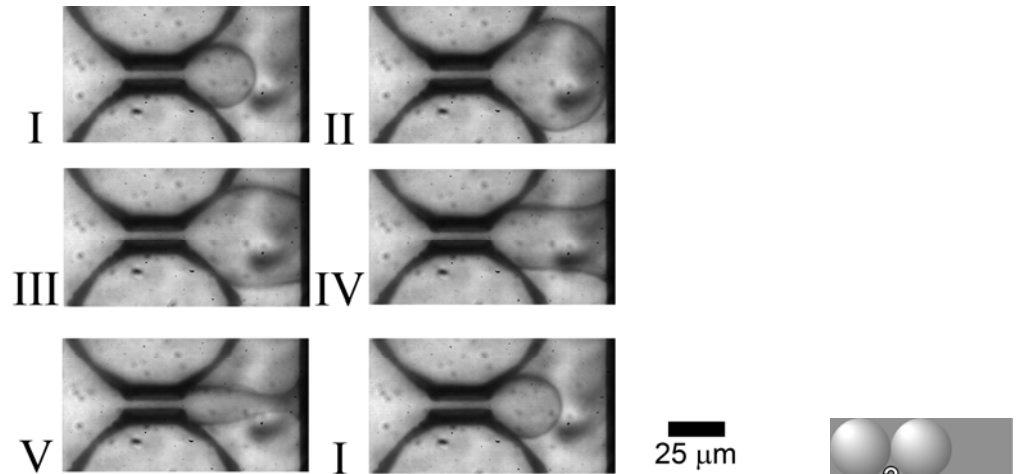


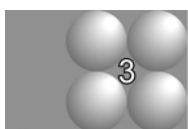
Figure 3. A droplet formation cycle; the oil is pushed into the microchannel from the left side of the image onto the terrace, where it forms a disk which eventually reaches the end of the terrace and snaps off to form a droplet.

Analysis. The number averaged diameters of around 100 produced droplets were measured using image analysis software (WinRoof, Mitani Co., Ltd., Fukui, Japan). Characteristic droplet formation times were also determined by the same software, one droplet formation cycle is depicted in Figure 3.

Simulations. To simulate a droplet formation cycle in a single microchannel, the fully three-dimensional Volume-of-Fluid method incorporated in CD-Adapco's Star-CD (version 4.0) was used. Details and validation of the method in this context are both described in chapter 2. The grid was adapted to the system used in this study, albeit that for simplicity reasons, we defined a rectangular terrace with $L_T = 50 \mu\text{m}$ and a terrace width (W_T) of $98 \mu\text{m}$. The square shaped supply channel was defined having a width $W_c = 8 \mu\text{m}$ and $L_c = 25 \mu\text{m}$. Both channel and terrace are $8 \mu\text{m}$ in depth and a symmetry plane was applied in the middle. We used a static inlet pressure boundary on the channel entrance, and a reference outlet pressure-boundary of 0 Pa . The contact angle (θ) was set at 10° to represent a realistic hydrophilic surface. Surfactant dynamics cannot be taken into account; we assumed no cross-flow of the continuous phase. At $t = 0$, the oil-water interface is flat at position $x = 23 \mu\text{m}$, just before the channel ends on the terrace. The

material properties were defined as measured for the systems with 1% SDS solution, except for the viscosity values. Contrary to the experiments, in the computations we could change the viscosity of the continuous phases without affecting the interfacial tension or density (in reality changes are caused by adding PEG as denoted in Table 1). As a result, we were able to define the applied pressure at a value just above the minimally required pressure for all systems, which allowed us to consider viscosity effects only.

The average computation time was about 5 days when the grid domain was divided over two nodes running under Linux 2.6.8.; each with two 2994 MHz Intel Pentium IV XEON processors and a physical memory of 3044 MB. Due to computation capacity limitations, only hexadecane was used in the simulations as dispersed phase. The pressure values at different positions and time stages during droplet formation were extracted with Pro-Star, the post-processing program of the software package and enhanced and combined with Canvas software (version 11, ACD Systems of America, Inc.); see Figure 6.



RESULTS AND DISCUSSION

Emulsification. Figure 4 shows three microscopic photographs of droplet formation in a grooved microchannel system just above breakthrough pressure where uniform droplets can be produced (a-c), and a picture of a system in the blow-up regime (d).

In (a), hexadecane droplets are formed in a continuous phase with viscosity $\eta_c = 4.83$ mPa s (giving a viscosity ratio of 0.48, see Eq. 2). The low viscosity of hexadecane results in a high rate of droplet formation. The droplets are non-spherical in front of the channel outlet: the viscous continuous phase hinders the motion of the droplets, and squeezes them together. Further away from the terrace, the droplets become more spherical. In a continuous phase with low viscosity, the droplets were spherical everywhere. Figure 4(b) shows droplet formation of a silicon oil with viscosity $\eta_d = 1000$ mPa s in a 20 wt% PEG - 1 wt% SDS aqueous solution with $\eta_c = 68.2$ mPa s (viscosity ratio = 14.7). Although the continuous phase is more viscous than in (a), the formed droplets are spherical and that is most probably due to the much slower droplet formation, which will be discussed later in more detail. In (c), oil with an even higher viscosity is used, in a 1 wt% SDS solution, and

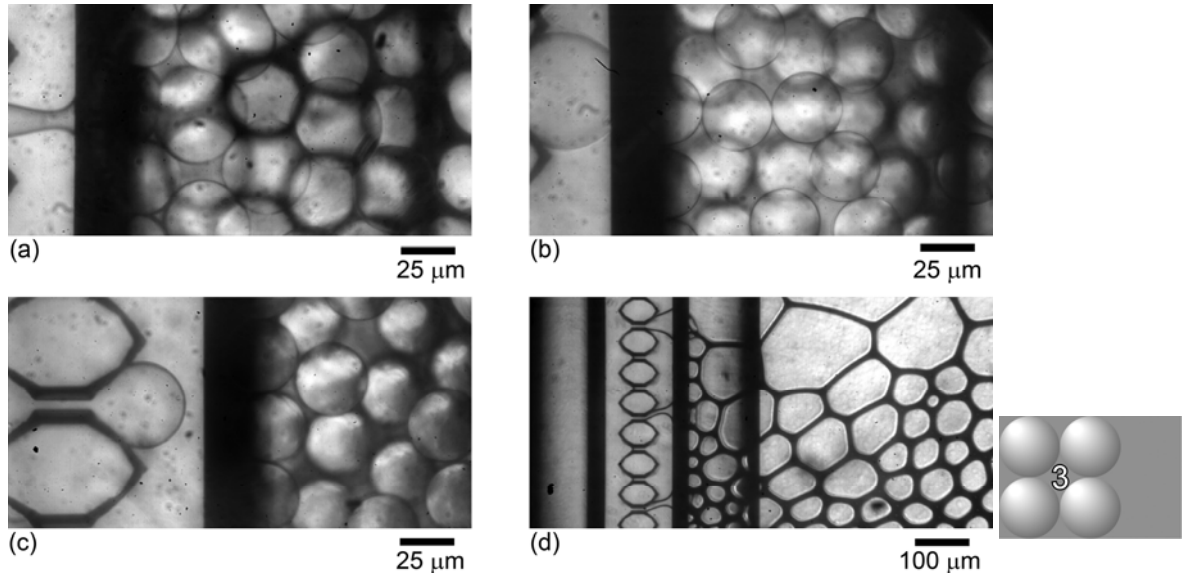


Figure 4. Typical emulsification results. (a) Squeezed hexadecane droplets in 5 wt% PEG – 1 wt% SDS solution, (b) Silicon oil ($\eta_d = 1000$ mPa s) in 20 wt% PEG – 1 wt% SDS solution (c) Silicon oil ($\eta_d = 5000$ mPa s) in 1 wt% SDS solution. (d) blow-up at elevated pressure, shown at lower magnification.

again spherical droplets were formed. Most emulsification experiments performed at pressures below the blow-up pressure resulted in equally sized droplets with a coefficient of variation below 5% (see also Table 2). In highly viscous continuous phases, the c.v. of droplets formed from low viscosity oils is somewhat higher, and this is probably caused by the deformed droplets, which are more difficult to characterize. In picture (d), blow-up of a soybean oil system in a continuous phase with $\eta_c = 68.2$ is shown (viscosity ratio 0.71). This occurs at elevated pressures, which is similar to earlier reported behavior of MC systems. In contrast to systems with lower viscosity of the continuous phase, this blow-up behavior is self re-enforcing: as soon as one channel starts to blow-up all active channels will follow shortly thereafter. Besides, for some systems with high continuous phase viscosity, we observed time dependent blow-up, which implies that after several hundred droplets blow-up occurred without increasing the pressure. Most probably, this is caused by limitation of surfactant transfer to the interfaces which will be discussed later. Table 2 shows an overview of the droplet diameters, corresponding coefficients of

Table 2: Results of performed experiments with chip design 1.

oil	η_c [mPa s]	D_{drop} [μm]	c.v. [%]	t_{drop} [ms]	oil	η_c [mPa s]	D_{drop} [μm]	c.v. [%]	t_{drop} [ms]
Hexadecane $\eta = 2.32$ mPa s	0.91	34.8	2.5	42	Silicon oil $\eta = 200$ mPa s	0.91	32.6	2	169
	1.40	36.8	3.7	30		4.83	34.6	4.1	303
	2.10	39.8	3.9	33		13.9	34.4	5.1	347
	4.83	41.6	9.6	34		68.2	36.2	9.3	470 *
	7.84	-				Silicon oil $\eta = 500$ mPa s	0.91	33.0	4.2
Soybean oil $\eta = 48.7$ mPa s	13.9	-			Silicon oil $\eta = 1000$ mPa s	0.91	33.6	2.7	442
	68.2	-			4.83	33.6	3.3	1236	
	0.91	32.0	2.1	404	13.9	33.6	4.1	1284	
	4.83	33.4	3.8	290	68.2	33.6	3.7	1714	
	13.9	34.4	2.9	518	Silicon oil $\eta = 5000$ mPa s	0.91	33.6	3.8	2420
68.2	39.6	12.2	432 *						

* = time dependent blow-up

variation and total droplet formation times of the experiments performed with microchannel design 1. To compare the experiments we have chosen to define the viscosity ratio (ξ) as the ratio of the to-be-dispersed phase viscosity (η_d) over the continuous phase viscosity (η_c):

$$\xi = \frac{\eta_d}{\eta_c} \quad (2)$$

and the dimensionless droplet diameter D as the resulting droplet diameter D_{drop} divided by the height of the terrace H :

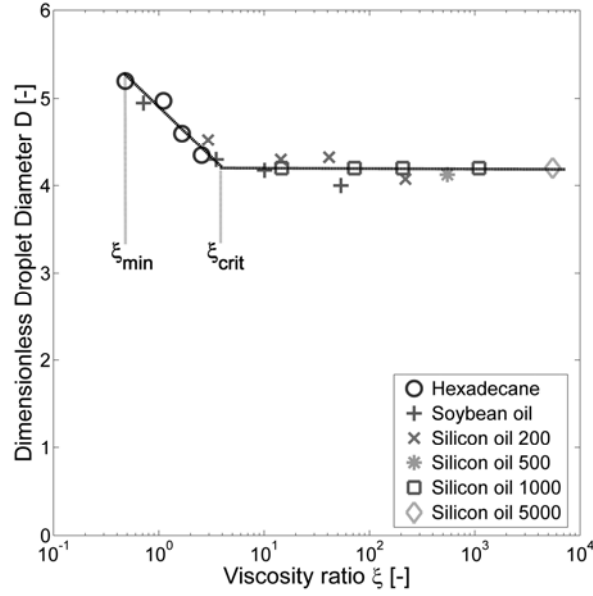
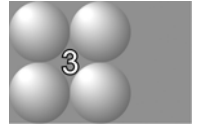


Figure 5. Dimensionless droplet diameter as a function of the viscosity ratio for chip design 1.

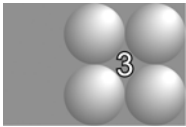
$$D = \frac{D_{drop}}{H} \quad (3)$$

The effect of the viscosity ratio on the dimensionless droplet diameter is shown in Figure 5.

In spite of the big variation in actual viscosity values of the to-be-dispersed and continuous phases, all data collapse onto a dimensionless master curve. If the viscosity ratio is above a certain value (ξ_{crit}), the droplet size is not influenced by the viscosity ratio. The droplet diameter is only affected at low viscosity ratio, below ξ_{crit} , where the droplet size increases with decreasing viscosity ratio. Below a minimal value of the viscosity ratio, $\xi_{min} = 0.48$, we were not able to form droplets with microchannel design 1. We will now discuss the observed results, also in relation to simulation results, taking two phenomena as a starting point: continuous phase inflow and dynamic interfacial tension.



Continuous phase inflow. For microchannel systems, it is known from literature that they facilitate inflow of the continuous phase near the location of droplet snap-off. In grooved microchannels, as well as in asymmetric straight-through channels, the terrace structure enhances microchannel emulsification (Sugiura *et al.*, 2002b; Kobayashi *et al.*, 2004; Kobayashi *et al.*, 2005b) and for oblong straight-through channels it is well documented that the aspect ratio of the channels needs to be larger than 3-3.5 in order to obtain monodisperse droplet formation. Through CFD simulations, it was shown that this minimal aspect ratio was indeed necessary to have enough intrusion possibilities for the continuous phase; *i.e.* water (Kobayashi *et al.*, 2004). At a lower aspect ratio, the growing droplet will completely block the microchannel, and inhibit the ingress of the continuous phase. This is however a static effect.



In this work, we take the CFD simulations a step further and use higher continuous phase viscosities to understand the observed dynamics in the experiments. As an example, we show in Figure 6 the pressure fields at similar stages in droplet formation plotted for a continuous phase viscosity of $\eta_c = 0.91$ mPa s ($\zeta = 2.55$) and $\eta_c = 4.83$ mPa s ($\zeta = 0.48$); both simulations are for hexadecane as to-be-dispersed phase, and other details are given in the materials and methods section.

In Figure 6, only half of the terrace structure is shown to allow detailed observation of the pressure field; a symmetry plane is used in the middle. As the computational grids are slightly rotated, the top views as well as the cross-sections are visible. The pressure values relative to atmospheric pressure are indicated in the ‘color’ bars (the one with the full color is for the negative range, the one with the hatched lines is for the positive relative pressures); the interface is at the black line. Due to the Laplace pressure over the interface between water and oil, the pressure values in the to-be-dispersed phase are much higher and gradients are larger compared to the continuous phase.

In Figure 6, stage I is the inflation stage where the oil flows onto the terrace in a disk-like shape. Similar behavior is observed in both situations, although at low ζ the process is somewhat slower. The crucial difference between high and low continuous phase viscosity ratios becomes visible during stage II, where the disk-like oil on the terrace

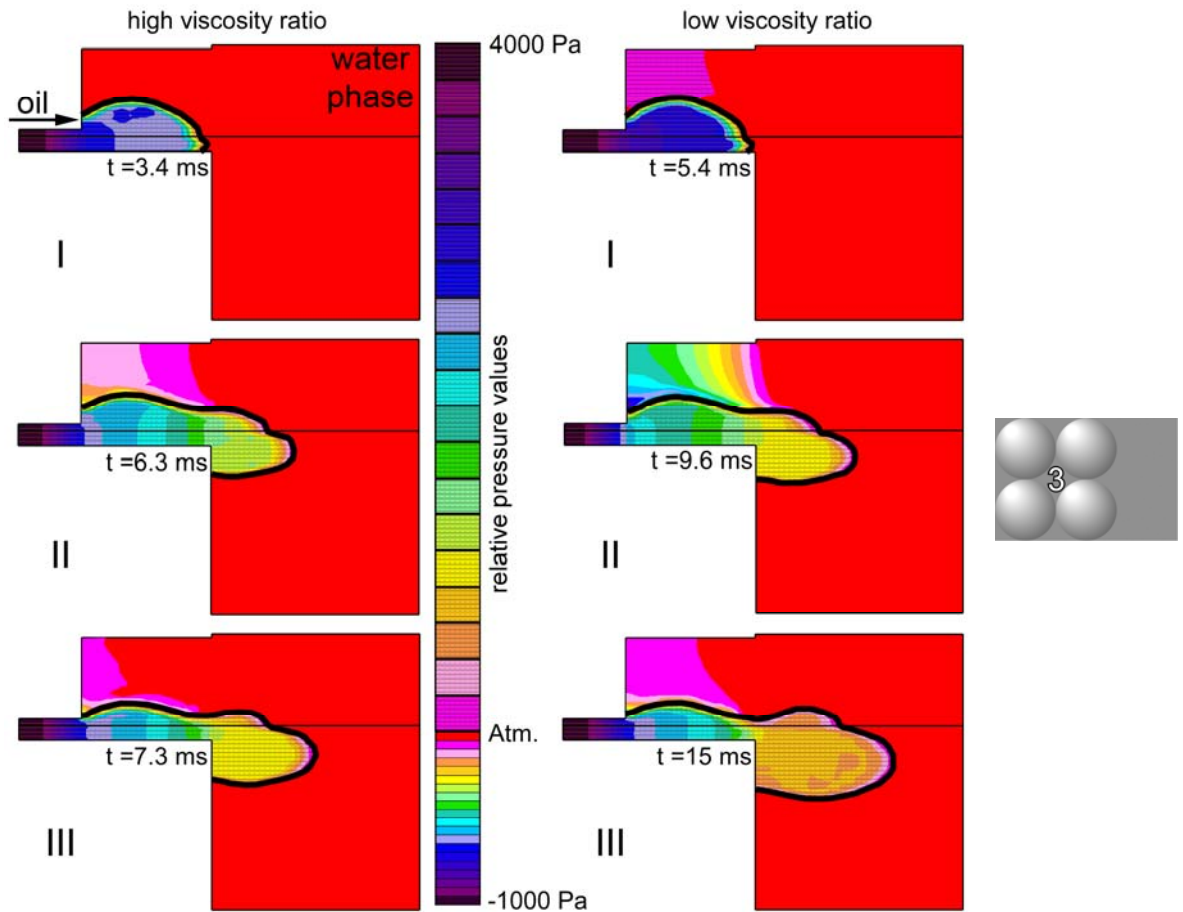
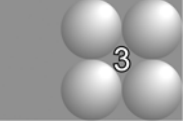


Figure 6. Pressure fields during 3 stages of droplet formation for emulsification systems with a high (left) and low viscosity ratio (right).

flows into the spherical growing droplet in the well. While the terrace is emptied, the generated inward gradient on the terrace causes the continuous phase to flow onto it. With a higher viscosity of the continuous phase, this gradient is clearly steeper, resulting in lower values of the pressure. In stage III, the droplet is close to snap-off, and the gradients that were present in the continuous phase during stage II, have practically leveled out again.

The analytical model derived for MC systems in Chapter 2, was developed for the situation with a high ζ (low viscosity of the continuous phase). Given the differences in local pressures that we noted in the simulation, the analytical model should be refined, since it is based on the local pressures at three locations in the system. For the model, we use the breakthrough pressure mentioned earlier (Eq. 1), which is the lowest pressure applied at the channel entrance which enables oil flow into the channel, the pressure in the oil on the terrace (P_d) and the pressure in the droplet (P_{drop}). Break-up occurs if the flux to the droplet (Φ_n : caused by a pressure difference between terrace and droplet) exceeds the supplying flux through the channel (Φ_{ch} : caused by a pressure difference between channel entrance and terrace), so:



$$\Phi_n > \Phi_{ch} \quad (4)$$

If this criterion is fulfilled immediately after emptying the terrace, the process generates small droplets and is in the monodisperse droplet generation regime. If not, a quasi-static neck will be present to supply oil to the droplet until the criterion is fulfilled.

The pressure in the droplet ΔP_{drop} , defined by:

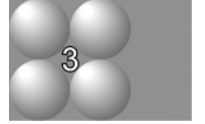
$$\Delta P_{drop} = \frac{2\sigma}{R_d} \quad (5)$$

(with, σ the interfacial tension, and R_d the droplet diameter), and the breakthrough pressure at the channel entrance (Eq. 1) will not be affected by the continuous phase viscosity. In contrast, as shown in the simulations, a higher continuous phase viscosity results in a steeper gradient and lower pressure values in the continuous phase on the terrace (P_c) as can be seen in Figure 6, and this effectively influences the pressure differences in the to-be-dispersed phase (P_d) on the terrace, which follow from:

$$\Delta P_{terrace} = P_d - P_c = \sigma \left(\frac{1}{R_1} + \frac{1}{R_2} \right) \cos \theta \quad (6)$$

In which, R_1 and R_2 are the principle radii of curvature of the oil shape on the terrace, and θ is the contact angle. R_1 is determined by the height of the terrace, H , while R_2 varies during stage II in Figure 6 (emptying terrace), and further, the contact angle is assumed to be constant. In case of a higher viscosity of the continuous phase, the pressure in the oil phase on the terrace (P_d) is lower, and consequently, the supply flow of dispersed phase from the channel to the terrace will be high. As a result, a larger volume of dispersed phase will flow into the well during this stage of droplet formation, and larger droplets will be formed at low ζ , as is visible in stage II of the droplet formation process in Figure 6.

Interfacial tension. From the results depicted in Figure 5 and Table 2, and the measured static equilibrium interfacial tensions shown in Table 1, we can conclude that there is no direct link between static interfacial tension and resulting droplet size. There seems to be a link between the static interfacial tension and the droplet formation times, as can be seen in Table 2. These observations are in line with the results from Sugiura *et al.* (2004b), who also reported an influence on the time of droplet formation. The reason for more rapid droplet formation at higher interfacial tension values is the larger absolute pressure difference between the local pressures defined in the previous paragraph (the curvatures are expected to be similar); which is co-determined by the local interfacial tension.



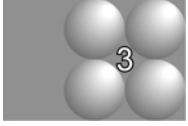
If the process is extremely slow in every sense, the surfactant will have sufficient time to cover the surface area, and the interfacial tension will be equal to the equilibrium interfacial tension. However, given the timescales at which emulsification occurs, it is reasonable that in at least some of the experiments, dynamic interfacial tension effects play a role. Here we try to evaluate the importance of the dynamic interfacial tension by investigating the timescale for diffusion of the surfactant molecules (τ_d) for molecular diffusion near the droplets in laminar flow at low Reynolds numbers (Lucassen-Reynders and Kuijpers, 1992):

$$\tau_d = \frac{2}{D_{diff}} \left(\frac{d\Gamma}{dc} \right)^2 \quad (7)$$

in which, D_{diff} is the diffusion coefficient of the surfactants, Γ the adsorbed amount and c the surfactant concentration. Further, the relative rate of new surface area creation (κ) can be defined as:

$$\kappa = \frac{d \ln A}{dt} \quad (8)$$

The numerical value of τ_d depends strongly on the concentration of the emulsifier, and its diffusion coefficient; theoretical values for SDS are in the order of 10^{-3} s (Vlahovska *et al.*, 1997; Sasaki *et al.*, 1977). The interfacial tension will be at its equilibrium value if the diffusion of the surfactant molecules is fast enough to cover the newly created interface instantaneously:



$$\kappa = \frac{d \ln A}{dt} \ll (\tau_d)^{-1} \Rightarrow \sigma \approx \sigma^{eq} \quad (9)$$

The interface will be free of emulsifier if:

$$\kappa = \frac{d \ln A}{dt} \gg (\tau_d)^{-1} \Rightarrow \sigma \approx \sigma^0 \quad (10)$$

From the definition of the time scale of diffusion, it follows that τ_d is inversely proportional with the diffusion coefficient D_{diff} , and we expect D_{diff} inversely proportional to the viscosity, if we follow the Stokes- Einstein relation:

$$D_{diff} = \frac{k_B T}{6\pi\eta r} \quad (11)$$

and this would imply that τ_d is proportional to the viscosity:

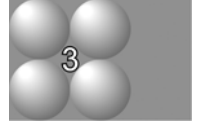
$$\tau_d \propto \eta_c \quad (12)$$

We can approximate the surface creation rate from the droplet surface area A_{drop} , and the initial oil disk area A_{start} and the droplet formation cycle time t_{drop} :

$$\kappa \approx \frac{\ln A_{drop} - \ln A_{start}}{t_{drop}} \quad (13)$$

Hexadecane has the fastest area creation rate in the performed experiments; κ ranges from 60-80 s^{-1} . Using the value of τ_d from literature, it can be concluded that for this low viscous continuous phase, diffusion is fast enough to cover the interface, $\kappa \ll (\tau_d)^{-1}$, and reduce interfacial tension instantaneously to a value close to its equilibrium value.

Increasing the viscosity of the continuous phase has two straightforward effects related to interfacial tension effects; it will lower the diffusional mobility of the surfactant (Eq. 12) and it will affect the droplet formation rate (see also Figure 6), and thus the surface creation rate (κ). In addition, several indirect effects can influence droplet formation. An increase in dynamic interfacial tension value will influence the droplet formation rate as described earlier for a static value, therewith affecting its own dynamic behavior. The generation of a great multitude of droplets or smaller sized droplets (total surface area formation larger) will result in a faster depletion of surfactant from the continuous phase, therewith inducing effects on droplet formation rate and stability. Further, we noted in our experiments that a cross-flow can be of great importance for supply of ‘fresh’ surfactant (and transport of formed droplets that may hinder the surfactant supply process) especially at a high viscosity of the continuous phase, where blow-up is more likely to occur.



In our CFD simulations, in which a constant interfacial tension was assumed, we see similar trends in droplet size as we found experimentally. For these low viscosity ratios, the influence of the dynamic nature of the interfacial tension on the droplet size in the monodisperse regime seems limited, and we expect that the differences in droplet size are caused by slower continuous phase inflow.

System design. Several aspects of droplet formation can be influenced with the design of the microchannel device. Based on the explanation of the observed phenomena, it should

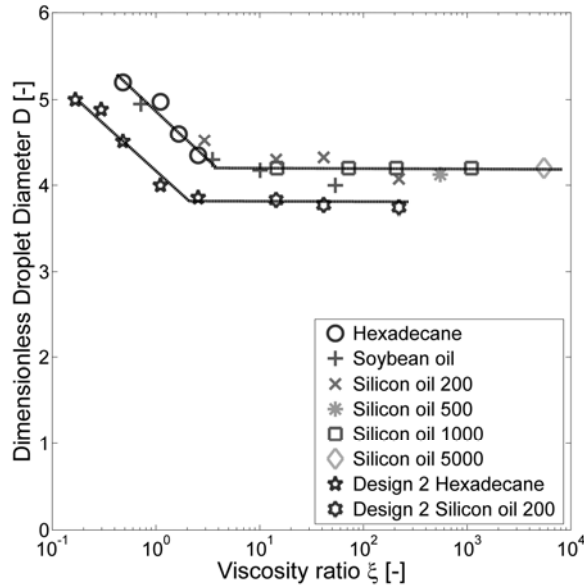
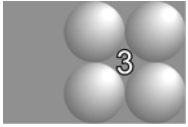


Figure 7. Dimensionless droplet diameter as a function of the viscosity ratio; effect of channel design.

be possible to shift the droplet diameter versus viscosity ratio curve, if the system is chosen such that it is beneficial for droplet formation at lower viscosity ratios. Therefore, we investigated a comparable MC system to prove that the design can indeed be used to improve the window of operation. In Figure 7, the dimensionless diameters of droplets obtained with a system with a longer channel and shorter terrace (design 2) are added to the data presented earlier.

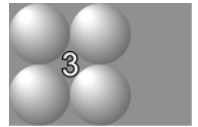
Because of the smaller terrace, smaller droplets can be formed, however more importantly, with this design, we were able to form equally sized droplets until a minimum value of $\xi_{min} = 0.16$. A shorter terrace length will result in a shorter inflow distance for the continuous phase which will be beneficial at low ξ . From literature (Sugiura *et al.*, 2002b) and Chapter 2 of this thesis it is known that longer channels result in more stable droplet generation, and this study adds to this finding that long channels are also beneficial to obtain droplets at low viscosity ratios. A longer channel means a higher hydrodynamic flow resistance, which slows down the flow from channel to the terrace

during droplet formation, therewith keeping the inflow of dispersed phase through the microchannel more constant.

In summary, from all our findings it is clear that not only the design of the microchannel itself is important for stable emulsification, but that also the design needs to be adapted to the components (dispersed and continuous phases, and surfactant) that are to be emulsified.

CONCLUSIONS

We report the effect of viscosity of both continuous and to-be-dispersed phases on microchannel emulsification. At high ratios of the viscosities of the dispersed and continuous phases, the droplet size is not influenced, but at low viscosity ratios, the droplets become larger, and there is a ratio below which successful emulsification is not possible. This minimum viscosity ratio at which emulsification can still take place can be influenced by the design of the microchannel device; for example, a shorter terrace and longer channel leads to a lower critical ratio.



From CFD simulations, we found that the increased droplet size at low ratios is caused by the increased oil supply to the terrace due to a steeper pressure gradient in the continuous phase that surrounds the dispersed phase that is draining from the terrace. Surfactant dynamics are expected to have minor effects during droplet formation, although some secondary effects could play a role in the blow-up of the process, where depletion of available surfactant is expected to occur.

ACKNOWLEDGEMENT

Koen van Dijke and the Food Process Engineering group of Wageningen University want to thank the National Food Research Institute and the University of Tsukuba for their hospitality and willingness for cooperation.



Chapter 4

SIMULTANEOUS FORMATION OF MANY DROPLETS IN A SINGLE MICROFLUIDIC DROPLET FORMATION UNIT

ABSTRACT

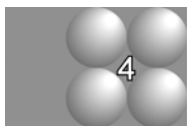
In this chapter, we introduce a new microfluidic droplet formation unit with which we are able to produce multiple monodisperse emulsion droplets simultaneously. In this Edge-based Droplet GEneration (EDGE) device, droplet formation occurs along the edge of a plateau located between the oil supply channel and the continuous phase channel. The EDGE system has a broad practical pressure range at which a monodisperse emulsion can be produced and is self-regulating. Next to that, it is hardly sensitive for fouling, and further it is reasonable to assume that these droplet formation units can be scaled-up easily.

*This chapter has been accepted for publication as: Van Dijke, K.C.; Veldhuis, G.; Schroën, K.; Boom, R.M. Simultaneous formation of many droplets in a single microfluidic droplet formation unit *AIChE Journal* **2009** DOI: 10.1002/aic.11990 Supplementary material online available at the journal's home page.*

INTRODUCTION

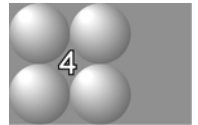
Narrowly dispersed emulsions with droplet size of 0.1-100 μm are of great importance in both science and industry. However, conventional emulsification techniques yield wide droplet size distributions with typical coefficients of variation of around 40% (Saito *et al.*, 2006). Next to that, most of the energy put into the product is dissipated as heat (Walstra *et al.*, 2006)

Recently, several new energy-efficient microfluidic droplet formation systems have been developed which give more monodisperse emulsions. Highly monodisperse droplets can be produced by single-drop technologies such as flow-focusing devices (Anna *et al.*, 2003; Garstecki *et al.*, 2005), co-flowing systems (Umbanhowar *et al.*, 2000), T-, Y- or cross-junctions (van der Graaf *et al.*, 2005; Nisisako *et al.*, 2002; Steegmans *et al.*, 2009), and microchannels (Kawakatsu *et al.*, 1997; Kobayashi *et al.*, 2002a; chapter 2). Some of these techniques produce droplets in the desired range; however, the volumetric productivity of one unit is considered too low to be of practical relevance for larger scale applications.



To realize a higher volumetric production rate it is essential to upscale these systems. In the single-drop technologies the droplets are formed sequentially, which requires mass parallelization of the droplet formation units (DFU). In shear-based systems such as flow-focusing, co-flowing devices, and e.g. T- and Y-junctions, both the to-be-dispersed and continuous phase flows need to be precisely controlled at each DFU as the flow rates have a huge influence on the droplet size. Consequently, a parallelized shear-based droplet generator is complex, since it not only involves more units but also the control of the flows in all units. Nisisako and Torii (2008) succeeded in mass-production of monodisperse droplets of around 100 μm with CV of 1.3% using large-scale microfluidic integration on a chip (256 droplet formation units). Although it is in principle possible to parallelize smaller channels, therewith leading to mass production of much smaller droplets, the difficulties with control of the flows are expected to increase exponentially as the characteristic size of the system decreases, and are expected to be far from trivial.

In microchannel (MC) systems as studied by Kawakatsu *et al.* (1997), Sugiura *et al.* (2000), Kobayashi *et al.* (2002a), and our group (Chapter 2), only the flow of the to-be-dispersed phase needs to be controlled. The continuous flow rate is not a parameter that plays a role in droplet generation, since droplet formation is induced by Laplace pressure differences, and is often referred to as spontaneous droplet formation. A low flow rate is only applied for droplet removal from the DFU, since otherwise it would be blocked by the droplets. These systems seem to be more suitable for scale-up; especially the straight-through microchannel devices of Kobayashi and co-workers look promising. Monodisperse emulsions with droplet diameters of 4.4 – 9.8 μm with CV from 5.5 – 2.7% were successfully produced using straight-through MC plates with different channel dimensions (Kobayashi *et al.*, 2008). Unfortunately, the channel efficiency, which is the percentage of droplet producing channels, was $< 1\%$ for the plate with the smallest microchannels, and only up to 12.3% for the larger ones. This is most probably due to pressure gradients in the system, as was extensively discussed by Gijsbertsen-Abrahamse *et al.* (2004) for emulsification with microsieves which resemble the devices of Kobayashi. Next to that, fabrication inaccuracies could also cause low channel efficiency as mentioned by Kobayashi and co-workers.



In the microchannels discussed in the previous section, droplets are generated one at a time from a so-called terrace that practically empties to form the droplet. In this Chapter, we present a new droplet formation unit, EDGE (Edge-based Droplet Generation), in which a multi-droplet formation mechanism occurs that generates many narrowly dispersed droplets simultaneously from the same droplet formation unit. Contrary to the microchannels, where the volume of the droplets is roughly in the same order of magnitude as the volume of the terrace from which they are spontaneously generated, the volume of the droplets formed in this new device is only a small fraction of the volume of oil present on the so-called plateau.

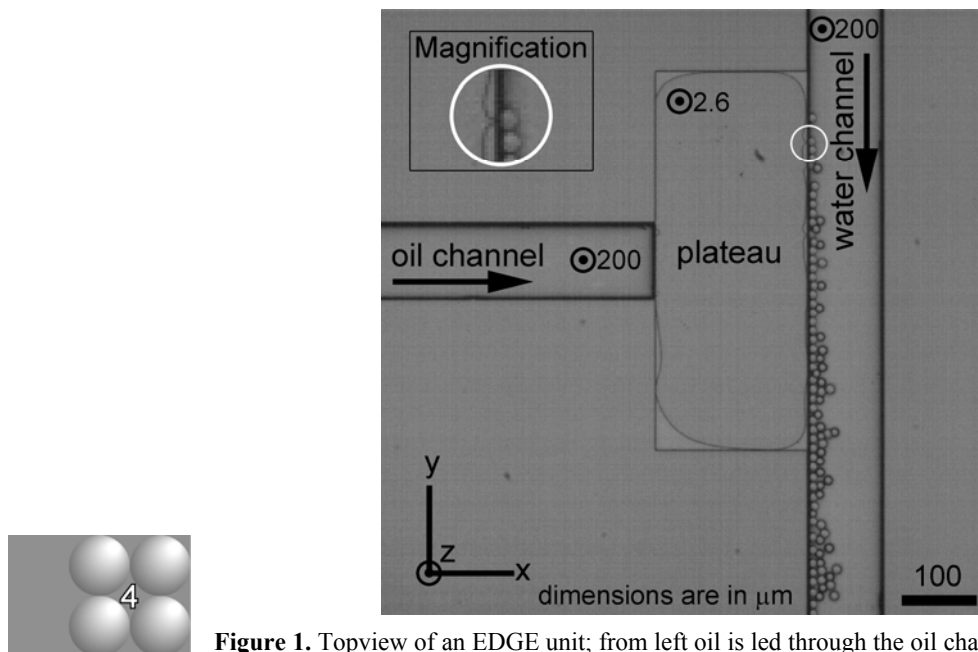


Figure 1. Topview of an EDGE unit; from left oil is led through the oil channel to the plateau and into the water channel after droplet formation at the edge of the plateau. A magnification of droplet formation is shown in the top left corner. Typical dimensions of the structure are indicated in the image.

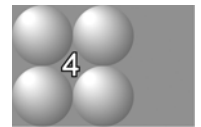
EXPERIMENTAL

The structures and channels were etched with the Deep Reactive Ion Etching (DRIE) technique (Micronit Microfluidics, The Netherlands) in a silicon microchip of 1.5 x 1.5 cm. A glass plate was bonded on top of the chip to close the channels. Hydrophilic surfaces needed for oil-in-water emulsion production were created in this way. The unit consists of an oil supply channel of 100 μm wide and 200 μm deep, and a continuous phase supply channel with similar dimensions. In between those channels, there is a plateau with fixed width ($W_p = 500 \mu\text{m}$) and length ($L_p = 200 \mu\text{m}$). The plateaus that were used have either of two depths (H_p): 1.2 or 2.6 μm ; the plateau being the actual the droplet formation unit in this EDGE system. We define both systems as EDGE-1.2 and EDGE-2.6 respectively (see also Figure 1 for an image of the lay-out and the dimensions). The oil, in our case hexadecane (viscosity $\eta = 3.34 \text{ mPa s}$), is guided to the plateau via the oil

channel. We use a digital pressure controller (Bronkhorst, The Netherlands) to set and control the applied pressure. The pressure needed for hexadecane to flow onto the plateau is determined by Laplace's law:

$$\Delta P = \sigma \cos \theta \left(\frac{1}{R_1} + \frac{1}{R_2} \right) \approx \frac{\sigma}{R_1} \quad (1)$$

where σ is the interfacial tension, R_1 and R_2 are the radii of curvature of the oil-water interface, and θ is the contact angle. For simplicity reasons, we assume a contact angle of 0° , and since the curvature R_2 is very large compared to R_1 , the minimal pressure needed here is determined by the smallest curvature, as shown in the right part of Equation 1. If the pressure exceeds this value, the oil flows on the plateau and droplets will be formed at the edge, where the droplets 'fall over the edge' into the channel with MilliQ ultra pure water with 1 % SDS as surfactant, which is supplied to the channel with a syringe pump. Typical flow rates for the continuous phase are 300-1000 $\mu\text{l}/\text{hour}$.



The emulsification process is visualized using a high-speed camera connected to a microscope. In Figure 1, a snapshot from a movie of a typical experiment with an EDGE-2.6 μm system is depicted; the view is straight from above, and the depth of the various structures is indicated in the image. In the top left corner, an enlarged image of a forming droplet is shown.

Droplet formation at the edge of the plateau occurs seemingly at random along the width of the DFU, and at many locations simultaneously, albeit that the corners of the plateau are not used due to Laplace pressure differences. In an EDGE system, similar sized hexadecane droplets can typically be formed at frequencies of >1500 and >2000 Hz per DFU, for EDGE-2.6 and EDGE-1.2, respectively.

RESULTS AND DISCUSSION

The droplet sizes of emulsions produced with both EDGE systems are analyzed through image analysis and with the Mastersizer 2000 (Malvern Instruments Ltd., United

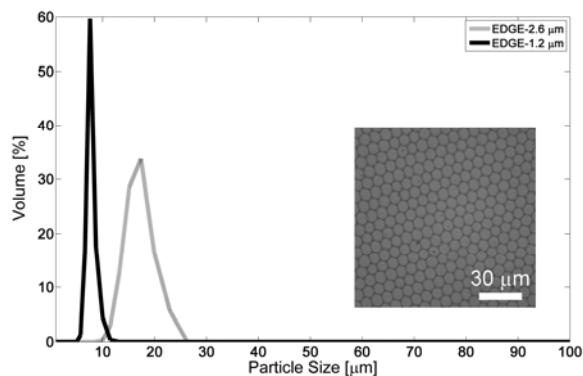
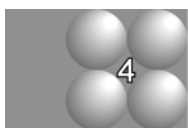


Figure 2. Size distribution of emulsions produced with EDGE-1.2 and EDGE-2.6, together with a micrograph of an emulsion produced with the 1.2 device.



Kingdom). The resulting size distributions are depicted in Figure 2, together with an insert of a photo of an emulsion produced with EDGE-1.2. When using image analysis, we find an average droplet size of 7.1 μm for EDGE-1.2, and 14.6 μm for EDGE-2.6 with a CV of approximately 5 % for both EDGE systems; and these CV's are very comparable to values reported in literature, e.g. in the work of Kobayashi who also used image analysis. When determined by Mastersizer, the volume weighted average for EDGE-1.2 is 7.20 μm with a CV of $\approx 10\%$; for EDGE-2.6, the size is 15.55 μm with a CV of $\approx 16\%$. There seems to be a systematic difference between both techniques and that may quite well be a result of the limited number of droplets that necessarily can be analyzed by image analysis. In spite of the different values, the produced emulsions have a narrow distribution, especially when compared to emulsions made by homogenization.

To study the droplet formation process in more detail, sequential close-up images of a single droplet were made. Figure 3 shows the typical shape of the interface during droplet formation. One should keep in mind that we look straight from above and we can only see one plane; the x-y plane. The droplet becomes visible in image b, and grows in time, until the neck with which it is connected to the plateau breaks (image g), and the interface retreats to fill the plateau again (image a).

Growth of the droplet results in a lower Laplace pressure in the droplet according to Equation 1 with both radii of curvature equal to droplet radius R_d . The droplet in Figure 3

b-f is still connected to the plateau through a neck. Very close to the edge of the plateau, it can be assumed that the local pressure in the neck will be approximately equal to the Laplace pressure in the droplet. And this implies that Laplace pressure due to the two curvatures of the neck has to be in accordance with that of the droplet. The curvatures can be found on the plateau, one of them (x-z plane) is fixed at a value of half the height of the plateau (R_{p1}). The curvature in the x-y plane (R_{p2}) can have different values and has to become negative if the droplet radius (R_d) becomes twice as large as the fixed curvature (R_{p1}) on the plateau, due to the decrease of the pressure in the growing droplet. We can describe this balance with:

$$\frac{2\sigma}{R_d(t)} = \frac{\sigma}{R_{p1}} - \frac{\sigma}{R_{p2}(t)} \quad ; \text{ if } R_d > 2 R_{p1}, R_{p2} < 0 \quad (2)$$

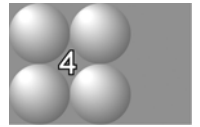
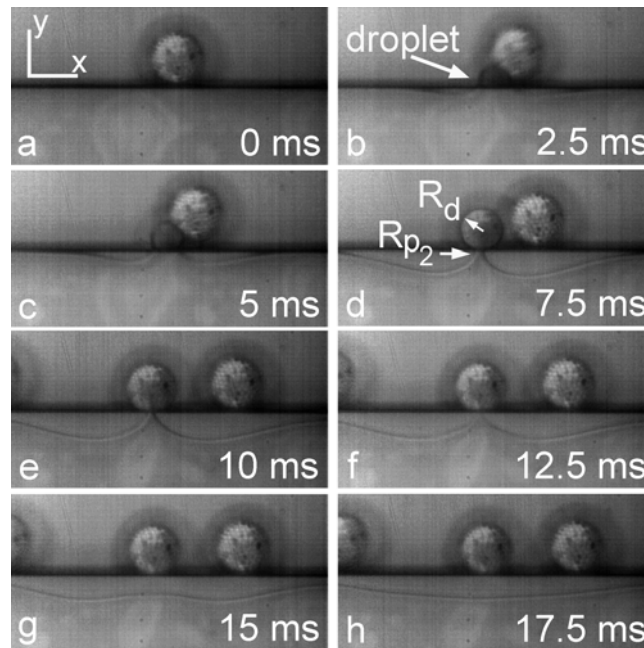


Figure 3. Droplet formation in an EDGE-2.6 device. In image a, the plateau is completely filled with oil, and in image b, the forming droplet becomes visible, in the subsequent images the droplet grows and is connected through a neck to the plateau, until in image g the neck breaks and a droplet is released.

In the close-up movies (Figure 3), we observed that the curvature in the x-y plane R_{p2} indeed becomes more and more negative in time, which underpins the explanation of the observed interfacial behavior. With the forced decrease in R_{p2} a quasi-static neck near the edge is created because the Laplace pressure in the droplet, and thus neck, does not change very rapid anymore with the growth of the droplet. As long as the amount of oil flowing into the droplet does not exceed the amount of oil flowing into the neck from the surrounding area on the plateau, the droplet will remain attached otherwise the neck will break.

This description also implies that the pressure dependency of the droplet size should not be very strong, unless blow-up of the neck occurs. This is investigated experimentally for both EDGE systems (Figure 4); D_{drop} is in this case determined with image analysis software (ImagePro Plus), and 100 droplets have been measured. To make comparison between both systems easier, the dimensionless droplet diameter D , defined as the droplet diameter D_{drop} divided by the height H_p of the DFU, is plotted versus the dimensionless applied pressure (the ratio of applied pressure and minimal pressure necessary to invade the plateau). At low pressures, D seems constant (around $6 H_p$); possibly, a very small

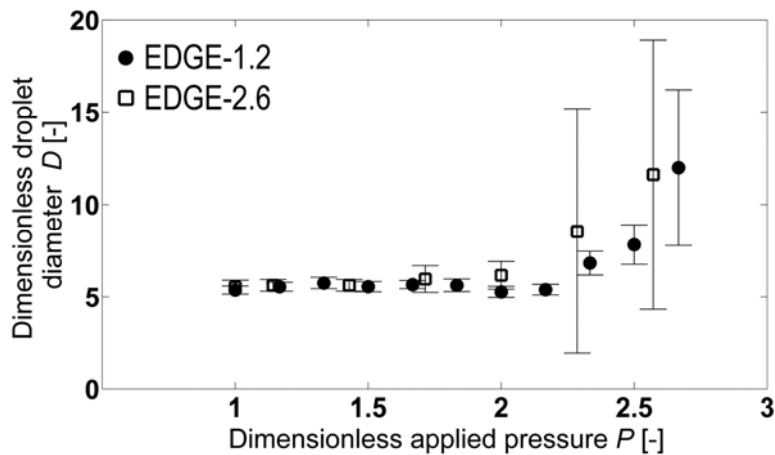
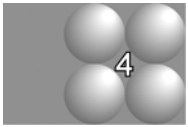
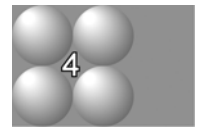


Figure 4. Dimensionless droplet diameter of emulsions produced with the EDGE-1.2 and EDGE-2.6 systems as a function of the dimensionless applied pressure.

increase could be noted, only when a certain pressure is exceeded the droplet size increases very rapidly.

The main factor that determines the droplet diameter in the pressure independent range (Figure 4) is the height of the plateau, (as mentioned, a scaling factor of 6 is found), and further investigation is necessary to elucidate this factor in detail. Compared to scaling factors reported for other microchannel systems, (2.5 – 4 times the smallest channel dimension), the values here are higher.

The droplet size generated by EDGE is not very sensitive to pressure changes and that is a big benefit compared to other micro technological emulsification devices. Further, problems that are mentioned in literature for other systems, e.g. fabrication accuracy (microchannels), flow conditions (any shear based technique), and pressure distributions (up-scaled microsieves or microchannels) are unlikely to happen.



The large plateaus are not a serious challenge for the modern etching techniques. In addition, each DFU can be considered as self-regulating; the droplet formation position along the edge is not forced to be on a specific spot but can be anywhere and at many places at the same time. Besides, we noted that operation of the plateaus was straightforward; after pressurization, the plateaus fill with oil, and even if some disturbing factor (e.g., a speck of dust) is present, which influences the flow pattern, the wide plateau system fills regularly. Overall, the system is very stable, which is essential for any practical application, and we expect EDGE to be a promising candidate for scale-up.

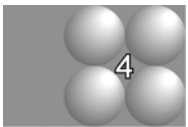
In addition to oil-in-water emulsions, the mechanism presented here is expected to be suitable for double emulsions (water in oil in water), and for the production of foam. If hydrophobic chips become available, it is also expected that W/O emulsions can be produced.

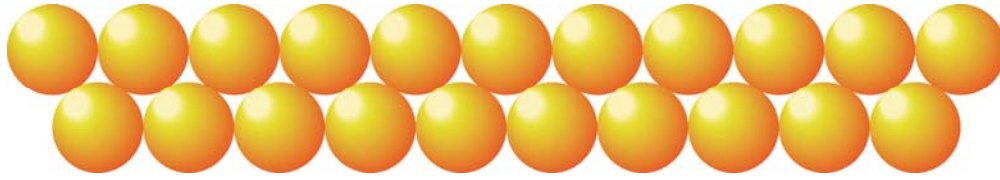
In summary, we have shown a new microfluidic droplet formation unit which simultaneously produces multiple micron-sized droplets with a narrow size distribution. Interfacial tension is the driving force for the process and the observed behavior can be described with basic physical laws. We believe that this EDGE-system is very suitable for

scale-up, which could be of great significance for further development of mild emulsification processes.

ACKNOWLEDGEMENT

We would like to thank Sophie Bartels and Abid Maan for performing the measurements.





Chapter 5

THE MECHANISM OF DROPLET FORMATION IN MICROFLUIDIC EDGE SYSTEMS

ABSTRACT

Edge based droplet generation (EDGE) emulsification, which produces multiple, monodispersed droplets simultaneously at one droplet forming unit (introduced in the previous chapter), is studied in more detail with high-speed imaging, computational fluid dynamics and geometric modeling as research tools. Complete filling of the plateau, essential for multiple droplet generation, is caused by the difference in pressure needed to invade the plateau and the pressure necessary to start droplet formation. In addition, the droplet formation unit has the highest hydrodynamic flow resistance in the system, which ensures oil supply and promotes plateau filling. The locations at which droplets are formed were found to be very evenly spaced with about 25 times the plateau height between them. CFD simulations showed that there is a scaling relation with the viscosity ratio, similar to that of microchannel systems. At high viscosity ratios, a minimal droplet diameter is found, which is typically 5.5-6.5 times the plateau height and can be estimated from geometric considerations only.

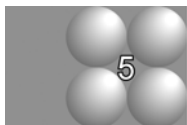
*This chapter has been accepted for publication as: van Dijke, K.C.; de Ruiter, R.; Schroën, K.; Boom, R.M. The mechanism of droplet formation in microfluidic EDGE systems *Soft Matter* DOI: 10.1039/b916141d.
Supplementary material online available at the journal's home page.*

INTRODUCTION

Conventional emulsification equipment such as high-pressure homogenizers, colloid mills, and mixers is energy inefficient (McClements, 1999) and produces emulsions with considerable polydispersity in droplet size (Sugiura *et al.*, 2002b). Novel emulsification techniques that use membranes or microfluidic devices, hold a considerable advantage over the classic techniques as they allow better control over droplet size and size distribution, through lower shear stresses, and consequently higher energy efficiency. However, these novel techniques are still in the initial stages of development, and more understanding of these processes is needed before industrial application can become a reality.

Microfluidic devices distinguish themselves from traditional membranes by their precisely designed geometry of pores and channels, which makes them suitable for the production of monodisperse droplets of small size. Microfluidic emulsification techniques reported in literature may use shear-induced droplet formation, as is the case in T- and Y-junctions (van der Graaf *et al.*, 2005, Garstecki *et al.*, 2006, De Menech *et al.*, 2008, Tan *et al.*, 2006, Steegmans *et al.* 2009), co-flow and flow-focusing devices which rely on extensional flow (Umbanhowar *et al.*, 2000; Utada *et al.*, 2007). Alternatively, the droplets may be snapped off driven by the interfacial tension, which is also called spontaneous droplet formation. This principle is exploited in microchannel emulsification (Chapter 2 and 3, Kawakatsu *et al.*, 1997; Sugiura *et al.*, 2002a; Kobayashi *et al.*, 2002a), in which no shear is needed. All mentioned methods have in common that they are single-drop technologies, in which the droplets are formed sequentially from one droplet formation unit.

Recently, we introduced a new microfluidic droplet formation system: the Edge-based Droplet GEneration (EDGE) device (see Chapter 4), in which multiple droplets are produced simultaneously from one droplet formation unit (see also Figure 1). Droplet formation occurs through a spontaneous mechanism, since no cross-flow is required for droplet formation. Scaling-up of these systems is less complex compared to single-drop



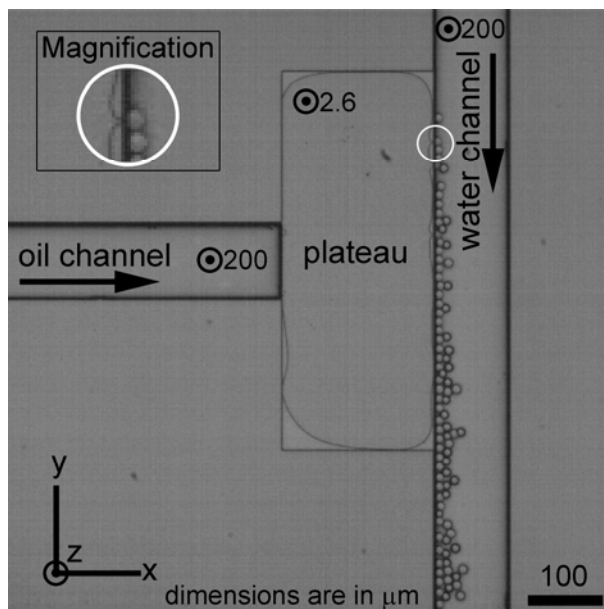
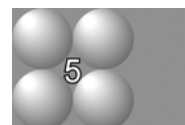


Figure 1. Top-view of Edge-based Droplet Generation. Multiple droplets are formed simultaneously along the edge of a shallow and wide plateau. In the upper left corner, a magnification of the characteristic curvatures during droplet formation is shown (see also Chapter 4).



and shear-based systems; Chapter 6 shows the suitability for scale-up of EDGE droplet formation units as they are relatively insensitive to flow conditions, including pressure distributions, and fabrication inaccuracy or fouling.

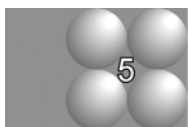
EDGE devices have been tested with food grade components; in the production of single and double emulsions and foams. The systems were found to operate in a remarkably stable way (Chapter 7). All these aspects make EDGE an interesting technique for larger-scale application; that is, if the underlying mechanism can be better understood, and from this, design rules derived.

As mentioned, droplet formation in EDGE systems is expected to be analogous to other spontaneous droplet generation processes. However, there are also distinct differences with e.g. microchannel emulsification. Typical behavior in EDGE is that droplet formation takes place seemingly at random along the edge of a completely filled plateau.

Comparable terrace or plateau structures are described in literature, but none of them shows the droplet formation found in EDGE devices (Kawakatsu *et al.*, 1997; Sugiura *et al.*, 2002c); here droplet formation takes place only at a fixed position, in the front centre of the microchannels. For EDGE, the droplet size scales with the height of the droplet formation unit as is the case for microchannel devices, but the proportionality factor in EDGE is considerably larger compared to other systems from literature. In this work, we study the EDGE process in more detail with experiments, computational fluid dynamics and through geometric analysis to elucidate various aspects of the droplet formation mechanism, with the ultimate aim to arrive at scaling relations.

MATERIALS AND METHODS

MATERIALS



Chemicals. In the experiments, n-hexadecane for synthesis from Merck KGaA (Darmstadt, Germany), and air were used as the dispersed phase. As the continuous phase, MilliQ ultrapure water with 1% (w/w) sodium dodecyl sulfate (SDS) from Sigma-Aldrich (Saint Louis, MO) was used. Some properties can be found in Table 1, such as density ρ , interfacial tension with water σ_{water} , and equilibrium interfacial tension with SDS solution $\sigma_{eq,SDS}$.

EDGE – chips. The microfluidics chips used in the experiments were produced by Micronit Microfluidics BV (Enschede, The Netherlands), and the codes that are used throughout the manuscript denote the height of their droplet formation unit, the plateau. The microfluidic chip was a silicon plate (1.5 x 1.5 cm), into which the microchannels and

Table 1. Some properties of the various phases used.

Dispersed phase	ρ [kg m ⁻³]	η [mPa s]	σ_{water} [mN m ⁻¹]	$\sigma_{eq,SDS}$ [mN m ⁻¹]
air	1.2	0.018	72 ^a	39 ^a
hexadecane	773	3.34	44 ^c	9.1 ^b

^a Nakahara *et al.*, 2008, ^b Chapter 3, ^c van der Graaf *et al.*, 2005.

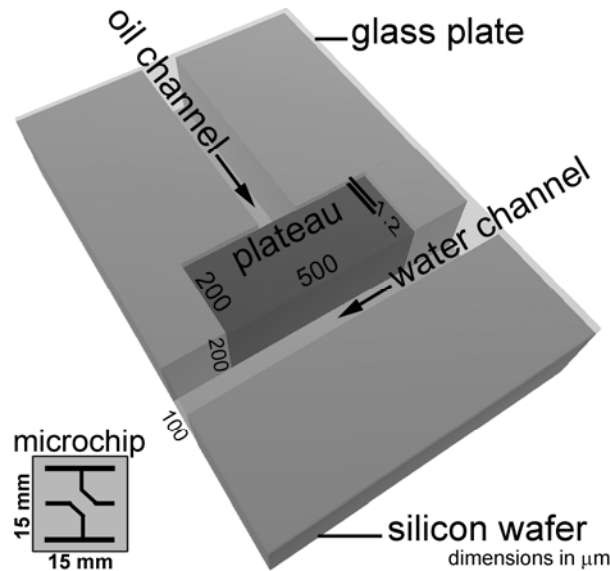
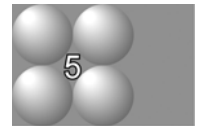


Figure 2. Schematic three-dimensional representation of a typical EDGE-system with a height of 1.2 micron; in the lower left corner the microchip lay-out is shown.

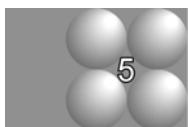
plateau were etched with deep reactive ion etching to ensure straight corners (round-off $< 1 \mu\text{m}$). A glass plate was bonded on top of the silicon plate to close the channels, thereby creating hydrophilic microstructures that are suitable for the production of oil-in-water emulsions. Figure 2 shows a schematic three-dimensional representation of a typical system with an oil supply channel, water channel and droplet formation unit (plateau) and in the lower left corner the microchip lay-out is shown.



The microchips used in the experiments generally contained two independent systems with a single droplet formation unit each; only one system was used at the same time. The emulsification system consisted of a dispersed phase supply channel of $200 \mu\text{m}$ high and varying widths (20, 100, 200 and $500 \mu\text{m}$), and a continuous phase transport channel of $200 \mu\text{m}$ high and $100 \mu\text{m}$ wide. These two channels were connected via a narrow plateau that can be characterized by its length (L_p), width (W_p), and height (H_p). The plateaus used in the experiments were generally $200 \mu\text{m}$ long, had a varying width ($500\text{-}4000 \mu\text{m}$), and were either 1.2 or $2.6 \mu\text{m}$ deep (these last two numbers are used for coding).

Peripherals. The droplet formation process was observed with a high-speed camera (MotionPro HS-4, Redlake MASD Inc., San Diego, CA) system, connected to a microscope (Axiovert 200 MAT, Carl Zeiss B.V., Sliedrecht, The Netherlands). The camera was controlled with MotionPro Studio software (Redlake MASD Inc.). The maximum magnification was 2500x (microscope: 10x, objective: 100x, and Optovar: 2.5x) and the maximum frame rate was 10,000 frames s⁻¹. The combination of magnification and frame rate is limited by the amount of light that reaches the high-speed camera. During all experiments, the shutter speed was chosen such that the best compromise between contrast and resolution of the images was obtained.

The continuous phase was guided into the continuous phase channel of the microstructure through 0.030" PEEK tubing (Grace Davison Discovery Sciences, Deerfield, IL) connected to a 10 mL Hamilton gastight Luer Lock syringe (Bonaduz, Switzerland). The continuous phase was flow rate controlled by placing the syringe in a Harvard Apparatus (Holliston, MA) PHD 2000 syringe pump; the continuous phase channel is thus wide that no pressure build-up occurs. The dispersed phase was guided into the dispersed phase channel of the microstructure through PEEK tubing connected to a pressurized vessel (hexadecane) or gas cylinder (air). The connections were NanoTight fittings in combination with quick connect female luer to female adapters, and Super Flangeless Ferules, all from Upchurch Scientific (Oak Harbor, WA). A digital pressure controller (Bronkhorst, Veenendaal, The Netherlands) was used to set and regulate the applied pressure of the dispersed phase, and was controlled with FlowPlot V3.25 and FlowView 2 V1.15 software (Bronkhorst). Two separate pressure controllers for hexadecane and air were used. The microchip was placed in a module designed by Micronit Microfluidics BV, and placed on the microscope table. The microchip was illuminated (KL 2500 LCD, Zeiss) via the objectives of the microscope, and the emulsification was observed with the microscope video system. After the experiments, the microchips were cleaned with ethanol and sonicated in ethanol for 90 minutes. After overnight drying in an oven at 550 °C, the chips were stored in MilliQ ultrapure water until further use.



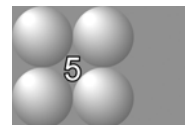
METHODS

Various aspects of droplet formation are investigated in this paper with high speed imaging, and Computational Fluid Dynamics simulation software to investigate the local pressures in the EDGE systems during droplet formation, and to investigate other system parameters systematically. A geometric analysis is used to elucidate the minimal droplet diameter in relation to plateau height and contact angle.

High speed imaging and image analysis. With the previously described microchips and equipment, high speed images were obtained during EDGE emulsification. The droplet formation process at the edge of the plateau was characterized by image analysis with a series of MATLAB routines. First, the analyzed movie was viewed frame by frame to select 100 consecutive droplets. For every droplet, two frame numbers were stored; the frame in which the neck was visible for the first time and the frame just before the droplet detached. The latter frame was used to identify the position of droplet detachment, which was stored together with its corresponding time.

CFD simulations. We modeled the EDGE system using a three-dimensional Volume-of-Fluid method incorporated in CD-Adapco's Star-CD (version 4.0). Details of this method and validation for spontaneous droplet formation in microchannels are described in Chapter 2. The grid was adapted to the system used in this study; a large shallow plateau (width $W_p = 96 \mu\text{m}$, height $H_p = 1 \mu\text{m}$ and length $L_p = 100 \mu\text{m}$) and a well. The total number of cells was 195,000. At both sides of the plateau and well, a periodic boundary was applied. A straight interface near the edge of the plateau was used as the starting configuration in this case, without problems with abrupt initial changes near wall boundaries, due to contact angle effects. This approach is efficient in computation time as the timescales of flow over the plateau and droplet formation are very different.

At $t = 0$, the oil-water interface is flat at position $x = 98 \mu\text{m}$. We used a static inlet pressure boundary on the DFU entrance, and a reference outlet pressure-boundary of 0 Pa in the well. The inlet pressure was chosen to be just above breakthrough pressure which was calculated with Laplace's law:



$$\Delta P_{\min} = \sigma \left(\frac{1}{R_1} + \frac{1}{R_2} \right) \cos \theta \quad (1)$$

where one of the curvatures (R_1) corresponds to the plateau height (H_p), and the other one (R_2) to the width of the plateau (W_p), which implies that this curvature is very large, compared to R_1 and can be neglected in the calculation of the minimum pressure. The contact angle (θ) was set at 10° to represent a hydrophilic surface. It was assumed that there was no cross-flow of the continuous phase. Surfactant dynamics (i.e., time or location dependent interfacial tension) were not taken into account in this method.

Geometric modeling. We start our geometric analysis with observations made through high speed recording. During droplet formation a quasi-static neck exists close to the edge of the plateau (see Figure 1 and Chapter 4). The geometric model presented here is based on the assumption that the curvature of the interface at the plateau is the result of the pressure drop generated by the growing droplet. In Figure 3a-d, the defined parameters are indicated in cross sections in several planes. The dispersed phase, surrounded by the continuous phase, has a contact angle θ with the silicon oxide walls, defined for the dispersed phase and indicated in Figure 3a. As a result of this definition, $-1 \leq \cos(\theta) \leq 0$. In Figure 3a, the solid curved line represents the droplet interface. Deviations from a spherical shape are neglected, so the Laplace pressure in the droplet is described by only one radius of curvature, the droplet radius R_d . In Figure 3b, the position of the interface at half the height of the plateau (a circle with radius R_{dp}) is indicated by the dotted line, the maximum size of the droplet (much deeper in the channel) is indicated with a solid line. The cross-sections of the neck in the y-z plane are shown in Figures 3c and 3d.

The first radius of curvature of the interface at the edge of the plateau, R_{p1} , is determined by the height of the plateau and the contact angle (see Figure 3c), and is positive and constant in time:

$$R_{p1} = \frac{-H_p}{2 \cos(\theta)} \quad (2)$$

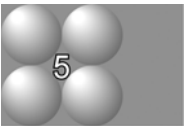
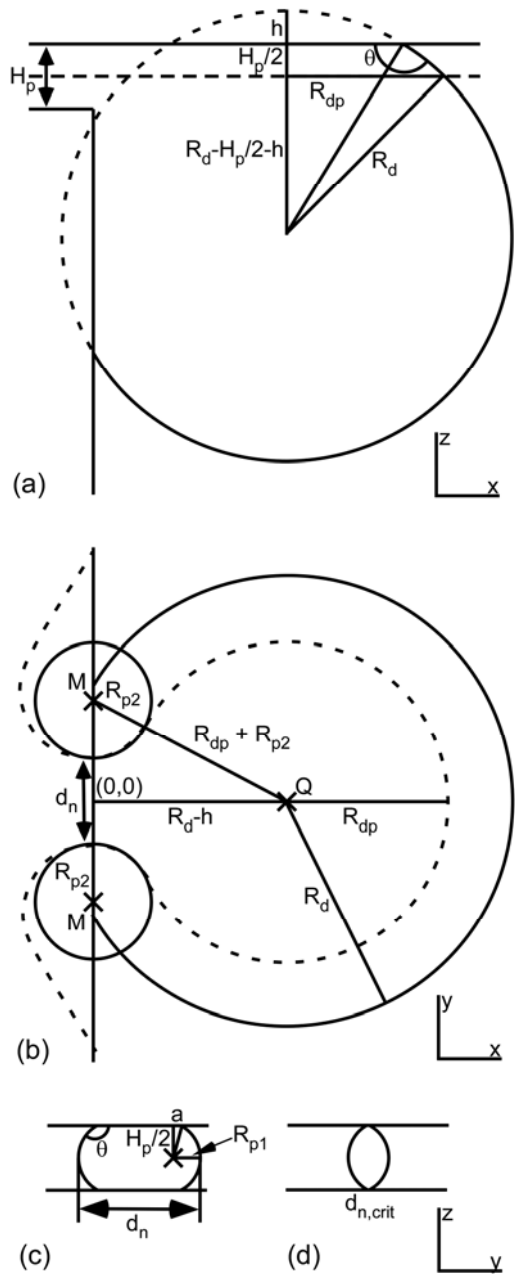


Figure 3. Geometric analysis of the droplet formation process in an EDGE-system. Cross-sections in several planes are depicted and parameters needed for the analysis are defined; the actual analysis is described in the main text.

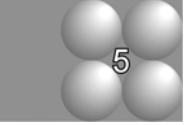
The second radius of curvature of the interface at the edge of the plateau, R_{p2} , is defined in Figure 3b. As shown in the following analysis, this second radius of curvature changes in time and becomes (more) negative upon droplet growth.

The Laplace pressures in the droplet and at the edge of the plateau are assumed equal during the droplet formation process, so:

$$\frac{2\sigma}{R_d} = \frac{\sigma}{R_{p1}} + \frac{\sigma}{R_{p2}} \quad (3)$$

As R_d increases during droplet growth and R_{p1} remains constant, R_{p2} changes in time to satisfy Equation 3, and:

$$R_{p2} = \frac{R_{p1}R_d}{2R_{p1} - R_d} \quad (4)$$



Equation 2 and 4 are combined to obtain an expression for R_{p2} that only depends on H_p , θ , and R_d

$$R_{p2} = \frac{H_p R_d}{2(H_p + R_d \cos(\theta))} \quad (5)$$

Please note that this relationship is assumed to be valid at the edge of the plateau only.

We assume that the neck can be defined by two circles with radius R_{p2} in the x,y-plane at half the EDGE plateau height, where the droplet has a radius of R_{dp} (see Figure 3b). The center of the circles is chosen at the edge of the plateau, thereby satisfying the assumption that the thinnest part of the neck – where ultimately detachment occurs – is at the plateau edge as soon as R_{p2} becomes negative. Further, we only consider the droplet formation process from the moment the droplet size satisfies Equation 6, as the growing droplet is assumed to be non-spherical at smaller radius (see also Equation 17):

$$R_d > \frac{-H_p}{\cos(\theta) + \cos(\theta + \frac{1}{2}\pi)} \quad (6)$$

As shown in Figure 3a, the radius of the cross-section of the droplet at half the plateau height R_{dp} is given by:

$$R_{dp} = \sqrt{R_d^2 - ((R_d - h) - \frac{H_p}{2})^2} \quad (7)$$

$(R_d - h)$ is the principal radius of curvature of the droplet minus the height of the spherical cap:

$$R_d - h = -R_d \cos(\theta) \quad (8)$$

Combining Equation 7 and 8 yields an expression for R_{dp} that only depends on H_p , θ , and R_d .

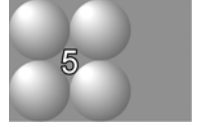
$$R_{dp} = \sqrt{R_d^2 - (R_d \cos(\theta) + \frac{H_p}{2})^2} \quad (9)$$

The coordinates of the centers of the two circles defining the neck ($M_{x,p2}$, $M_{y,p2}$), as well as the coordinates of the circle of the cross-section in the growing droplet ($Q_{x,dp}$, $Q_{y,dp}$; see Figure 3b), both at half the plateau height can be described as:

$$M_{x,p2} = 0 \quad (10)$$

$$M_{y,p2} = \pm \sqrt{(R_{p2} - R_{dp})^2 - (R_d \cos(\theta))^2} \quad (11)$$

and



$$Q_{x,dp} = -R_d \cos(\theta) \quad (12)$$

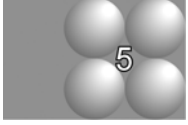
$$Q_{y,dp} = 0 \quad (13)$$

The neck diameter is equal to the distance between the two circles along the edge that define the neck:

$$d_n = 2(R_{p2} - M_{y,p2}) \quad R_{p2} > 0 \quad (14)$$

$$d_n = 2(M_{y,p2} - |R_{p2}|) \quad R_{p2} < 0 \quad (15)$$

In Equation 15, for $R_{p2} < 0$, we had to take the sign of R_{p2} into account, as the value is negative. The neck contracts during droplet growth, until the critical neck diameter, $d_{n,crit}$, is reached, see Figure 3d. Further contraction of the neck results in a continuing and fast increase of the local Laplace pressure – as R_{pl} start to decrease –, leading to rapid collapse of the neck. This detachment criterion is adapted from Van der Zwan *et al.* (2009b) to include the contact angle θ . The theoretical critical neck diameter varies from zero at $\theta = \pi/2$ to H_p at $\theta = \pi$:



$$d_{n,crit} = 2(R_{p1} - a) = 2\left(\frac{-H_p}{2\cos(\theta)} - \frac{-H_p \tan(\theta)}{2}\right) = H_p \left(\tan(\theta) - \frac{1}{\cos(\theta)}\right) \quad (16)$$

The neck diameter with increasing droplet diameter is calculated by a MATLAB routine. As soon as Equation 16 is fulfilled, i.e. the critical neck diameter is reached, the corresponding droplet diameter R_d is defined to be the diameter of the minimal generated droplet of an EDGE system with height H_p and contact angle θ .

RESULTS AND DISCUSSION

Invasion of the DFU. In Figure 4, the typical behavior during oil invasion of an EDGE droplet formation unit is visible in 3 stages. Due to the length of the plateau, only approximately half of the plateau is visible. The oil supply channel is in the lower left corner of the microscopy photos, and the oil is pushed from left to right, into the well, the dark area on the right side. In photo (a), the oil just invades the plateau; in photo (b), the interface reaches the edge of the plateau in the middle of the DFU, where some droplets are formed as can be derived from the shape of the interface. Next, the plateau fills up further, and droplets form along the length of the plateau as shown in photo (c). In general, EDGE devices fill completely with dispersed phase (see Chapter 6 & 7), only designs with very narrow oil supply channel (20 μm) show incomplete filling.

This remarkable behavior can be explained by the difference in pressure needed to invade and subsequently flow over the plateau, ΔP_{in} , and the minimal required droplet formation pressure at the edge, ΔP_{edge} , if we adopt the following reasoning. The dispersed phase forms a cylinder segment at the edge of the plateau. Interfacial instability and thus droplet formation can only occur after the minimum radius of curvature of the cylinder segment,

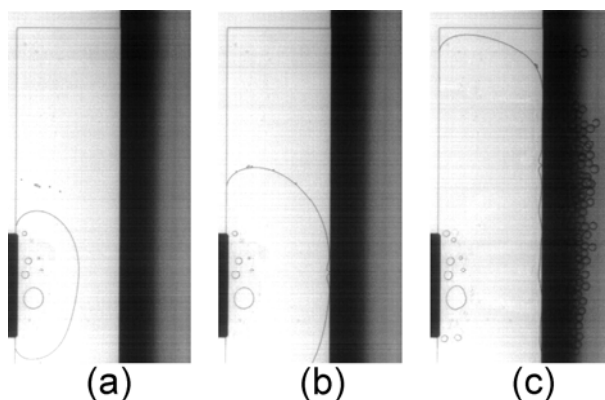
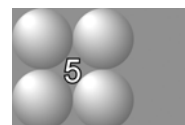


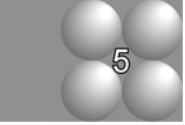
Figure 4. Invasion of a droplet formation unit with hexadecane. As soon as the oil reaches the edge of the plateau, droplet formation starts (b), but the plateau also fills up further (c) and more droplet formation positions appear. One can note that some continuous phase remains on the plateau, visible as small circles. These do not disturb the operation of the EDGE unit at all.

and therewith the highest pressure ΔP_{edge} , is reached. The radius of curvature in a grooved system, i.e. with a glass cover plate and a well, can be defined by:

$$R = -\frac{H_p}{\cos \theta + \cos \varphi} \quad (17)$$

if θ is the contact angle with the disperse phase with the glass plate and φ is the contact angle of the dispersed phase with the substrate relative to the plateau, and H_p the height of the plateau. The contact angle of the dispersed phase on the plateau with the glass plate is assumed constant during droplet formation. For the corner φ between the substrate and oil interface holds $\varphi = \theta$ at the plateau and $\varphi = \pi$ at the edge of the plateau, when the critical pressure is reached. According to Laplace's law, the pressure is:

$$\Delta P = -\frac{\sigma(\cos \varphi + \cos \theta)}{H_p} \quad (18)$$



with σ the interfacial tension. Only the small curvature caused by the plateau height is essential here, as the one determined by the width is very large. In Figure 5, dimensionless

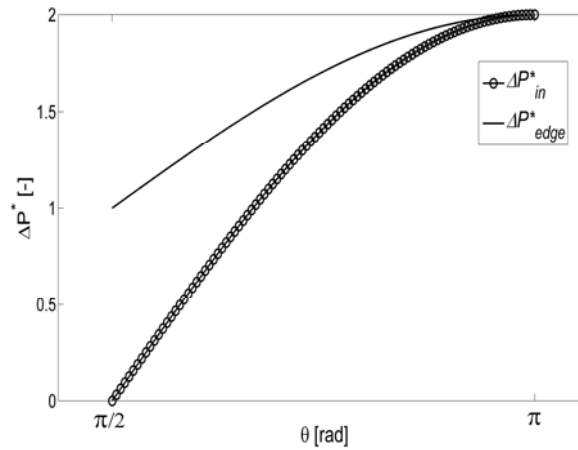
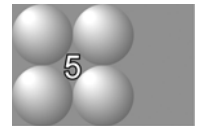


Figure 5. Dimensionless invasion (ΔP_{in}^*) and edge (ΔP_{edge}^*) pressures as function of the contact angle.

ΔP_{in}^* (with $\varphi = \theta$) and ΔP_{edge}^* (with $\varphi = \pi$) values are plotted as function of the contact angle (ΔP made dimensionless by multiplication with H_p/σ). The differences between the two pressures are large at small contact angle θ , which implies that the pressure needed to start droplet generation is significantly higher than the pressure needed for the to-be-dispersed phase to fill the plateau if surface properties are in that range, resulting in complete filling. The difference in pressure becomes smaller as the contact angle θ gets larger, and it reaches zero at $\theta = \pi$. This implies that with a system with $\theta = \pi$, or complete wetting by the continuous phase, the dispersed phase will not spread over the plateau if the oil supply is more narrow compared to the plateau, and efficient use of the available EDGE length is unlikely to happen.

In several other studies known from literature, a wide terrace was used, but no complete filling was observed (Kawakatsu *et al.*, 1997; Sugiura *et al.*, 2002c, chapter 3). This is expected to be caused by the difference in design of the microdevices. In EDGE, we do not use a narrow supply channel, and the invasion pressure is determined by the plateau only. In e.g. microchannels, the narrow supply channel requires a high pressure to push the oil onto the terrace, and if this pressure exceeds ΔP_{edge} , the to-be-dispersed phase will not fill the terraces completely. Furthermore, the highest flow resistance in these systems is in the microchannels, while in EDGE systems, it is the plateau that has the highest hydrodynamic resistance in the whole system. Therefore, in the EDGE system, the dispersed phase will spread over the plateau, and droplet generation will occur along the length of the system.



Location of droplet formation. The typical locations at which droplet detachment took place are shown in Figure 6, with -1 being the lower end, and 1 being the upper end of the plateau. The time at which the first droplet detached was defined as $t = 0$ s. Figure 6 shows an example of a result for constant applied pressure. Each marker indicates the detachment position and detachment time of one analyzed droplet. The acquired droplet detachment positions, and the times at which the droplets started to form and finally detached, were subsequently used to calculate the mean distance, δ_{drop} , between two neighboring locations for droplet detachment and droplet formation frequencies. As

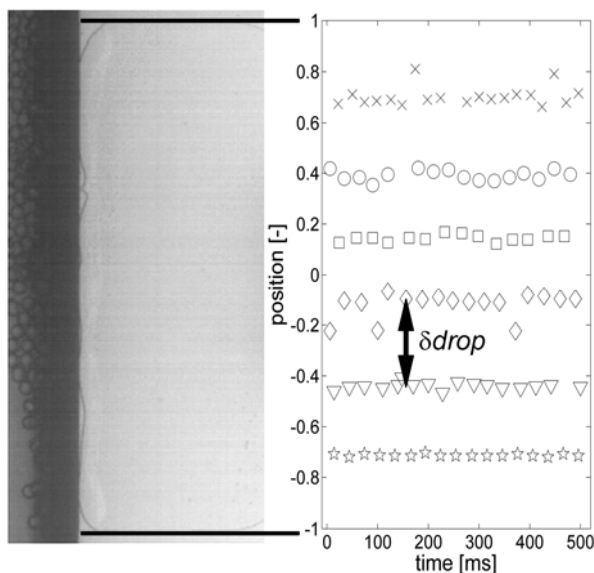
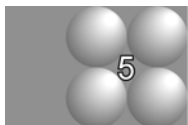


Figure 6. Droplet formation positions in a completely filled EDGE-2.6 plateau producing equally sized droplets. The locations are spaced regularly with sometimes a clear deviation from the formation position.



observed in Figure 6, the droplets detached rather evenly spaced although positions shifted temporarily, which is an indication that the locations of droplet formation are not determined by local defects in the system geometry.

In Figure 7, the average droplet formation locations are shown as a function of applied pressure. Droplet formation starts as soon as the front of the interface reaches the edge of the droplet formation unit, which is at relatively low pressure. By increasing the pressure, the oil spreads further over the plateau, and the EDGE length available for droplet formation becomes longer resulting in more droplet formation locations (see $\Delta P_{applied} = 143$ mbar). Increasing the pressure after the plateau has been completely filled results first in an increased droplet formation frequency ($\Delta P_{applied} = 154$ mbar). An extra droplet formation location occurs if pressure is increased further, and all the other locations adapt to this, resulting in a decrease in droplet formation distance ($\delta drop$) and a shift in positions, however, the droplets are no longer monodisperse at $\Delta P_{applied} = 220$ mbar. The distance between formation positions for an EDGE-2.6 system in the monodisperse

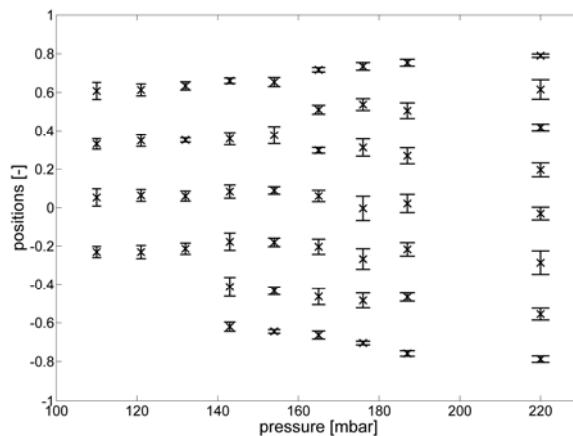
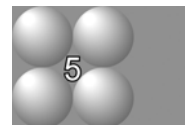


Figure 7. Droplet formation positions as a function of the applied pressure. At low pressures, the available EDGE-length is not completely used, i.e. the plateau is not totally filled. With an increase in pressure, the DFU fills up and more formation spots appear. When the plateau is completely filled, an increase in pressure results in more droplet formation positions but also in polydisperse droplet formation.

droplet formation regime is between 65 μm and 70 μm for oil droplets ($D_{drop} = 14\text{-}15 \mu\text{m}$), and this value is the same for air bubbles ($D_{bubble} = 40\text{-}50 \mu\text{m}$). In an EDGE-1.2 system, δ_{drop} could only be determined for oil droplets and was around 29 μm . Remarkably, the droplet or bubble formation distance scales with the height of the plateau ($\approx 25x$), and is independent of the droplet or bubble size.



CFD simulations. The simulations show similar behavior as observed in the experiments, as illustrated in Figure 8, where the focus is on the edge of the DFU. The interface moves to the edge of the plateau in Figure 8a, and droplet generation starts at the edge as soon as the cylindrical shaped interface flows into the well, Figure 8b. The droplets grow further, and at neighboring locations, a similar procedure starts. After droplet formation, the interface retracts on the plateau and moves relatively slowly to the edge again. In Figure 8d, three equally sized droplets are visible, while one is still forming. The distances between droplet formation positions for this virtual EDGE-1.0 system are 22-24 μm ; and this is in the range that was expected from linear extrapolation of experimental δ_{drop} in EDGE-1.2 system values, i.e., around 24 μm .

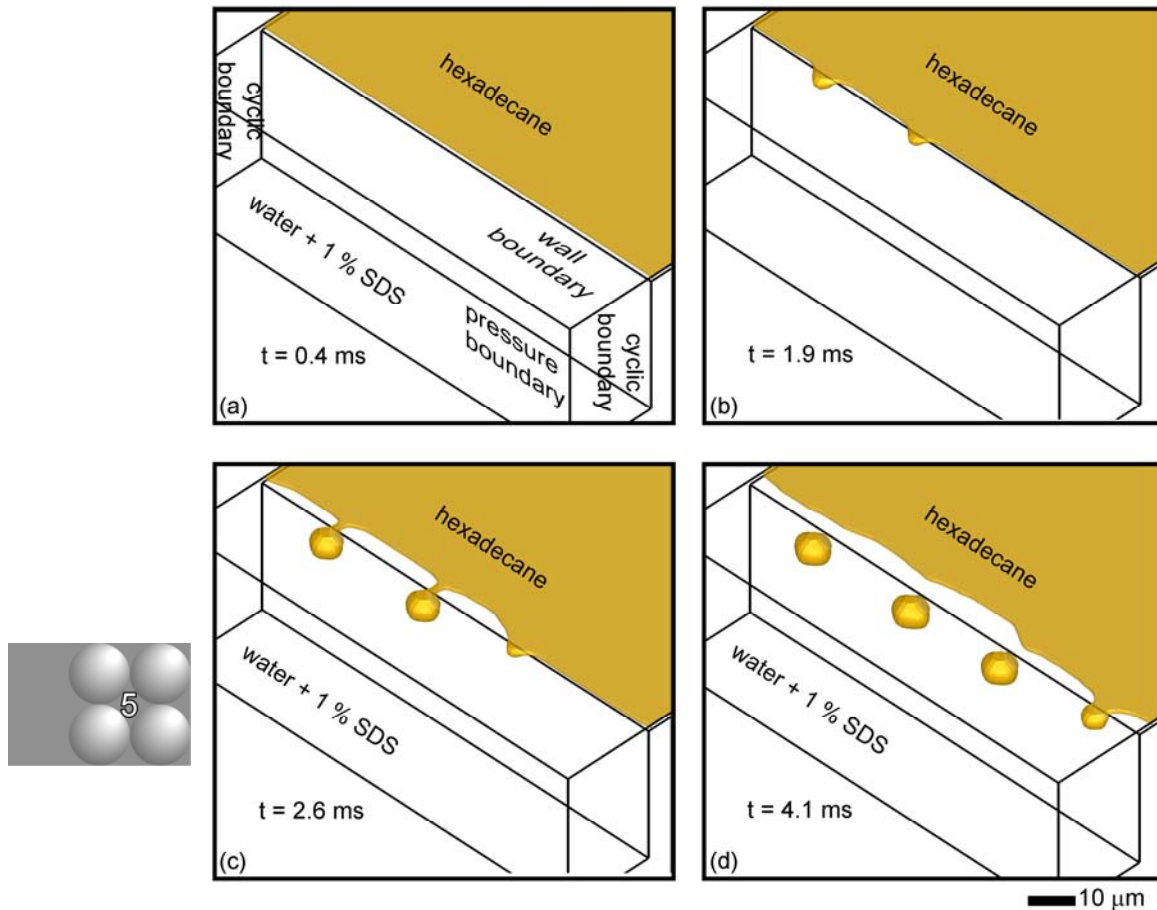


Figure 8. Four stages of droplet formation in an EDGE system, extracted from a typical simulation result. Generated droplets stay in front of the plateau as no cross-flowing continuous phase is present.

Pressure field during droplet generation. The pressure fields on part of the plateau were extracted from the CFD data and are shown in Figure 9. Far away from the edge, a gradual and parallel pressure drop is present. In the proximity of the forming droplets, relatively steep pressure gradients in radial direction are observed. This typical pressure distribution can explain the robustness of the system to some extent; pressure fluctuations only act locally, near the edge, but do not disturb the flow over the plateau. Vice versa, a change in the overall (modest) pressure distribution over the terrace (e.g. by a speck of

dust) will not influence the much steeper local pressure gradients near a forming droplet. Given the pressure profile, it is unlikely that droplet formation is linked along the whole width of the DFU. Although it can not be excluded that droplet formation is delayed until a neighboring droplet is formed, we did observe simultaneous droplet formation at two neighboring locations, and this would point to autonomous behavior (i.e. droplet formation independent of any neighboring location).

Viscosity ratio. In Chapter 3, in a study on spontaneous droplet formation in microchannels, we found both experimentally and computationally, that the ratio of the viscosities of the dispersed and continuous phases has a pronounced effect on the droplet size. It was found that there is a range of viscosity ratios (disperse / continuous) in which the droplet size is not affected, while at low viscosity ratios the droplet size increases.

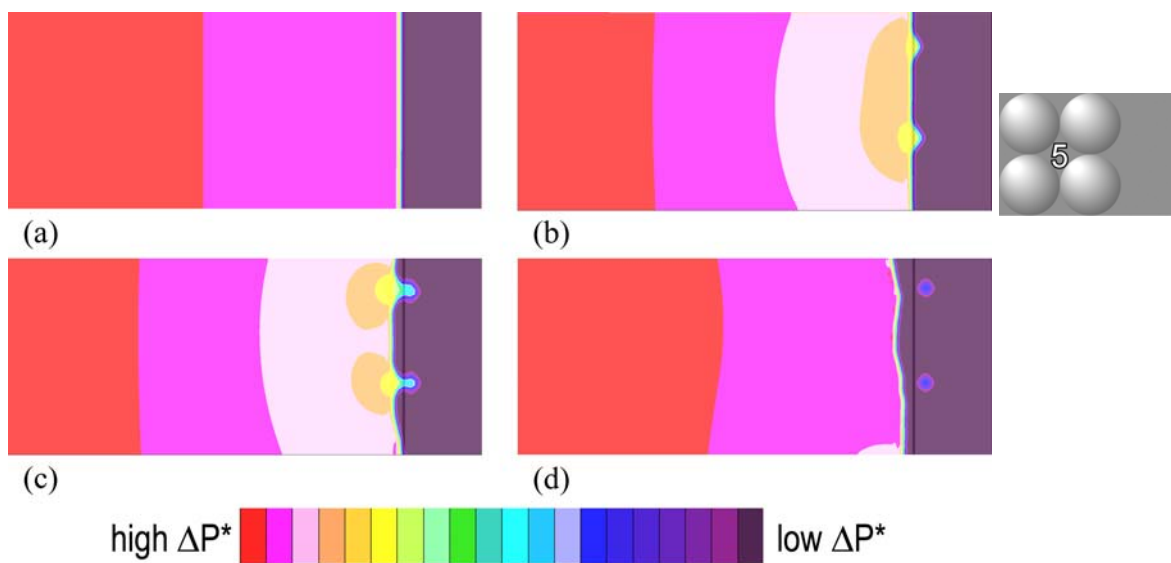


Figure 9. Pressure gradients during droplet formation in an EDGE system. In (a), the plateau is filled with liquid and the pressure gradient is flat, across the entire plateau, except for the front of the liquid (Laplace pressure). Once the liquid reaches the end of the plateau (b), the liquid starts forming droplets at some locations. At these positions, the pressure gradients become steeper, and become more pronounced when the droplets become bigger (c). When the droplets detach, the interface retreats on the plateau, after which the oil supply pushes the interface towards the EDGE again.

This was linked to the ease with which the continuous phase can invade the terrace structure in the microchannel. Although invasion of such a terrace needs to take place over a considerably longer distance than in EDGE, we still expect that also for EDGE systems, these effects play a role, and this expectation is fed by the notion that in Chapter 7, we found that droplets and bubbles formed by EDGE technology (having very different viscosity ratios) have different sizes. Droplets formed at a high viscosity ratio are considerably smaller than bubbles. CFD simulation was used to evaluate whether similar effects occur in EDGE as in microchannels.

Simulations gave the same droplet size irrespective of whether an interfacial tension of 9 mNm^{-1} (corresponding to 1% SDS) or 50 mNm^{-1} (bare surface) was used as was found previously for microchannels (Chapter 3). Also for air bubbles, the bubble size was not affected by the interfacial tension, although bubbles (and droplets) are formed considerably faster at higher interfacial tension, as was also the case in grooved

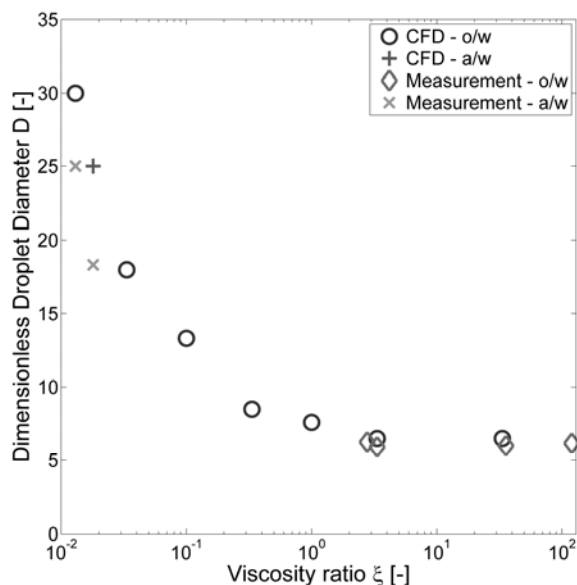
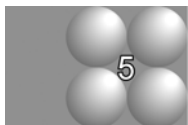
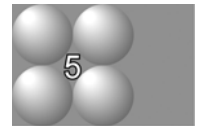


Figure 10. Calculated and measured (Chapter 7) dimensionless droplet or bubble diameter as function of the viscosity ratio for EDGE. For the CFD calculations, an interfacial tension of 50 mNm^{-1} was used for both oil-in-water (o/w) and air-in-water (a/w) systems.

microchannel systems. The size of the bubbles was considerably bigger than of the droplets, and this may well be caused by the difference in viscosity ratio, which is discussed further in the next section. In Figure 10, the droplet and bubble diameter calculated by CFD simulation is shown for various viscosity ratios, together with experimental data.

The calculated droplet sizes are found in good agreement with the measurements. As could be expected, for bubble size, some difference is noted, but this is reasonable given the experimental challenges that did not allow close-up observation of the bubble size. A similar effect of the viscosity ratio on droplet size is found as for grooved microchannels; at high ratios, the droplet size is constant, and we can define this size as the minimal droplet diameter for EDGE. Its value scales with the height of the plateau: we systematically found a factor 5.5-6.5 between droplet size and plateau height. At lower ratios, the droplet or bubble size increases, and this is in accordance with the larger bubbles found at $\zeta = 0.018$ (air-water viscosity ratio).

Interesting is further that there is no indication of a critical minimum viscosity ratio for EDGE, as was found in chapter 3 with oil-in-water systems in grooved microchannels. At smaller viscosity ratios, these systems have no monodisperse droplet regime, but immediately show blow-up with increasing pressure, directly after becoming active. This behavior is not observed for EDGE.



In the next section, we focus on the minimal droplet diameter, through geometric analysis, which also allows us to investigate contact angle effects.

Minimal droplet volume model at high viscosity ratio. Through the geometric analysis described in the materials and methods section, we investigated the droplet formation process. The diameter of the droplet is determined as function of the contact angle for $H_p = 2.6 \mu\text{m}$, and $H_p = 1.2 \mu\text{m}$ (see Figure 11a), and it was found that the droplet size decreases with increasing contact angle.

The horizontal lines in Figure 11a indicate the experimentally determined droplet sizes (it was not possible to reliably obtain direct experimental values for the contact angle).

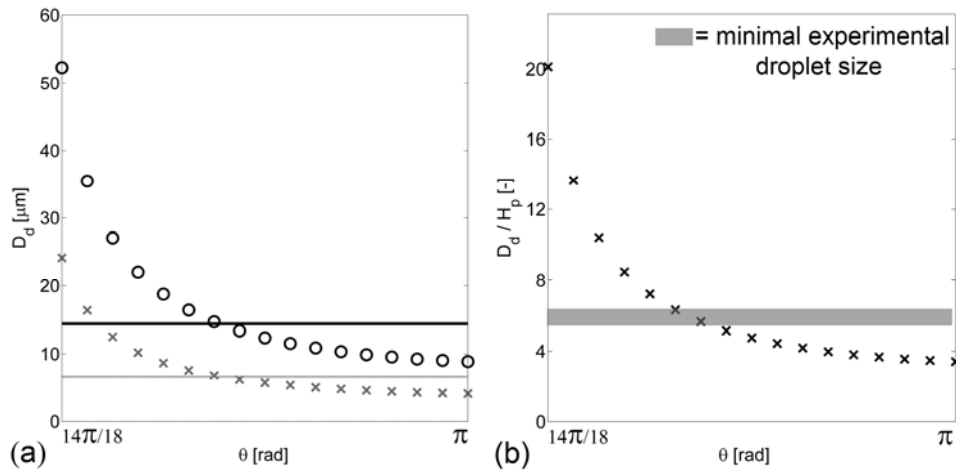
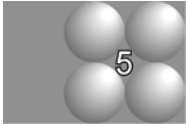


Figure 11 (a) The predicted diameter of the obtained droplet as function of the contact angle for (circle) $H_p = 2.6 \mu\text{m}$, (cross) $H_p = 1.2 \mu\text{m}$. The straight lines represent the experimentally obtained values for the hexadecane droplets (14.6 μm and 7.1 μm , for EDGE-2.6, EDGE-1.2 microstructures, respectively). (b) The data collapse if the diameter of the obtained droplet is divided by the height of the plateau. The gray area defines the minimal droplet sizes found for all EDGE systems.



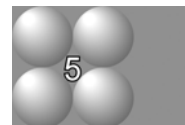
Assuming that this diameter is equal to the principal diameter of curvature just before detachment, the contact angle during droplet formation can be estimated from Figure 11. For both microstructures, EDGE-1.2 and EDGE-2.6 microstructures, a contact angle of about 155° is obtained for hexadecane droplets, which is in line with earlier experimental results with the same materials (van der Graaf *et al.*, 2006). The relationship between R_d and θ also implies that the radius of the droplets will be lower in very hydrophilic microdevices, which may be within reach through surface modification. However, we earlier concluded that with very hydrophilic systems, the complete filling of the plateaus is more critical (see Figure 5), especially if the oil supply to the plateau is narrow, therefore a good balance between both effects needs to be established.

In Figure 11b, the droplet diameter was made dimensionless by dividing the droplet size by the plateau height. As the data for the different EDGE microstructures then collapse into a single master curve, the diameter of the generated droplets is linearly dependent on

the plateau height. This dependency was also observed during the experiments, and provides a relatively easy way to control the size of the generated droplets. Because process dynamics such as slow invasion of the plateau by the continuous phase at low viscosity ratio, are not covered, the geometric analysis is only valid at high viscosity ratio when EDGE is operated in the monodisperse droplet formation regime. In that case, the outcome of the geometric analysis indicates the best case scenario; *i.e.* the smallest possible droplet.

Typically, the ratios between plateau height and droplet size are 5.5 – 6.5 for EDGE, where for terrace-based or straight-through microchannel emulsification, these values are 2.5-4 (Sugiura *et al.*, 2002a, Kobayashi *et al.*, 2004). As described in Chapter 2, the droplet size in terrace-based microchannels in the monodisperse droplet generation regime is determined by the volume that is present on the terrace structure. In EDGE-systems, only a minimal amount of dispersed phase flows into the well during droplet formation, therewith making the system intrinsically more stable, and tunable.

CONCLUSION



In this paper we studied the fluid dynamics in an EDGE system in detail. The results of this research are summarized here:

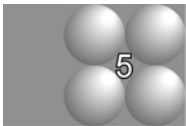
- The even filling of the wide and shallow plateaus, allowing multiple droplet formation, can be explained through the difference in invasion and minimal droplet formation pressure at the edge. The highest hydrodynamic resistance of the system is located in the droplet formation unit which ensures a steady oil supply to the plateau, which was confirmed by CFD.
- Both experiments and CFD simulations show that the droplet formation locations are quite regular and organized. The distance between droplet formation spots is determined by the height of the plateau and the applied pressure, but is independent of the droplet or bubble size in the monodisperse droplet generation regime.

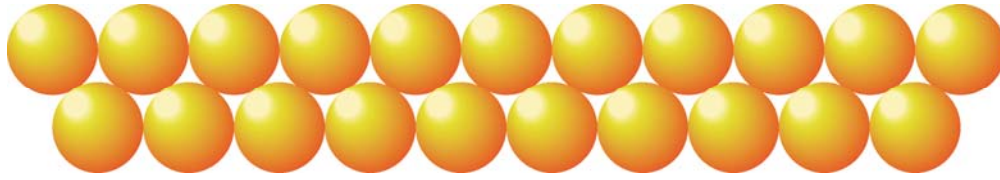
- The droplet size is primarily determined by the plateau height, and further a scaling relation with the viscosity ratio was found. The droplet size is constant at high viscosity ratios, which can be described with an analytical model, while at lower ratios an increase in droplet (or bubble size) is observed.

The here presented mechanistic considerations of the EDGE emulsification process seem to us a sound basis for the next steps toward larger scale implementation of this process.

ACKNOWLEDGEMENT

The authors thank Albert van der Padt for useful suggestions and Pieter Kroon for technical assistance with the simulations.





Chapter 6

PARALLELIZED EDGE-BASED DROPLET GENERATION DEVICES

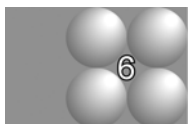
ABSTRACT

We here report on three parallelized designs of the new Edge-based Droplet GEneration mechanism, which, unlike existing mechanisms, produces many equally sized droplets simultaneously at a single droplet formation unit. Operation of the scaled-out systems is straight forward; only the oil inlet pressure has to be controlled to let all the units produce oil droplets, given certain basic design constraints. For systems with a typical nozzle depth of 1.2 μm , the mean droplet diameter is 7.5 μm and the coefficient of variation is below 10%. The number of droplets that is formed per unit can easily be increased by increasing the length of the unit. The stable pressure range in which monodisperse droplets are formed can be extended by small adjustments to the design. Overall, the EDGE devices are simple in design and robust in use, making them suitable for massive outscaling.

This chapter has been published as: van Dijke, K.C.; Veldhuis, G.; Schroën, K.; Boom, R.M. Parallelized Edge-based Droplet Generation Devices *Lab Chip* **2009** 9, 2824 - 2830. Supplementary material is available on the journal's website.

INTRODUCTION

For numerous complex fluids used in food, pharmaceuticals, and cosmetics, a simple and mostly single emulsion is used as the basic structure. These emulsions, in which one phase is dispersed as droplets in the other phase, are normally produced by methods which use brute forces to disrupt larger droplets into smaller ones, and as a result also heat up the product leading to thermal damage (Walstra, 2003). Because of this, there are severe limitations to the process conditions that can be used in the production of emulsions, and therewith in the products that can be realized. In addition, in spite of the large amount of energy used, the produced emulsions have a broad droplet size distribution with a typical coefficient of variation (CV) of around 40 % (Saito *et al.*, 2006). In recent years, several alternative techniques were proposed based on micro-engineered devices which are known to be more energy efficient and allow better control over the droplet size. In Figure 1, examples of such microsystems are shown. For all of them it is claimed that they produce monodisperse emulsions ($CV < 10\%$) at relatively low energy consumption.



The basis for droplet formation in these systems can be diverse. In T- and Y-junctions, droplet formation is induced by the shear forces exerted by the cross flowing continuous phase. In flow-focusing both liquids flow in the same direction, but the continuous phase does so at much higher speed, therewith inducing droplet formation. In all shear driven systems, the flow of the continuous and to-be-dispersed phase have to be controlled precisely to obtain monodisperse emulsions, and in parallelized systems, this may turn out to be an extra challenge.

In microchannels, spontaneous droplet formation is a result of interfacial area minimization, and contrary to shear-based systems, the droplet size is only dependent on the geometry of the microchannel, as long as the oil phase flow rate is kept within a certain range. Therewith, these systems promise simpler operation than shear-based systems (also concerning scale-up which will be discussed later).

In all aforementioned systems, droplets are formed sequentially from one droplet formation unit (DFU). The productivity of a single microfluidic droplet generator is

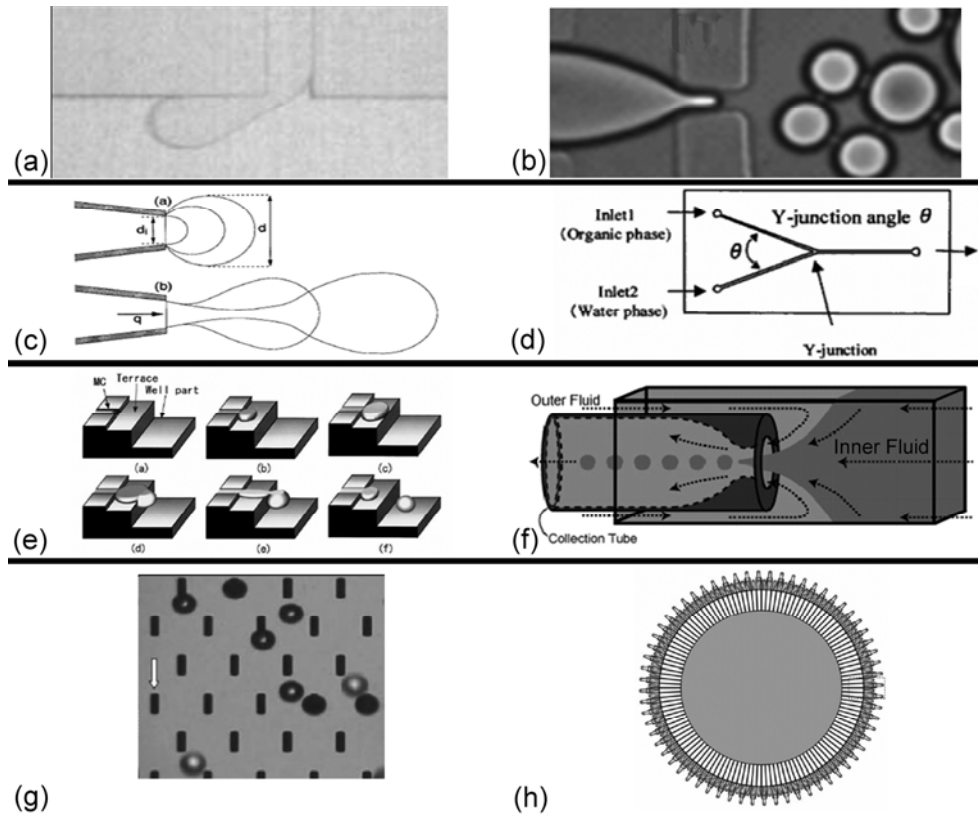
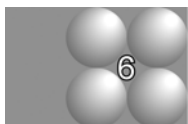


Figure 1. Several examples of microfluidic devices which all are able to produce monodisperse droplets: (a) T-junction (van der Graaf *et al.*, 2005) (b) Flow-focusing (Anna *et al.*, 2003) (c) Co-flowing system (Umbanhowar *et al.*, 2000) (d) Y-junction (Kawai *et al.*, 2002) (e) Microchannels (Sugiura *et al.*, 2000) (f) Microcapillary device (Utada *et al.*, 2007) (g) Straight-through microchannels (Kobayashi *et al.*, 2002a) (h) Parallelized cross-flow junctions (Nisisako and Torii, 2008).

therefore rather low and up-scaling (or out-scaling) is important. In theory, massive parallelization of the units is possible, and therewith, higher throughputs should be within reach. Unfortunately, parallelization is not straightforward. Ideally, all units should be operated at the same conditions, but this is hard to realize. Flow control and fabrication complexity are the main difficulties here. Shear-based systems with parallelized units have been reported by Li *et al.* (2008), Barbier *et al.* (2006), Hashimoto *et al.* (2008) and Nisisako and Torii (2008). Li *et al.* (2008) report the use of a quadra-droplet generator

(QDG), which comprises of four parallel microfluidic flow-focusing devices. They report a slight increase in polydispersity of the droplets due to a weak coupling between the parallel units. Still, a monodisperse emulsion with mean droplet diameter of 100-200 μm can be produced, with sizes strongly depending on flow-rate ratios. Barbier *et al.* (2006) have studied two T-junctions in parallel and found complex dynamic behavior. Only in the synchronization regime, a well-defined monodisperse emulsion is formed. Hashimoto and co-workers (2008) found little variation in formation of droplets in coupled flow-focusing generators. In contrast, bubble formation showed a variety of complex dynamics. The authors concluded that the difference in dynamics originated from the compressibility of the dispersed fluids. Nisisako and Torii (2008) designed a complex large-scale parallelized droplet generator with 16-256 shear-based DFU's and produced droplets of around 100 μm (Figure 1h); the droplets were very monodisperse with a coefficient of variation of around 1%.



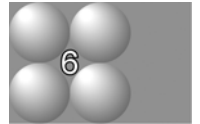
For all the parallelized systems mentioned here, the microchannel geometry and droplet sizes are relatively large, and control over the liquid flows is therefore relatively easy given the size of the channels (i.e. the Laplace pressure is low compared to the applied pressure), albeit far from straightforward as indicated earlier. For most practical applications of emulsions, the droplets need to be considerably smaller, and given the underlying mechanisms, this implies that the channels need to become smaller, flow control needs to be more accurate, and consequently, will have more influence on the emulsification efficiency. For spontaneous droplet formation, this was nicely illustrated in the work of Kobayashi *et al.* (2002a) with straight-through microchannels. For this technology, only the to-be-dispersed phase flow has to be controlled; the single purpose of the continuous phase is to move the droplets downstream. When producing monodisperse soybean oil droplets of around 30 μm with straight-through microchannels (Figure 1g) at an oil flow rate of several tens of milliliters per hour, the results looked very promising (Kobayashi *et al.*, 2005c). However, when downsized straight-through microchannels were used to produce droplets below 10 micron, the maximum oil flow was only 50 μl per hour (Kobayashi *et al.*, 2008). The bottleneck in the downsized systems seems to be the very low percentage of active channels. For the smallest straight-through microchannels

presented by Kobayashi and coworkers, the droplets had an average droplet diameter of 4.4 μm , but the percentage of active channels was below 1 %. This means that 1% of 92,575 channels produced monodisperse droplets just before the first blow-up (generation of anomalously large droplets) occurs somewhere in the system, and the system becomes unstable. For slightly larger channels producing droplets of 6.7 μm , this percentage was 5.2%. The percentage increased further, and for the largest fabricated channels (which produce droplets of 9.8 μm), a value of 12.3% was found.

The low percentage of active channels is probably caused by pressure gradients just below the straight-through plate as was reported by Gijsbertsen-Abrahamse *et al.* (2004) for microsieve systems and by Van Dijke *et al.* (2009) for terrace-based microchannels. These pressure gradients only allow a pore to become active if it is at a certain distance from a pore that forms droplets. Besides, narrow straight-through channels are difficult to fabricate due to the aspect ratio between etching depth and channel depth, which is as high as the state of the art production techniques allow. If fabrication inaccuracies occur, this is immediately reflected in the monodispersity of the emulsion, and in the number of active channels.

The percentage of active channels is not an issue in droplet formation with a submicron-channel array (Kobayashi *et al.*, 2007). However, there are some points that have to be taken into account when considering this system for scale-up. The terraces in the array need to be very shallow, and silicon seems to be the only material that allows this shallow etching. An interesting material from a practical point of view is stainless steel, but this material cannot be fabricated precisely below a 10- μm scale (Tong *et al.*, 2001). Further, packing of arrays to form a bigger unit for up-scaled processes may turn out to be a big challenge, therefore, straight through microchannels seem to be a more obvious choice for up-scaling, in spite of the low number of active channels.

It is thus obvious that there is a challenge in the design of systems which produce droplets below 10 micrometer, with all droplet forming units working, given the current technical options. In a previous chapter we proposed Edge-based Droplet Generation (EDGE) where simultaneous formation of many oil droplets in a single DFU occurs. Unlike the



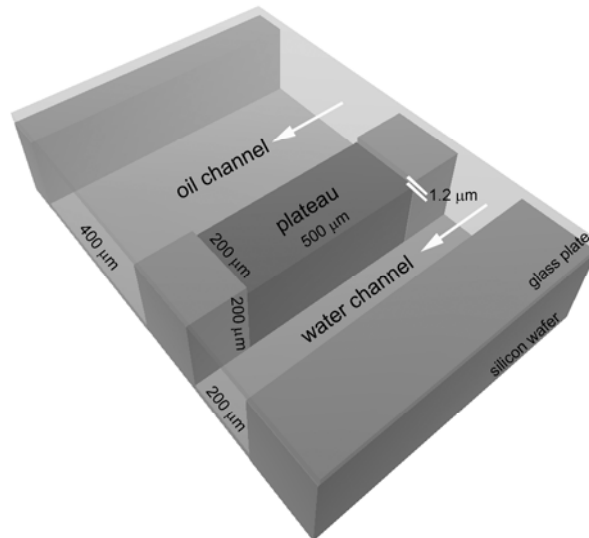
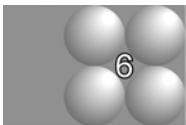


Figure 2. Three-dimensional drawing of a single EDGE-unit, which is etched in a silicon wafer together with the oil supply channel and the water phase or emulsion channel.

The dimensions are not to scale, but underline the depth differences.



system presented by Tan and Lee (2005) where parent and satellite droplets are formed simultaneously, which need to be separated in order to obtain monodisperse emulsions, with EDGE technology equally sized droplets are formed, which makes EDGE less elaborate. The DFU consists here of a shallow, very wide slit through which the to-be-dispersed phase flows (see Figure 2). The dispersed phase forms a string of droplets simultaneously at the exit of the slit. Multiple equally sized droplets per DFU have the advantage that less DFU's are needed, and control over the oil phase is expected to be less cumbersome than in single droplet DFU's. Besides, the design of the units is rather simple, and does not challenge the current state-of-the-art etching technology that is used to produce them. In principle, the EDGE units can even be fabricated without etching complex structures in the substrate. For example, we tested a prototype that consisted of stacked glass plates with adequate spacers, and with this unit, we could demonstrate the EDGE emulsification mechanism. Next to that, the units themselves are self-regulating because the droplet formation position is not forced to a specific position but can take place anywhere along the edge simultaneously.

Whether these positive points are an advantage in parallel EDGE systems is investigated in this Chapter. We study the ‘upscalability’ of the EDGE-system, and investigate the percentage of active DFU’s through high speed imaging. The droplet sizes are related to the performance of a single unit, as described in Chapter 4 and 5. In the discussion, scalability of EDGE technology amongst others is compared to that of other microtechnological emulsification systems.

EXPERIMENTAL

Microchip designs. The microchips were produced with a Deep Reactive Ion Etching (DRIE) technique in a silicon wafer (Micronit Microfluidics, The Netherlands). The chips were closed by a glass plate on top. The silicon and glass surfaces were hydrophilized by oxidation, which makes them suitable for oil-in-water emulsification. From the contact angles that were observed during experimentation, it was obvious that the microchips were hydrophilic, and remained hydrophilic, therefore, no further surface treatment was necessary.

In this work, we studied the behavior of three different structures with similar depth of 1.2 μm (see Table 1). The first basic structure is a rectangular plateau, which will be further referred to as EDGE-R. In EDGE-R we have 196 DFU’s with dimensions 200 x 500 x 1.2 μm (length x width x depth; see Figure 2) with 200 μm of bonding area between two plateaus. This structure is a parallelized version of the single DFU systems presented in Chapter 4 of this thesis. The second basic structure is a plateau between two channels without any bonding area, which gives a very wide plateau. The dimensions of the DFU in these EDGE-W devices are 200 x 9500 x 1.2 μm . This plateau was designed to maximize droplet formation length and thus increase productivity. The third basic structure has the

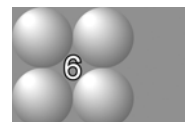


Table 1. Dimensions of EDGE systems.

DFU designs	depth [μm]	length [μm]	width [μm]	Number of plateaus
EDGE-R	1.2	200	500	196
EDGE-W	1.2	200	9500	14
EDGE-T	1.2	200	200 \rightarrow 1200	112

shape of a truncated triangle. The base line, which is at the continuous phase channel side, is 1200 μm and the triangle converges to 200 μm at the oil supply channel side; this is EDGE-T. The depth is 1.2 μm , and 112 units are present in one chip. The triangular shape was designed to increase pressure stability of the device.

Figure 2 shows a schematic three-dimensional drawing of a *single* rectangular plateau (not to scale), which is positioned between the oil and water channels. In this drawing, the depth differences are visualized. The dark-gray plateau is the DFU in this system. The oil is pushed from the oil channel onto the plateau, and ultimately the oil flows from the edge into the water channel in the form of droplets.

In the scaled up design, the various EDGE structures are connected through a ‘winding’ channel, which is used as continuous phase channel and droplet collection area. The oil supply is via a forked channel, the winding channel of the continuous phase is wrapped around the legs of the fork. In Figure 3 a top-view photo of an EDGE-R microchip is shown. In the photo of the EDGE-R microchip, in the top right corner a powder blasted hole is visible, which acts as the water channel inlet. The hole in the upper middle of the

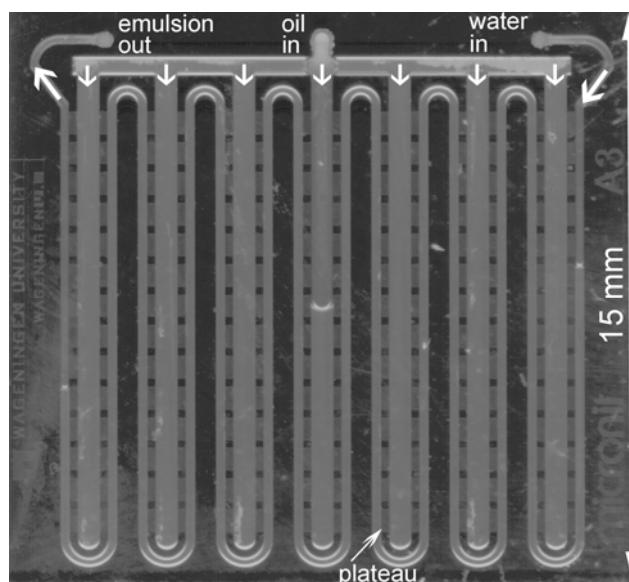
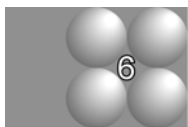
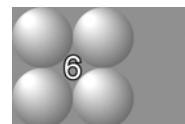


Figure 3. Photo of the microchip with the parallelized EDGE-R system.

chip is the oil phase inlet and in the left-hand corner, the produced emulsion flows out of the chip. In between the parallel parts of both channels, the plateaus are etched. The support pillars between the plateaus, for bonding and spacing, are visible as darker areas.

Essential in the design of the parallelized EDGE-devices is ensuring a comparable pressure drop over all the plateaus throughout the device. This is done by minimizing the pressure drop in the to-be-dispersed phase channels as well as the continuous phase and/or product channel. The channels should be designed such that they only allow a pressure drop of a few millibar over the length of the channel. The oil channels should therefore be relatively wide in order to have steady oil supply. The continuous phase channel should also be wide; in spite of the low viscosity of the continuous phase, the increasing amount of oil droplets will increase the viscosity of the fluid in this channel considerably, and thus increase the related pressure drop.

Peripherals. The microchip is placed in a module (Micronit Microfluidics, The Netherlands) and connected via flat-bottom ferrules with nuts from Upchurch Scientific to 1/16" PEEKTM tubing with an inner diameter of 0.75 mm. The applied pressure on the oil phase is controlled with a digital pressure controller (Bronkhorst, The Netherlands). The typical pressure range that was investigated is 150 to 350 mbar. For the continuous phase, we use hydrostatic pressure, or a syringe pump, as we only need a pressure difference in the order of several millibar; as the continuous phase does not shear the droplets off, but only removes the droplets. Typical continuous phase flow rates in the microchip were between 0.4 and 1 mL/hr. The emulsions that were produced contained up to 30% of oil, depending on the set flow rate of the water phase and oil pressure.



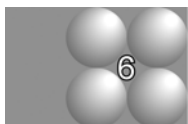
To visualize droplet formation in the EDGE-system we used a high-speed camera (Redlake MASD Inc., USA) connected to a microscope (Carl Zeiss B.V., The Netherlands). The module with the microchip was placed on the microscope table and illuminated via the objectives with a halogen cold light source (Schott, Germany). To start the experiment, the vessel with the continuous phase was lifted to increase the pressure to around 7 mbar. Subsequently, the applied pressure on the oil phase was increased

stepwise via the controller until the oil flowed onto the plateau. The droplet sizes were determined with image analysis software.

Chemicals. As the to-be-dispersed phase, n-hexadecane ($C_{16}H_{34}$, 99%), synthesis grade, from Merck KGaA (Darmstadt, Germany) is used. As the continuous phase, MilliQ ultra-pure water with 1 wt% sodium dodecyl sulphate (SDS) is used. The viscosity of both phases is 3.34 and 1.00 mPas, respectively. The static interfacial tension of this system is 8 mN/m, but the actual interfacial tension during droplet formation may be higher. Depending on the time scales at which various effects take place, the actual value of the interfacial tension may be anything between this value and the measured interfacial tension of a ‘clean’ surface (44 mN/m).

RESULTS AND DISCUSSION

Given the goal that we have set for this work, we will systematically check various aspects that are of essence for up-scaling of the EDGE design. The number of active units is investigated first, followed by the stability of the process, and finally a general comparison of available techniques in literature and EDGE will be made.



Active units. The chips are filled as described in the materials and methods section. After that, the applied pressure on the oil phase is increased gradually. Once the minimum required Laplace pressure ($\Delta P_{Laplace}$) is reached, the oil intrudes onto the plateaus. This pressure can be estimated with Laplace’s law: $\Delta P_{Laplace} = \sigma(R_1 + R_2)^{-1}$, where σ is the interfacial tension between both phases and R_1 and R_2 are the primary radii of curvature of the interface. The smallest curvature (R_1) is found between the plateau and the glass plate, and because of its value, it dominates the Laplace pressure here.

It is observed that all DFU’s filled completely with oil around this pressure, and once the oil reaches the edge, regular-sized oil droplets are produced (see Figure 4). The percentage of active units was 100% in each system tested. Typical droplet formation frequencies from the individual plateaus (EDGE-R and EDGE-T) can be as high as 1500 s^{-1} , depending on the size of the droplet and the applied pressure. For EDGE-W, it is impossible to determine the frequency because the entire plateau can not be visualized at

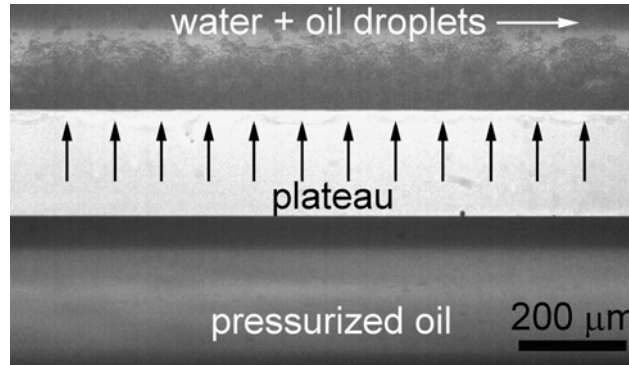
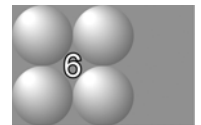


Figure 4. Part of active Droplet Formation Unit in EDGE-W system; 1200 μm of the total length of 9500 μm is visible.

the same time (Figure 4). An indication is 250 droplets per second per 100 μm plateau length, and this is in accordance with what was found for microchips with single plateaus. Also for the pressure dependency of the droplet size, similar results were obtained, as will be discussed later.

In all chips, all structures are active, and the frequencies of the structures seem comparable, therewith indicating that the channel dimensions were chosen appropriately; the pressure drops in the oil and water phase were indeed minimal as intended. In some cases, the droplet formation is so fast or channels are so full that we cannot determine the frequencies, but since at higher water flow rates, and in chips with less plateaus we always observed that the plateaus behave similar, we can safely assume that EDGE can be scaled out successfully.



To illustrate how droplet formation takes place, in Figure 5 the upper right corner of an EDGE-T chip is shown at a magnification of 25 times. In the left part of this figure, the triangular plateaus are outlined with black lines to help the reader locate the DFU's. All plateaus are filled with oil, as illustrated in the magnified rectangle in the middle. The contact angles in this image clearly indicate the hydrophilicity of the chip surface. In the right hand figure, a small part of the interface at the edge is magnified, where droplet formation takes place. The actual formation of a single droplet is visible only at the highest available magnification. As described in Chapters 4 and 5, the droplet formation

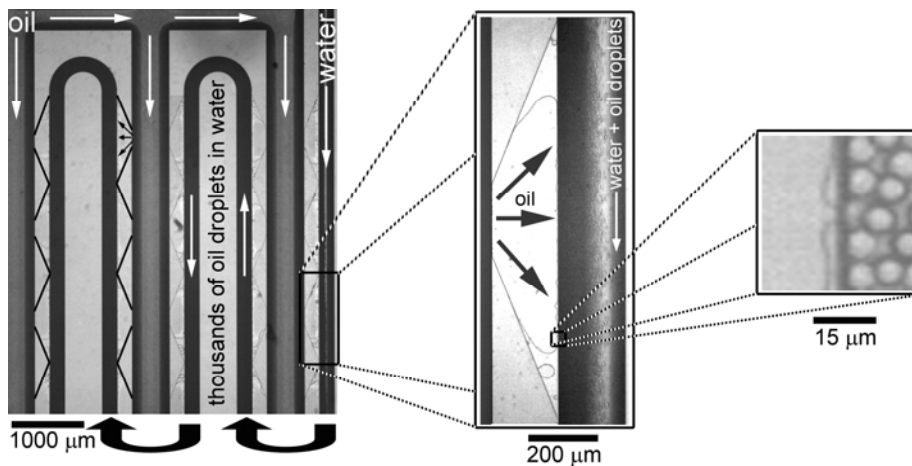
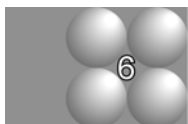


Figure 5. Screenshots of a part of an EDGE-T device at different magnifications.

takes place at the edge of the plateau and is not forced to occur on a specific position. The process seems thereby less sensitive to disturbances (see also disturbances section). As expected, the oil does not fill the far corners of the structures. This effect is larger for the triangular plateaus than for the rectangular plateaus which fill virtually completely. The available area is best used in the EDGE-W design as there are fewer corners on these wide plateaus.



Stability of the process

Pressure. Since all units fill with oil, and show appreciable frequencies, the next step was to investigate the pressure dependency of the droplet size, and its coefficient of variation. Both parameters were determined using image analysis on 100 droplets produced at the beginning of the continuous phase channel (this was found to be a good indicator for the rest of the units since visibility is optimal and we did not observe other droplet sizes further down the structure in spite of less visibility). The result is shown in Figure 6; a constant oil droplet size is observed starting from the minimal Laplace pressure needed to push the oil onto the plateau until a critical value is reached. Above this value, an increase in diameter is observed. The coefficient of variation seems somewhat more pressure sensitive than the droplet size, but its absolute value is still small, indicating rather monodisperse emulsions.

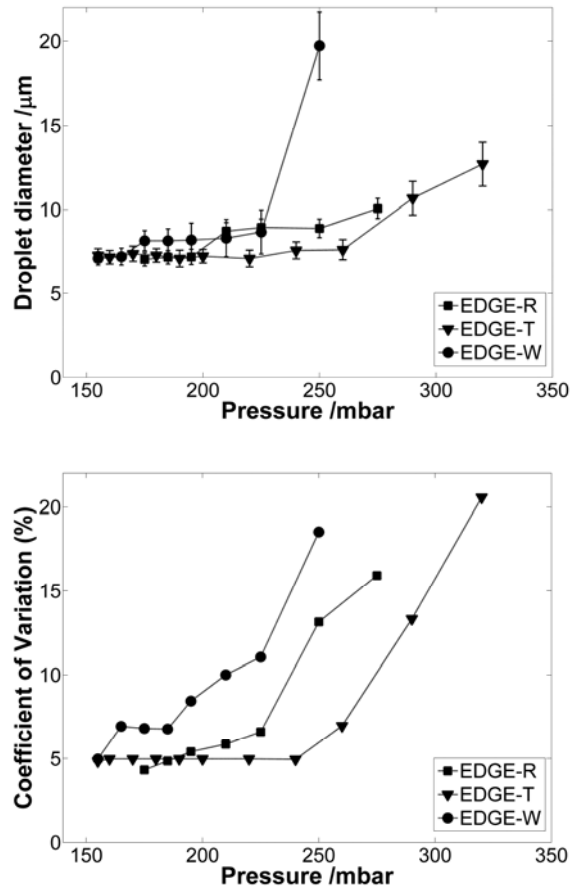
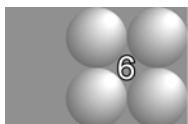


Figure 6. Pressure dependency of the droplet size and coefficient of variation of droplets produced with EDGE technology. In the stable droplet size region, droplet formation frequencies were typically around 250 droplets per 100 mm of plateau length.

We define here the stable monodisperse pressure zone as the pressure interval in which monodisperse droplets are formed (i.e., coefficient of variation below 10%), which is obviously of relevance for the application of spontaneous droplet formation systems. The stable monodisperse pressure zones for EDGE-R, EDGE-T and EDGE-W are broad enough for practical application. The triangular design shows an even broader working range (albeit at the expense of productivity due to suboptimal use of available EDGE area)

as it squeezes the oil supply, which has the same effect as increasing channel length in microchannel emulsification (Sugiura *et al.*, 2002b and Chapter 2 of this thesis). A longer microchannel results in a higher flow resistance in the channel, as discussed in Chapter 2, and the smaller cross-section in a triangular plateau also aims at creating such an increase in resistance. In spite of the decrease in EDGE-length, the resulting wider operation range for constant droplet size and coefficient of variation in EDGE-T systems may turn out to be advantageous. Especially with low viscous, and thus pressure sensitive, oils it can be important to have a more stable process as the droplet formation frequency will be high anyway.

Disturbances and robustness. An added benefit of the wide plateaus is that even if there is an obstruction on the plateau (sometimes dust particles are stuck on the plateau) the oil simply fills the area around the obstruction and continues with droplet formation at the edge of the structure as further explained in Chapter 5, Figure 4. The droplets that are formed still have the same size, which makes the process robust. When comparing mechanical robustness of the designs, we did notice that the widest plateaus seemed more fragile, and were thus more susceptible to breakage.



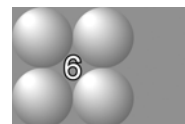
Long-term operation. The EDGE system was subjected to long-term operation, implying constant usage for 3 consecutive days. During the entire experiment, the process was stable. Visual inspection of the process showed that the droplet size did not change as a function of time. The stability, and activity, of the EDGE process can be explained by the droplet formation taking place only at the edge of a DFU. Since the plateau is large compared to the droplets, the droplet detachment is not accompanied with large pressure fluctuations, which could induce coupling effects. The relatively large plateau thus acts as a buffer and pressure gradients around a forming droplet only affect the fluid flow very locally. EDGE units seem to be self-regulating droplet generators.

Comparison to other microfluidic emulsification techniques

In Table 2, microfluidic droplet generation techniques from literature are qualitatively evaluated on system characteristics such as monodispersity of the emulsion, the size of the droplets, productivity per droplet forming unit, complexity of fabrication, and scalability.

Table 2. Qualitative comparison of microfluidic emulsification techniques.

	size distribution -- polydisperse ++ monodisperse	droplet size -- large ++ small	production per DFU -- low ++ high	fabrication -- complex ++ simple	parallelization -- challenging ++ simple
T / Y junctions (Van der Graaf <i>et al.</i> , 2005; Kawai <i>et al.</i> , 2002)	++	0	++	+	-
Flow-focusing (Anna <i>et al.</i> , 2003; Nisisako and Torii, 2008; Hashimoto <i>et al.</i> , 2008)	++	+	++	0	--
Microcapillaries (Utada <i>et al.</i> , 2007)	++	--	+	--	--
Microchannels (Sugiura <i>et al.</i> , 2000; Kobayashi <i>et al.</i> , 2007)	+	++	-	-	++
STMC (Kobayashi <i>et al.</i> , 2002a)	+	+	-	-	0
EDGE (chapter 4 and 5)	+	+	+	++	++



A fair quantitative evaluation is in our opinion difficult, because various aspects are interlinked. For example, the droplet size influences the production rate per droplet formation unit since smaller droplets are generated at higher frequency, albeit that the total oil flux is in general lower. In spite of this, some general aspects can be noted. The monodispersity is highest for shear-based emulsification techniques (first three entries in the table), but this is only true for a single DFU and with ideally controlled phase flows. Second, these techniques are mostly reported for preparation of rather large droplets ($> 10 \mu\text{m}$). For small droplets, spontaneous emulsification techniques (last three entries in the table) are more suited, but their production rate can be low compared to shear-based

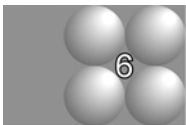
techniques. When considering the various techniques for up-scaling, other aspects become important such as the fabrication of the devices and the ease of parallelization. For both aspects, EDGE technology seems to have an edge over the other techniques due to its simple design, and the scalability shown in this paper.

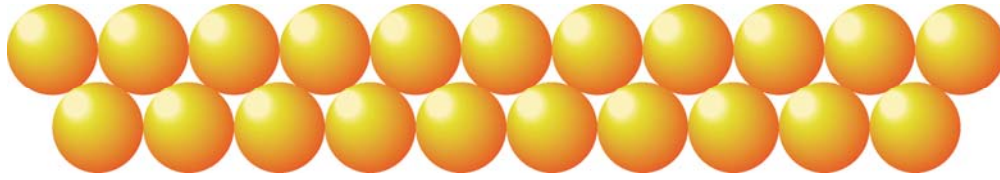
CONCLUSION

The recently proposed EDGE technique for production of narrowly dispersed emulsions with average droplet sizes below 10 μm was successfully parallelized. The scaled-out EDGE technology is robust, easy to implement, giving narrow droplet size distributions, and this makes EDGE a promising technique for the production of emulsions with small droplets.

ACKNOWLEDGEMENTS

The authors thank Abid Maan for performing the measurements.





Chapter 7

EDGE EMULSIFICATION FOR FOOD-GRADE DISPERSIONS

ABSTRACT

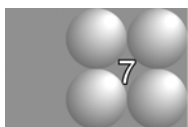
In this paper, we use the Edge based Droplet GEneration (EDGE) emulsification method to produce food grade emulsions (including double emulsions) and foams. This newly developed mild technology proved to be very stable and robust in the production of all these products. The products are made with food grade components in an up-scaled micro device, which does not show any changes in time in wettability and fouling, and the size of the droplets and bubbles is as needed for food stuffs. Air bubbles generated with EDGE were much larger than emulsion droplets, which could be explained through the viscosity ratio of the phases and changes in interfacial free energy caused by dynamic interfacial tension effects. In the outlook section of this paper, the obtained results are related to the dimensions of upscaled devices, which are in a practically feasible range, also due to the simplicity of the EDGE structure and its operation. Preliminary estimations show that a 300L system can produce 1 m³/hr of 4 % (v/v) emulsion.

This chapter has been submitted as: Van Dijke, K.C.; Schroën, K.; Van der Padt, A.; Boom, R.M. EDGE emulsification for food-grade dispersions.

INTRODUCTION

Food grade dispersions, e.g. emulsions and foams, are generally produced via established technologies such as high pressure homogenizers, colloid mills, in spite of their inefficient energy usage and wide span of droplet sizes. Typically, 1-5 % of the applied energy is used to make the emulsion droplets, and the rest is dissipated as heat, which may lead to heat damage of the product and its ingredients (McClements, 2005). For this reason, repeated passage at less extreme conditions is generally needed to give the product the desired properties. In addition, repeated passage is applied to allow extra time for the surfactants to do their stabilizing work after new interface has been created; the surfactants cannot be supplied sufficiently fast to timely stabilize all the area that is created during a single passage.

Emulsification processes based on micro-engineered emulsification devices consume considerably less energy and are therefore an interesting alternative emulsification technology; however, this technology still needs further maturation. Although many different concepts have been proposed, important steps have to be made to make emulsification by microtechnology practically relevant. These steps should be taken with respect to the size of the droplets, the ingredients that can be used, and the scalability of the devices.



Many microtechnological devices do not generate droplets in the same size category as those generated by conventional technology; and since the product properties are co-determined by the droplet size, there is little room for compromise. Further, many different emulsifiers are used in high concentrations in microtechnological research, but most of these tend to be non-food grade (Hashimoto *et al.*, 2008; Kobayashi *et al.*, 2002a; Vladislavljevic *et al.*, 2008; all other chapters in this thesis). Often the same is valid for the tested oils. Exceptions are the work of Kobayashi and Nakajima (2002b) and Saito and co-workers (2005), who worked on straight-through microchannel emulsification, using various food components; however the droplets generated were typically around 40 μm , which is an order of magnitude larger than desired for food products. Further, many

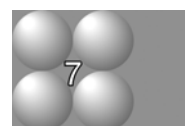
results have been published for single devices, while only in a few examples devices have been scaled up (e.g. the microchannel device by Kobayashi and co-workers, and the microsieve invented by Van Rijn and Elwenspoek (2005) and applied within Nanomi technology as stated on their website (www.nanomi.com)).

Wetting and fouling of microdevices is often neglected (except in Saito's work); and this is unjustified since these aspects are crucial for robust prolonged operation and cleanability. Together with the three points that were mentioned in the previous section, this should determine whether microtechnology may become a true alternative for emulsion and foam production.

The recently proposed Edge based Droplet GEneration (EDGE) emulsification technique has been successfully used to produce small, narrowly dispersed hexadecane droplets in pure water with SDS as a surfactant (Chapter 4). The droplet formation units are simple in design, being shallow plateaus between two channels, and this configuration has been shown to be suitable for scale-up through parallelization (Chapter 6). We here extend the use of EDGE technology to products with food-grade ingredients (e.g. whey protein concentrate, skim milk, and sunflower oil), ranging from single emulsions, to double emulsions and to foams.

Vulnerable products, such as double emulsions, can hardly be produced by classic technology; a broadly dispersed double emulsion with large droplets can be made, however this leads to unstable products with unsatisfactory properties (Garti and Bisperink, 1998). Here, a more gentle technique such as membrane and microchannel emulsification could prove to be of even greater benefit (Lambrich *et al.*, 2004; Kawakatsu *et al.*, 2001; Mine *et al.*, 1996), and we expect that this also holds for EDGE technology.

In foams, (as was the case for emulsions) evenly distributed and well defined small bubbles are desired for reasons of sensory perception and product stability. The conventional technologies such as steam injection, turbulent mixing (Saint-Jalmes *et al.*, 1999), and rotor-stator equipment (Bals and Kulozik, 2003), are rather energy inefficient, and give wide size distributions. In literature, it is reported that with static membranes,



(which are micron sized devices) foam can be produced at much lower energy input using the shear flow stresses of the continuous phase. This process can be further improved through controlled shear forces by an inner cylinder relative to an outer cylinder (Müller-Fischer *et al.*, 2007). In this work, we use spontaneous bubble formation in the EDGE devices with food-grade ingredients, targeting narrow size distributions.

All tested (food) systems are compared in the last section, and the performance of EDGE will be discussed. Further, a short perspective on EDGE technology for different food products will be given.

MATERIALS AND METHODS

EDGE-chips. The structures and channels were formed with Deep Reactive Ion Etching in a silicon wafer and closed off by bonding a glass plate (Micronit Microfluidics, The Netherlands). In this work, a parallelized EDGE microchip with 196 plateaus, which each

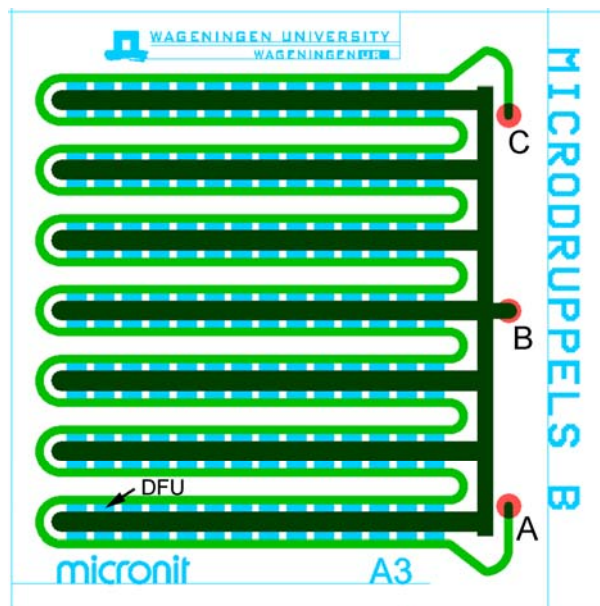
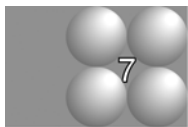


Figure 1. Design of the EDGE microchip used in this research. The dark channel guides the to-be-dispersed phase, the green ‘winding road’ is the continuous phase channel and the rectangular areas in between are the droplet formation units (DFU).

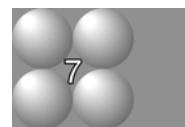
have a length of 200 μm , a width of 500 μm , and a depth of 1.2 μm was used for all experiments. The EDGE droplet formation unit and the parallelization are described in detail in chapters 4 and 5 of this thesis. In Figure 1 a schematic drawing of the microchip is shown.

The winding green line, that starts at A and continuous all the way to C, is the continuous phase channel which is shaped around the darker oil channel, which starts at B and forms a fork-shaped lay-out. Where the two channels run parallel to each other, the rectangular droplet formation units (blue) are placed. The three holes A, B, and C (red) at the backside of the chip act as inlets for continuous phase, dispersed phase, and outlet for product respectively. The chips were used without further treatment.

Chemicals

O/W emulsification. Whey protein concentrate was kindly provided by FrieslandCampina (Deventer, The Netherlands). A 6% (w/v) WPC solution was prepared on a magnetic stirrer by dissolving the powder in water at slightly elevated temperature (40 °C which is below the denaturation temperature). The protein solutions were kept in the fridge overnight before use; the viscosity is 1.2 mPa s according to Walstra *et al.* (2006). Friesche Vlag Langlekker skim milk (FrieslandCampina, The Netherlands) from a local supermarket was also stored in the fridge prior to use ($\eta = 1.65$ mPa s). Sunflower oil of viscosity $\eta = 50$ mPa s was also purchased at the local supermarket and used without any pre-treatment. Hexadecane was from Merck KGaA (Darmstadt, Germany).

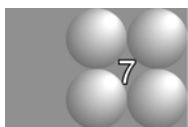
W/O/W emulsification. The droplets in the water-in-oil emulsion were prepared in such a way that they were small enough to enter the 1.2 μm deep plateaus of the EDGE devices so they can be incorporated in the double emulsion. To sunflower oil with 10% (w/w) PGPR (Givaudan, Vernier, Switzerland), 30 % (w/w) water was gradually added during 20 minutes, and the emulsion was mixed with an Ultra-Turrax homogenizer (T18 basic, IKA-Werke, Staufen, Germany) at 11000 rpm. The resulting average water droplet size was 0.4 μm (Mastersizer 2000, Malvern Instruments Ltd., UK), which is small enough to flow unhindered through the droplet formation unit (DFU). The viscosity of this W/O emulsion was measured in a rheometer (MCR 301, Anton Paar, Graz, Austria) with a



Couette geometry (DG 26.7). Rate sweeps were performed with shear rates from 1 s^{-1} to 900 s^{-1} . For each viscosity measurement, a forward and a backward rate sweep was performed in duplicate at a controlled temperature of $23 \text{ }^\circ\text{C}$; the value was found to be 170 mPa s . For the production of the double emulsion, 6% (w/w) Whey Protein Concentrate and skim milk were used as the continuous (outer) phase.

Foam. We used air at room temperature in the foaming experiments. Next to skim milk and WPC solution, we also investigated 1% (w/w) SDS in MilliQ Ultrapure water as reference continuous phase.

Procedure and peripherals. The microchip was placed in a standard microfluidic chip module (Micronit Microfluidics, Enschede, The Netherlands) and connected to the chip holes via $1/16''$ PEEK tubing with inner diameter of 0.75 mm with the use of Super Flangeless fittings from Upchurch Scientific. The to-be-dispersed phase flow was controlled accurately through a digital pressure controller (Bronkhorst, Veenendaal, The Netherlands) which could be connected to either a valve for liquids (O/W and W/O/W) or a valve for gases (Air/W). The pressure system was operated via software on a personal computer. A syringe pump was used to generate a flow in the continuous phase channel to transport the formed droplets or bubbles in such a way that they did not cause channel obstruction. Typically, applied flows were $100 - 1000 \text{ } \mu\text{l/hr}$, which corresponds to a pressure difference of only a few millibar over this channel.



After the chip was connected, the continuous phase flow was initiated and after some minutes a steady flow was developed. Subsequently, the pressure on the to-be-dispersed phase was gradually increased until the minimum required pressure for entering the plateau was reached. This pressure is a function of interfacial tension (σ), contact angle (θ) and relevant curvatures R_1 , and R_2 ; according to Laplace's law, this minimum pressure is:

$$\Delta P_{\min} = \sigma \left(\frac{1}{R_1} + \frac{1}{R_2} \right) \cos \theta \quad (1)$$

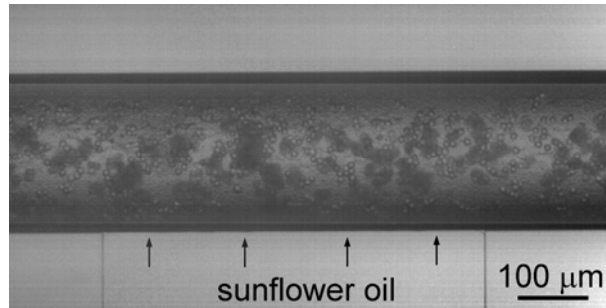
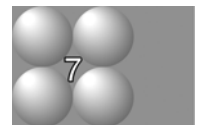


Figure 2. EDGE-emulsification of sunflower oil in 6 % whey protein concentrate solution.

where one of the curvatures (R_1) corresponds to the plateau height (H_p), and the other one (R_2) to the width of the plateau (W_p), which implies that this curvature is very large, compared to R_1 . In effect, the largest curvature can be neglected in the calculation of the minimum pressure. For emulsification of oil in water as presented in this work, this pressure was typically in the range of 300 - 400 mbar, for foam typically around 700 mbar with 1% SDS, and 1 bar with whey proteins as surfactant. This will be discussed in more detail in the results section.

Long term operation and storage of the microchips. Typical experiments to investigate the droplet / bubble size as function of pressure were carried out for 30 minutes. However, EDGE emulsification was also tested for longer times, and it turned out that it was possible to run overnight without visual change of the process due to fouling or other disturbances. After emulsification, the chip was flushed with and stored in water.

Droplet and bubble size measurements. We used image analysis software to determine the number-average droplet size and distribution. Next to that, a Mastersizer 2000 from Malvern Instruments Ltd. (Malvern, United Kingdom) was used to determine size distributions.



RESULTS AND DISCUSSION

O/W emulsions. Figure 2 shows an image of emulsification of sunflower oil in 6% WPC solution at the droplet formation unit indicated in Figure 1. The plateau is completely

filled with sunflower oil and the droplets are formed simultaneously along the edge, as we found previously for hexadecane; the entire length of the plateau generated droplets.

The droplet diameter was 7.2 micrometer with a coefficient of variation of 11.8 %, which is comparable to the values found for the hexadecane and the water-SDS system described in Chapters 4, 5 and 6 of this thesis. We also tested hexadecane with 6 % WPC solution; droplets of 7.5 μm were found, which is once more in good agreement. The highest droplet formation frequency, at which the sunflower droplets were generated, was about 30 droplets per 100 μm of EDGE length per second, and this frequency is typically a factor of 20 lower compared to hexadecane. This is most probably related to the viscosity of sunflower oil, which is a factor 18 higher than the viscosity of hexadecane; hence the flowresistance of the DFU will be 18 times higher. In the discussion section, this is evaluated further.

As can be seen in Figure 2, there are clusters of droplets flowing through the channel. However, after collection of the product no clusters could be detected by visual inspection

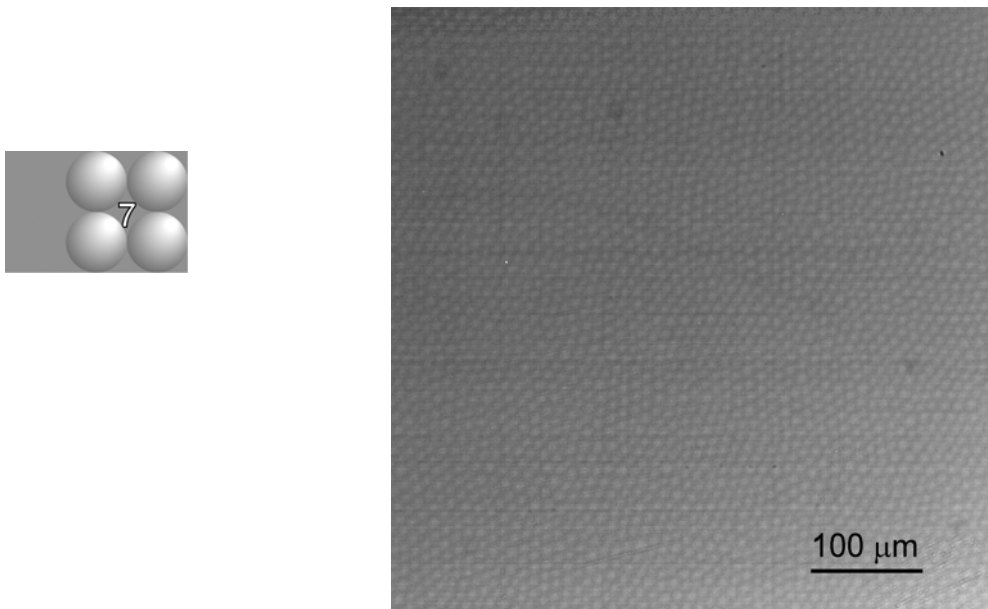


Figure 3. Sunflower oil droplets in 6 % whey protein concentrate solution.

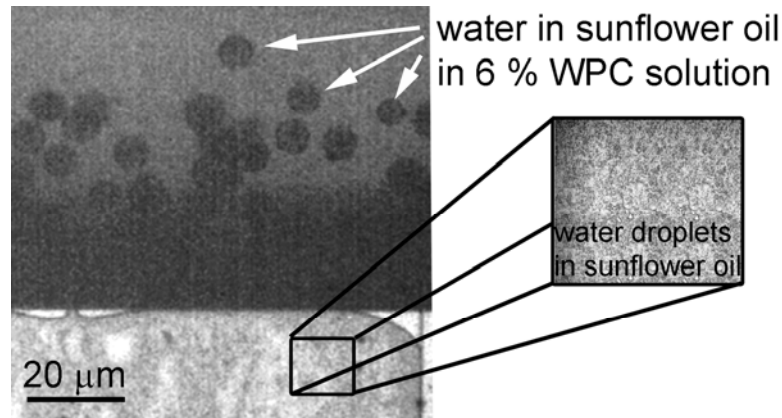


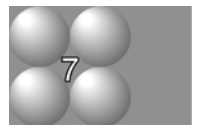
Figure 4. Production of double emulsion droplets in 6 % whey protein concentrate solution via EDGE emulsification of a single water-in-sunflower oil emulsion.

(see Figure 3, for the emulsion at 250x magnification) nor in the Mastersizer 2000 spectrum, which detected only droplet sizes equal to the single droplets observed in the channel. We assume that initially the amount of protein is sufficient to prevent coalescence, but not sufficient to cover all droplets completely, enabling some bridging flocculation. When allowed sufficient time, the proteins rearrange on the oil-water interfaces, and/or more protein adsorbs resulting in the stable emulsions that were detected at the outlet of the microchip.

We obtained similar results for the experiments in which skim milk was used as the continuous phase, albeit that visual inspection is harder due to the lower transparency of milk. The sunflower oil droplets in milk are in the same range as with 6 % WPC; their size is 7.4 μm with CV = 12.1 %. The frequency at which the droplets are formed is also the same as for WPC.

W/O/W emulsions. Double emulsions are visually different from single emulsions since they carry small water droplets dispersed in the sunflower oil, which are visible (although not easily) as black dots. In Figure 4, a double emulsion is formed in 6% WPC solution.

It is only possible to determine the size of the water-filled droplets by image analysis, because the internal water droplets disturb the laser scattering measurement in the Mastersizer. The sizes that were determined by image analysis are in the same size range



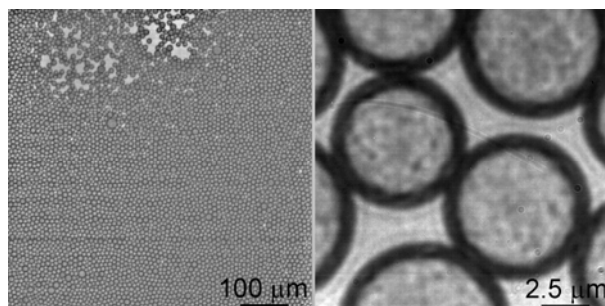
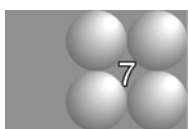


Figure 5. Sunflower oil droplets containing water in skimmed milk, i.e. double emulsion.

as for the single emulsion droplets: $7.4 \mu\text{m}$ with a C.V. of 6 %. Although the coefficient of variation seems lower, as mentioned in earlier work (Chapter 3), we think that the distribution coefficients obtained from image analysis are consistently lower than with laser scattering or equivalent techniques. Therefore, it seems safe to assume that the double emulsion droplets are comparable to single emulsion droplets and formed in the same way, which is in line with the microscopic observations at the edge of EDGE-systems. The droplet formation frequency is 25 Hz per $100 \mu\text{m}$ EDGE length which is slightly lower than for the single sunflower oil emulsification. We will discuss the droplet formation frequency later in more detail.

As with the single oil droplets, double emulsions can also be made with skimmed milk: the sizes are very comparable, as is the case for the coefficient of variation. In Figure 5, W/O/W emulsion droplets in skim milk are shown, and when magnified one can see that the oil droplets are all filled with water droplets, which is one of the major advantages compared to high shear-based methods.



In general, all oil droplets formed in this work have similar diameters to the hexadecane ($\eta = 3.34 \text{ mPa s}$) droplets described in earlier work. This confirms the spontaneous droplet formation mechanism described in Chapter 2, which implies that the dispersed phase viscosity only affects droplet formation time, but not the diameter. This is discussed further in the comparison section of this chapter.

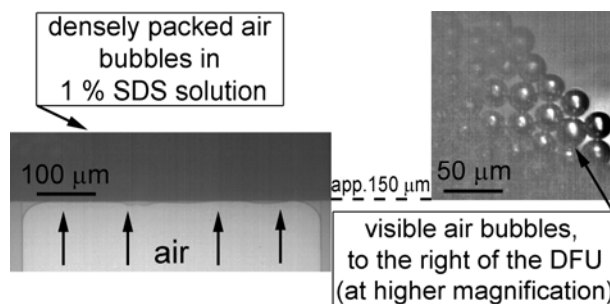
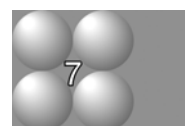


Figure 6. Formation of air bubbles in 1 % SDS solution. Left: a whole droplet formation unit filled with air and the completely filled channel in front of the DFU. Right: separately visible air bubbles approximately 150 μm to the right of the DFU.

Foam. The formation of bubbles with EDGE is in principle the same as with oil droplets; however, because EDGE was not previously tested for bubble formation, first a simple surfactant is tested, to show a proof of principle.

In Figure 6, the formation of air bubbles in a 1 % SDS solution at the DFU indicated in Figure 1 is illustrated. The droplets are shown at some distance from the right side of the droplet formation unit as only there the separate bubbles can be recognized. In front of the plateau, the channel is completely filled with bubbles, which cannot be distinguished from each other.

For bubbles, only an indication can be given for the diameter because we have to use image analysis for bubbles that move very rapidly, and therefore cannot always be recorded sharply. Nevertheless, it is clear that the bubbles formed in the 1% SDS-solution (app. 20 μm) are considerably larger than oil droplets. The bubble formation frequency could be estimated from the number of necking processes visible on the plateau. The frequency is very high: approximately 1000 bubbles per 100 μm EDGE-length. Therefore, it can be concluded that EDGE can be used effectively for foam formation.



The next step is to test with food grade ingredients. In Figure 7 the produced bubbles in 6% WPC-solution are shown in the channel of the microchip. Their size (approximately 30 μm) is considerably larger than found for SDS. For skimmed milk, the bubbles have the same size as for WPC; apparently the type of emulsifier does influence the size of

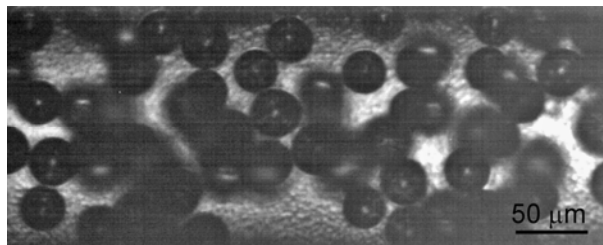


Figure 7. Air bubbles in 6 % WPC solution flowing through the channel.

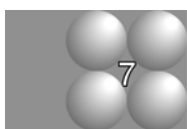
bubbles, where this was not the case for the emulsions. In spite of this, the process of bubble production is robust and steady, and we did not observe any changes in bubble diameter in time, nor any fouling of the chips that would disturb operation. The frequency was around 400 Hz per 100 μm , which is lower compared to 1% SDS, but since the SDS-bubbles are considerably smaller, this is logical.

Comparison and discussion of different systems

The behavior of the various systems is compared and discussed in this section. In Table 1,

Table 1. Characteristic values of several tested EDGE-systems.

System	ΔP_{min} [mbar]	η [mPas]	ζ [-]	$D_{droplet}$ or D_{bubble} [μm]	Max. frequency / 100 μm [Hz]
Hexadecane in 1% SDS	132	3.34	3.34	7.1	550
Hexadecane in 6% WPC	293	3.34	2.78	7.5	440
Sunflower oil in 6% WPC or skim milk	310	50	35.7	7.2	30
W/O emulsion in 6% WPC or skim milk	400	170	120	7.4	25
Air in 1% SDS	700	$18 \cdot 10^{-3}$	$18 \cdot 10^{-3}$	20	1000
Air in 6% WPC or skim milk	1000	$18 \cdot 10^{-3}$	$13 \cdot 10^{-3}$	30	400



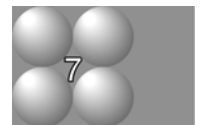
some characteristic (measured) values are shown, such as the minimal pressure needed to have the dispersed phase invade the plateau, and the diameter and frequencies of the generated droplets and bubbles.

The minimum required pressure is primarily related to the dimensions of the DFU, the interfacial tension and the contact angle (Equation 1). In the case that the contact angle remains unchanged (i.e., surface properties of the device remain unchanged), any difference in minimum pressure has to be caused by differences in interfacial tension. For gas bubble production, the value of ΔP_{min} was higher compared to the oil droplet systems due to higher surface tension between air and the continuous phase. Indeed, SDS was expected to lower the interfacial tension more (and faster) than WPC, and this is observed in the ΔP_{min} values.

The droplet size is strongly dependent on the geometry of the DFU (Chapter 4, 5) and the viscosity ratio of both phases (Chapter 5). As the geometry is the same in all experiments in this work, the ratio ζ of the viscosities of the dispersed phase (η_d) and the continuous phase (η_c), defined as:

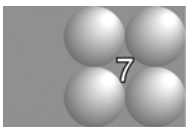
$$\zeta = \frac{\eta_d}{\eta_c} \quad (2)$$

can be used to explain the difference in droplet and bubble sizes. As found in chapter 3 for a grooved terrace-based microchannel system, the relative rate of the continuous phase flow onto the terrace affects the resulting droplet size significantly, and this is also the case for EDGE technology (Chapter 5). In other words, if the viscosity ratio ζ is high enough, similarly sized droplets will be generated. Near a critical value ζ_{crit} , which is dependent on the geometry (chapter 3, 5), the droplet size increases. The ζ_{crit} for EDGE is much lower compared to the grooved terrace system studied in chapter 3 as the inflow length is considerably shorter and the plateau length, which can be compared to channel length, is much longer.



The viscosities of the continuous phases used here (water-SDS, water-WPC and skim milk) are all in the same order of magnitude, so the to-be-dispersed phases will determine the viscosity ratio differences, shown in Table 1. The liquid/liquid systems studied in this work all have $\zeta \gg \zeta_{crit}$; consequently the droplet sizes are comparable. In case of air as dispersed phase for which ζ is very low (0.01-0.02), ζ is below ζ_{crit} and consequently the bubble size increases significantly as described in Chapter 5..

Even though the viscosity ratio explains the trend, the difference in bubble size between air in SDS solution and air in WPC solution remains remarkable, and this was also previously reported by Yasuno *et al.* (2004) for terrace systems. To explain this, dynamic interfacial tension effects have to be taken into account, especially, for very high interfacial area expansion rates (Chapter 3). In general, the surface free energy of the system becomes lower when going from the ‘constricted cylindrical shape’ on the plateau, to the droplet shape in the deeper continuous phase channel. A measure for the interfacial free energy can be calculated from the product of interfacial tension and surface area ($\int \sigma dA$). If the surface tension of the quickly growing bubble is not equal to the surface tension on the plateau, the surface increase has to be higher than minimally required in order to decrease the interfacial free energy sufficiently, resulting in larger droplets. This qualitative description can explain the emulsification results of Sugiura *et al.* (2004b) for various surfactant concentrations, and the aeration results of Yasuno *et al.* (2004).



The viscosity of the to-be-dispersed phase itself is expected to only affect the formation frequency. This is indeed the case for most of our investigated dispersed phases, and a linear relation with the viscosity holds (e.g. for hexadecane and sunflower oil). A remarkably small difference in droplet formation frequency was observed between sunflower oil and a water-in-sunflower oil emulsion, which was not expected based on the measured viscosity difference in the rheometer. Most probably, the macroscopic viscosity as determined in the rheometer, does not correspond to the situation on the plateau where the droplets are next to each other (as can be seen in Figure 4), and the emulsion droplets are constrained in two dimensions. Due to their size, the droplets are in the middle of the terrace, where the shear rate is lowest. Near the terrace wall, where most of the shear takes

place, the liquid is depleted in droplets. In the rheometer, droplets can interact with others in three dimensions, and this is not the case on the plateau. Therefore, it is logical that the actual viscosity in the EDGE device is determined by the continuous phase (sunflower oil), and that the frequency is similar to that for sunflower oil only. This is of importance for the production of these shear sensitive emulsions, for which in EDGE devices production rates can be established that are comparable to those of single emulsions, which is impossible when using classic technology.

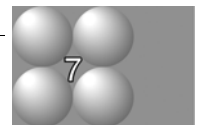
CONCLUSION AND OUTLOOK

Edge-based Droplet GEneration (EDGE) systems were used for emulsification and foaming in food grade systems, based on whey protein concentrate, skim milk and sunflower oil. The system was found to be very robust in operation over longer time. The droplet size was found to be 6 times the terrace depth for emulsions, and at least 17 times the terrace depth for foams. This could be explained based on the viscosity ratio and the recently introduced critical viscosity ratio.

The rate of emulsification is linearly dependent on the viscosity of the dispersed phase. Double emulsion generation was found to be much faster than expected; probably the

Table 2. Required EDGE length and volumes to produce 1 m³/hr of sample products.

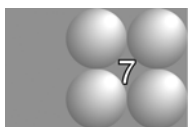
Ingredients	Possible product	required EDGE length [km]	EDGE 'chip-system' volume [liter]	EDGE sieve system volume [liter]
oil in skim milk (4 % (v/v) single emulsion)	recombined milk	170	270	30-40
water in oil in skim milk (4 % (v/v) double emulsion)	'tasty' low-fat milk	200	320	30-40
air in skim milk (50% (v/v) foam)	milk foam for e.g. deserts	19	30	3-4



macroscopic viscosity of the dispersed emulsion is lower when constrained into the shallow terrace.

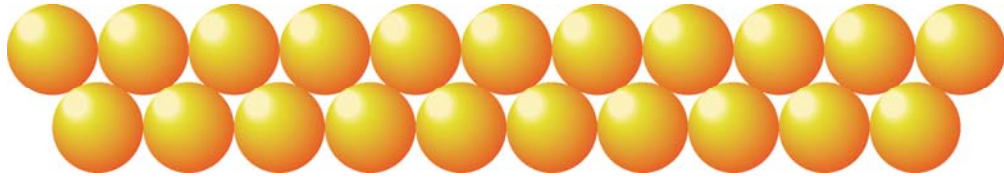
To obtain an indication for the feasibility of the EDGE principle in the food industry we calculated the required total EDGE lengths to produce 1 m³/hr of product based on the experiments we investigated. Table 2 shows the required lengths and virtual system volumes.

Although these lengths, especially for the liquid-liquid systems, seem enormous, the volume of the systems would typically be around 250-300 liter for emulsions and 30 liter for foams, when assuming a thickness of 1 mm for the EDGE microchips, stacked EDGE plates and neglecting the space needed for connections to the outer world. Furthermore, the parallelization of the chips used in this work is still not very efficient, while the microchip design constraint for visual inspection is of course not required for massive scale-up. One may consider a straight-through variant in which EDGE nozzles are constructed vertically like a microsieve to generate a massively parallelized EDGE system, which can decrease the system volume significantly. Although it is not trivial to produce an apparatus as suggested, the important advantages of EDGE technology are the simplicity of the design, the ease of scale-up, robustness of operation and its insensitivity towards fouling. These aspects may turn out to be drivers for further development of this technology.



ACKNOWLEDGEMENTS

The authors thank Riëlle de Ruiter and Peiheng He for performing several measurements and for contributing to stimulating discussions.



Chapter 8

DISCUSSION AND OUTLOOK

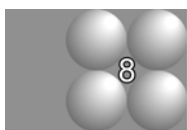
ABSTRACT

This discussion chapter starts by describing shortly how emulsification with microstructured systems is investigated in literature. After this, the strategy used in this work is summarized, which may be instrumental in faster development of (new) emulsification devices. The strategy is illustrated by examples from the chapters in the thesis, and other literature sources. It is aimed at developing insight on the mechanisms of droplet formation captured in scaling relations, which ultimately also leads to generalized rules for scale-up, and suggestions for large-scale emulsification devices, which are presented in the last part of this chapter.

Current emulsification research with microstructured devices

In literature, various emulsification systems have been discussed, and in the last decade, many systems based on microstructured devices have been presented. Much experimental work has been done on all these devices, be it for shear based systems like T- and Y-shaped junctions (De Menech *et al.*, 2008; Steegmans *et al.*, 2009; Van der Graaf *et al.*, 2005), co-flowing or flow-focusing devices (Anna *et al.*, 2003; Umbanhowar *et al.*, 2000; Nisisako and Torii, 2008), or cross-flow membrane emulsification (Abrahamse *et al.*, 2002; Nakashima *et al.*, 1991), or for spontaneous emulsification systems such as microchannels (Kawakatsu *et al.*, 1997; Kobayashi *et al.*, 2002a; Chapter 2 and 3), and EDGE systems (Chapters 4-7). The results are essential for understanding of emulsification, and in general give a good indication of the possibilities and impossibilities of a specific design. However, it is not straightforward to translate the knowledge gained from one particular design to another or to extract the precise effect of system parameters on the process. For this, detailed insight in the emulsification mechanism is needed. Aside from experimental work, a logical instrument in this is through computer simulations.

Abrahamse and coworkers (2001) reported CFD results, and showed that the interfacial tension and the surface properties, as reflected in the contact angle, are major determinants of the droplet size in cross-flow microsieve emulsification. Rayner and coworkers (2004) used the Surface Evolver (a package calculating the interfacial shape under static conditions) for spontaneous microchannel emulsification, and they could predict the droplet size within 8%. Kobayashi and colleagues (2004; 2006) used the volume of fluid (VOF) method which generated insight in the velocities and pressures during droplet formation. Lattice Boltzmann simulations were used by Van der Graaf *et al.* (2006), to describe droplet formation in T-shaped junctions, and they found good agreement with their experimental observations, as was the case in very recent research by Van der Zwan and co-workers (2009a) who applied the same technique to microchannel emulsification.



The simulations do not directly yield insight; it merely shows the consequences of a

limited set of assumptions. When the assumptions in the simulation indeed lead to the correct behavior, a causal relation may be present. However, it is essential that the findings are translated into a framework of understanding, which shows the direct relations between groups of parameters, and the system behavior.

Secondly, even though the VOF and lattice Boltzmann methods are powerful instruments for obtaining insight, the simulations are time-consuming and thus can only be carried out for a limited set of systems and configurations. This has to do with the fact that incorporating interfacial tension effects in any simulation is far from standard procedure. Because of this, considerable time is needed to set-up and validate the computer code, and besides, computing the results takes a lot of time.

For both reasons, it is important that the CFD simulations are interpreted with simpler models that e.g. use geometrical analysis as presented by van der Zwan and co-workers (2009b), to compile and integrate the total understanding of the systems, and to speed-up the design of microdevices for emulsification.

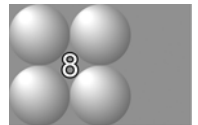
For this, we refer to the schedule in Figure 1 that Allen and Tildersley (1987) presented, giving the relation between experiments, simulations, and theory formation.

In this thesis, we combined experimental work, simulations and analytical models, in a similar way as proposed by Allen and Tildersley, but with some adaptations and extensions. The ultimate goal is developing design rules for practically and economically feasible emulsification devices. If a process is understood in detail, design rules are within reach, as is described in the next section on our design strategy.

Design strategy

Experimental

In order to investigate droplet formation mechanisms in detail, the microchannel emulsification devices were reduced to systems with only one microchannel and equipped with a glass top plate to allow visual observation (Chapter 2). The choice for one channel was also made because it is known that in some microchannel devices communication between channels takes place, which complicates parameter studies on droplet formation.



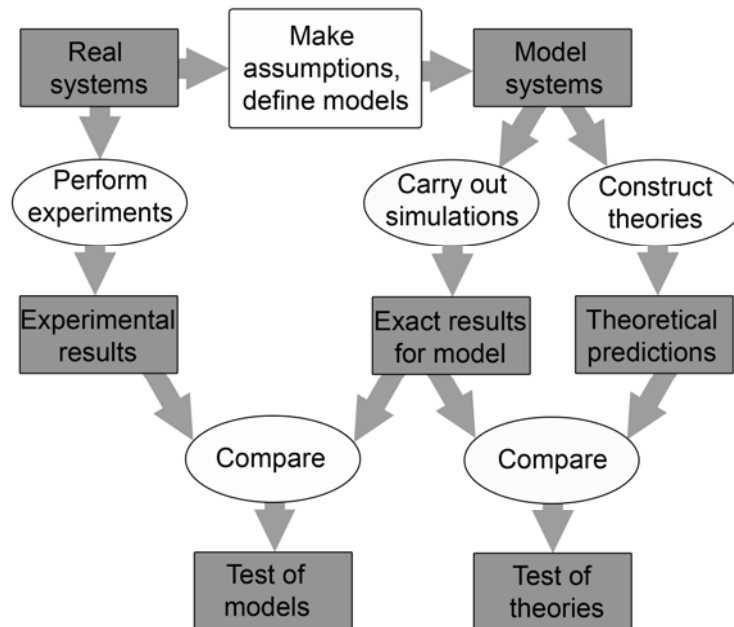
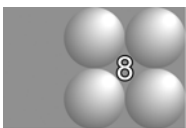


Figure 1. The connection between experiment, theory, and computer simulation according to Allen and Tildesley (Adapted from Allen and Tildesley, 1987).

The ingredients that were used at the beginning of the research were ‘simplified’ into pure and well-defined ingredients such as hexadecane and SDS in water; always keeping the ultimate goal of the production of food emulsions in mind. In this respect, there is a slight difference from Allen and Tildesley, as we propose to carry out experiments with ‘model’ systems also, i.e. strongly reduced in complexity. This is probably also prompted by the complexity of food, in general, which determines our point of view as food technologists.



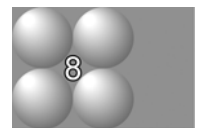
For experiments involving spontaneous droplet formation in microchannels, one should keep in mind that small pressure fluctuations can have a major influence on the flow characteristics, and at the same time, relatively high pressures may be necessary if the interfacial tension between the phases is high. Spontaneous droplet formation is actually an example of the sensitivity to pressure and demonstrates the importance of a properly designed set-up to avoid side effects. As soon as the dispersed phase forms an external droplet of a minimum size, the pressure on the terrace suddenly drops, which results in

outflow of the dispersed phase into the external droplet. This should be fast compared to the inflow from the supply channel: a precise balance between pressure drop between terrace and droplet, and overall pressure drop is needed. This illustrates that a good pressure controlled system is necessary. The applied pressure drives the droplet formation as is indicated in various Chapters in this thesis, and not the applied fluxes or velocities, which may be very different from what one would assume based on the value given by the pump. For example in shear-based Y-junctions, the fluxes can be orders of magnitude different because of the local pressures inside the microchips (Steggmans *et al.*, 2009).

Computational

In Chapter 2 of this thesis, experiments with single grooved microchannels were performed in which a clear effect of the terrace structure was observed. Extraction of understanding of the process was not straightforward however; therefore, a Volume-of-Fluid model incorporated in CD-Adapco's STAR-CD was used to simulate spontaneous droplet formation. The main advantages of this method are that changes in topology are taken into account in detail, that the mass of each flow component is conserved exactly, and the interface shape is not constrained, as is the case in some other methods (James *et al.*, 2004). The interface location is captured as it moves through the grid by tracking the local volume fraction. This should be done with a high resolution reconstruction scheme as the interface curvature determines the Laplace pressure over the interface, and it is therefore important to calculate the curvatures as precisely as possible (see also analytical section). An important limitation of the used method is the impossibility to model dynamic interfacial tension. Incorporating such dynamics, which is far from trivial and also not available in other packages, is still in development and could probably be incorporated within a few years (James *et al.*, 2004). On the other hand, parallelization of the simulation over several computers is relatively easy with this software which is a great advantage to keep the computation time within practical limits.

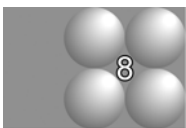
Although it is impossible to simulate reality completely, the CFD simulations performed in this research, based on a set of assumptions which simplify the system, were in reasonable agreement with experimental observations as shown in Chapters 2, 3, and 5,



but more importantly gave useful information about the dynamics of spontaneous droplet formation. Since these calculations are very time consuming in the set-up of the models, and in the calculations themselves, it is not an option to evaluate the design of a microstructure in this way in all its details. Still they are, especially in combination with experiments, a very valuable tool to separately and systematically study the influence of several process parameters that are not easily accessible experimentally. From these findings, the essence of the droplet formation mechanism could be derived, and we found this the biggest benefit of the CFD simulations, since this leads to much better analytical models (the right column in Allen and Tildesley's scheme), which are discussed in the next section. Moreover, we think the CFD models are in this respect essential, and therefore propose to place the right column of the scheme after the simulation steps, not parallel to it, as can be seen in Figure 2.

Analytical

The insights derived from CFD simulations focussed on the local pressures in the system, which have lead to the flux criterion for microchannel systems in Chapter 2 (and a geometrical analysis that describes the minimum size of the droplets for the EDGE system in Chapter 5). Using the flux criterion, a wide range of process conditions and design criteria for microchannels could be evaluated in a matter of hours, using a simple MATLAB script as illustrated in Chapter 2. These simple models are essential in capturing the understanding following from the CFD simulations, are practically useful, and give more insight in the total system behaviour. Developing such models from scratch would have been extremely hard without the CFD results to guide us in choosing the most relevant parameters for microchannel emulsification, which ultimately also lead to the design of the new EDGE system that is presented in this thesis. These models can therefore be seen as the theory formation as indicated by Allen and Tildesley.



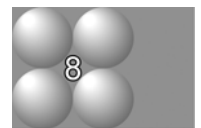
Edge-based Droplet GEneration is introduced in Chapter 4 of this dissertation. It consists of a wide but shallow nozzle in between properly designed oil and water channels (one at each side). It makes use of the insights in Laplace pressures and the terrace-structure function found for the microchannel systems presented in Chapters 2 and 3. In principle,

the biggest resistance in the EDGE emulsification system should be on the plateau in order to fill it up completely and to allow multiple droplet formation that can be controlled easily. Narrowly dispersed emulsion droplets are formed along the edge in a broad pressure range and the system seems to be self-regulating even if there is a disturbance in the flow pattern on the plateau or in the channels. Fundamental questions were raised (Chapter 5), of which we found some of the answers to be similar to those for microchannel emulsification (Chapter 2 and 3). Besides, scale-up (Chapter 6) and the use of food grade ingredients (Chapter 7), were investigated for EDGE, which are both essential for whether the technology can indeed be applied in the practice of food production. For all these questions, we found that EDGE shows genuine promise (as illustrated in the results shown in the various Chapters of this thesis).

We first summarize the strategy that we followed; it is in essence based on the scheme of Allen and Tildesley (1987) with some changes in routes and some extensions to the real application and upscaling. We found that it helped us to evaluate more process conditions than any of the individual techniques (experimental, computational, and analytical) would have allowed us to do.

In Figure 2, our strategy for fundamental understanding leading to design rules and innovation is schematically summarized and illustrated with figures from several Chapters of this thesis. Its steps are:

- I Identification of process of interest, and in this case this was microchannel emulsification.
- II Drastic reduction of complexity of the system, in this case to a single droplet formation unit suitable for inspection.
- IIIa Relatively uncomplicated experiments with simple or well-defined materials under controlled conditions (applied pressure in our case).
- IIIb Extensive simulations of the reduced system allowing some margins for limitations and errors.



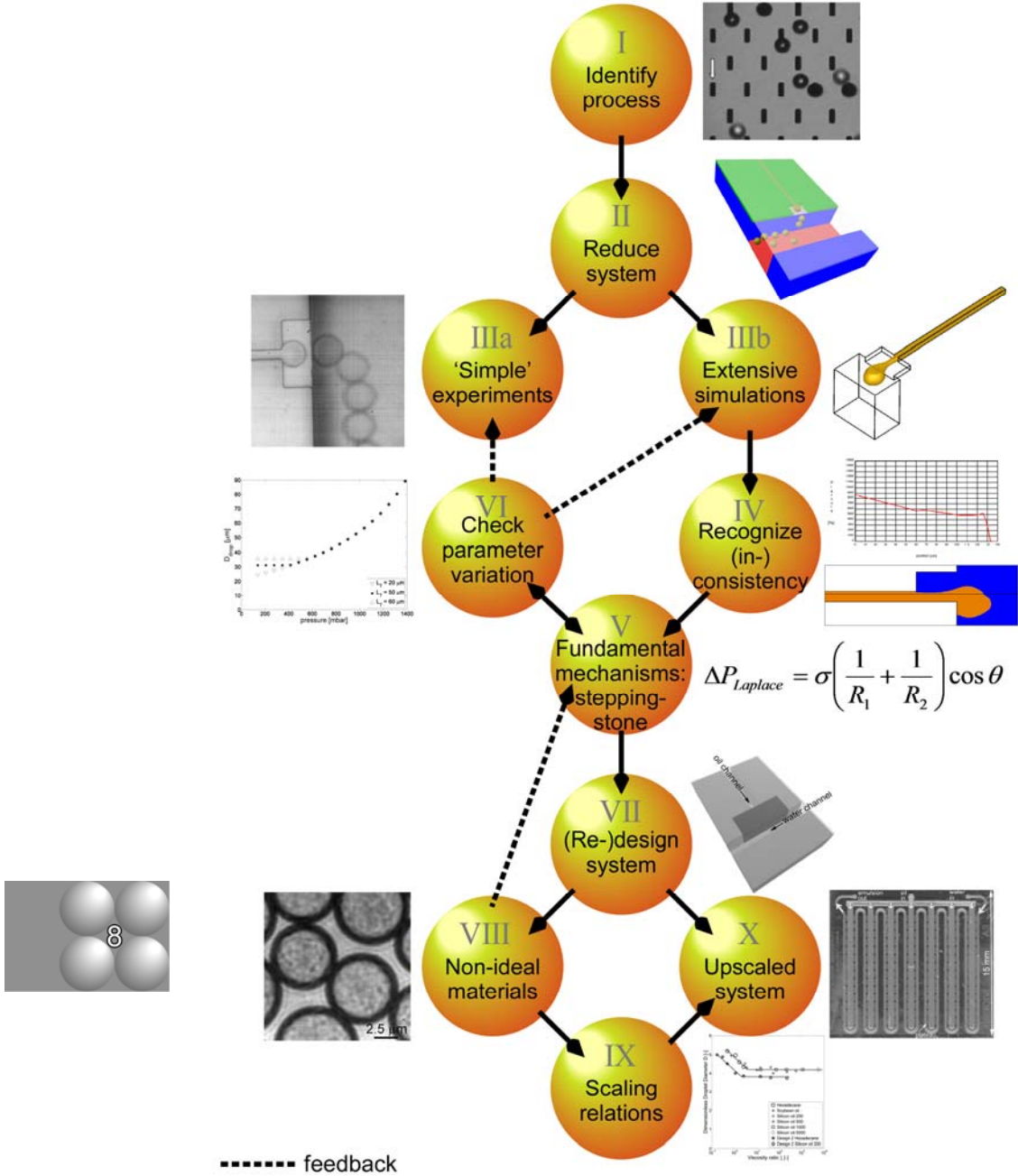
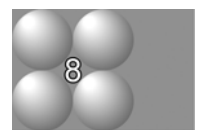


Figure 2. Schematic summary of design strategy followed in this thesis.

-
- IV Extract essential information (parameters) from simulations, and recognize consistencies and inconsistencies in behaviour.
 - V Use the results for defining the fundamental mechanisms, based on well-known physics laws and simple mathematics and use this as a steppingstone for further understanding of more complex behaviour.
 - VI Perform parameter variation with the mechanistic description of the process obtained in step V, and compare with experiments and simulations. Ideally, extend the steppingstone towards more complex behaviour, and derive basic scaling rules.
 - VII (Re-)evaluate system options, including new designs and up-scaled systems.
 - VIII Test the system with non-ideal materials.
 - IX Derive scaling relations for parameters which are beyond the basic model (e.g. estimation of dynamic interfacial tension effects based on a series of simulation at different static interfacial tension). With the knowledge of the process gained until now, one can set up experiments simply and solely focussed on the scaling relation. The scaling relations will be part of the design guidelines in step X.
 - X Set-up a larger scale system using insights obtained in previous steps, operationalized according to design guidelines.

Steps IIIb, IV and V were the most time-consuming research activities, while the actual evaluation based on analytical models hardly took any time. It is expected that our strategy can also be applied to other (emulsification) systems, therewith facilitating faster and better design. Experimental, iterative optimization can lead to a local optimum, while optimization based on fundamental knowledge is expected to lead to the global optimum, therewith directly rewarding the effort put into deriving fundamental mechanistic insights. In order to make this work, a good combination of experimental, computational, and analytical work is needed, and this should become standard procedure in food related research. Various relatively user-friendly computer codes are now available which are able to perform useful simulations of complex multiphase processes, which brings an important step to more detailed understanding of various processes and products within



reach of a larger group or researchers. It is essential to realize that simulations do not have to describe reality exactly, but should cover a limited set of properties and assumptions, and should be used to evaluate whether this set gives rise to the phenomena under study. If so, then a causal relation between the set of properties and the phenomena is likely.

Comparison, scale-up, and outlook

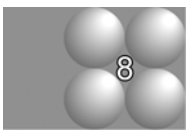
A fair comparison between different microfluidic emulsification systems is not trivial, but we attempted to do so in Chapters 6 and 7; in general, it is known that microchannel and membrane emulsification are closer to EDGE than to the classic techniques. We here compare the EDGE-technology with devices that are more traditional, such as high-pressure homogenisation, colloid milling, or other high-shear devices. We start with general aspects such as droplet size and droplet size distribution, and then discuss more complex matters, such as the layout of a scaled-up EDGE device. Table 1 summarizes this comparison.

The EDGE devices reported in this thesis are all capable of producing emulsions with much narrower droplet size distributions than the traditional devices. As for any microtechnological emulsification technique, the process conditions are much gentler, and

Table 1. Comparison traditional emulsification and EDGE.

	Traditional techniques	EDGE
Size distribution	-	+
Droplet size	0	0
Throughput	+	-
Energy efficiency	-	+
Gentle processing	-	+
Costs	+	-
Process control	-	+
Fouling	0	*

+ good, 0 reasonable, - poor *no problems with the systems tested until now

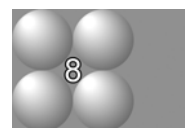


this also allows production of e.g. double emulsions, that otherwise cannot be produced without disrupting the internal phase. Besides, process control is much easier for EDGE, as the height of the droplet formation unit mainly determines the droplet size, and the resistance on the plateau needs to be high compared to other resistances in the system, in order to control the system completely. For classic emulsification technology, process control is not straightforward, only some empirical relations between energy input and droplet size are available.

Although microfluidic devices become more common practice in the research environment, there is still a big challenge in producing sub-micron droplets, as is also the case for traditional techniques. The biggest challenge for EDGE is however the throughput which is low in one microdevice but will obviously be larger in a scaled-up version. The conventional emulsification devices already operate on large scale and therefore have a big advantage in this respect. In a scaled-up EDGE, also the surface properties of the device should be properly maintained since this is of direct influence on emulsification, as is also lined out in Chapter 5. Until now however, no problems with fouling were observed over several days of continuous operation, and in between runs.

The strong interest of various industries and academic groups in producing equally sized small droplets in a gentle way, leads us to believe that a scaled-up process is relevant. If we focus on EDGE, droplet sizes are in the size range which is suitable for many applications, and it can be expected that the size can be reduced further, given the straightforward scaling relation between droplet size and plateau height. A first step in parallelization was made in Chapter 6 of this thesis. Unlike the microchannel systems and cross-flow membrane emulsification, the EDGE droplet formation units are all active at the same time, without pressure dependent channel activation as observed in straight through microchannel systems. Besides, we expect that given the simplicity of the EDGE design, manufacturing is easier compared to that of more complex structures.

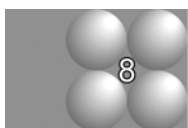
In Chapter 7 some basic calculations for the device volumes of a system producing $1 \text{ m}^3/\text{hr}$ of product are given. These volumes are well within reach, especially for foam production as the system volume indication is as low as 4 litres. Although it is not trivial



to fabricate such systems (and it is expected to be expensive), it shows good prospect for further maturation of the EDGE technology. For the food industry, the devices need to be big given typical high throughputs, but for the pharmaceutical industry, the volumes are considerably less because the focus is more on monodispersity than on bulk production, and application could be easier to realise. Alternatively, small-scale production in on-demand machines, with which consumers can choose their specific products demands at home or in the supermarket, and the product is made instantaneously, could be an interesting way to go.

EDGE is in theory not restricted to emulsions and foams; also, aerosols or sprays are expected to be possible products, and this could lead to an interesting spin-off in e.g. spray-drying processes (Wu *et al.*, 2007) in various industries. The high-pressure nozzles in conventional spray towers give a wide size distribution, and therewith, a difference in drying behaviour in the various droplets, resulting in product quality differences, which makes it difficult to optimize the process. If the drying process could be started with similarly sized droplets, the process conditions are better controlled for each particle and thus less variety is expected, which enables better overall product quality and probably higher process efficiency as well.

Away from large-scale applications, in medical applications a benefit can be expected if droplets generated by e.g. an inhaler are of a specific size. In that case, it would be possible to direct the droplets to a position in the patient where the medicine is most effective, and therewith, reduce side effects (Higashi *et al.*, 1995). Although one inhaler is not big in size, the total market for inhalers could still make EDGE an interesting new concept.



Fabrication of EDGE structures is quite simple; there is only one dimension that needs to be very precisely defined and maintained and that is the height of the plateau. For viscous dispersed phases, it is important to have droplet formation units which are not too long, because the resistance will be unnecessarily high, but still this dimension can be hundreds of times the height of the plateau, and should not be an issue in the production of EDGE-devices. In addition, the systems that have been developed in this thesis are not yet fully

optimised. Improvements are possible with plateaus that may contain a sequence of plateau heights, or that are tapered.

New techniques for multi-stack bonding of more than 20 glass wafers have become available. They result in monolithic glass devices with an internal volume over 100 ml, therewith indicating that it is technically feasible to increase throughput volumes in microchip technology (www.micronit.com). Additionally, for a multiple stack of EDGE plates, precisely aligning the edges seems to be not important, given the structure of the EDGE-systems tested in this thesis, and this may well give considerable flexibility for the design of a large-scale system, as is reflected in some of the suggestions for scale-up shown in Figure 3.

A logical starting point for scale-up would be a design similar to the straight-through microchannels presented by Kobayashi *et al.* (2002a) (Figure 3a). Although it is currently impossible to fabricate a slit with an extreme aspect ratio, as preferred for EDGE, it would

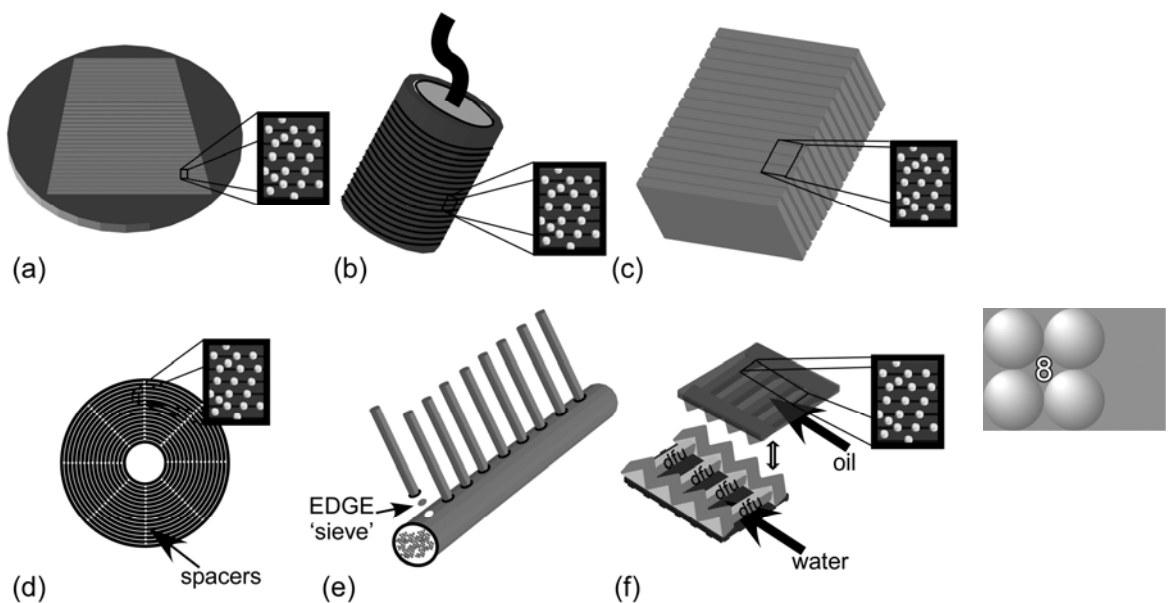
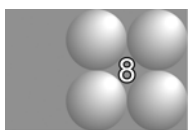


Figure 3. Several suggestions for upscaled EDGE systems. Only the plateau depth and the applied pressure on the dispersed phase need to be controlled precisely.

be a very efficient way to parallelize the EDGE system. The micro- or even nano-technological mechanical engineering techniques are developing quickly and it is expected that this will become a viable concept in the near future.

For cleaning purposes, a system that can be disassembled and reassembled easily is preferable. One can think of stacked flat plates or rings of any well-defined and rigid material (Figure 3b and c) kept apart by appropriate spacers. In Liquid Crystal Displays, silica or polymeric spacers are used to maintain the cell gap (the distance) between the front and rear pieces of glass used to make the display and this cell gap has comparable dimensions as needed for the EDGE systems presented in this thesis. Kim *et al.* (2007) prepared spacers which can be used for flexible LCD applications, and these may be applied in EDGE systems as well, therewith tackling mechanical fragility and brittleness issues (Figure 3d, showing a flexible layer wound into a spiral, while spacers keep the distance fixed). Alternatively, accurate spraying or printing techniques could be used to produce thin layers that can act as spacer. All these new developments could lead to a structure comparable to a microsieve, with high DFU density, better cleanability, and robustness.

Recently, Unnikrishnan and co-workers (2009) developed a ‘plug-and-play’ platform which is compatible with standard Swagelok connectors. Depending on the desired droplet size, a suitable connector with the correct EDGE device (like in Figure 3a and 2d) can be plugged onto the large channel, and if multiple connections to a relatively large continuous phase channel can be realized as shown schematically in Figure 3e, a convenient apparatus can be developed, which can be applied in a flexible way. The ‘zipper’ construction in Figure 3f is another initial idea which could facilitate easier cleaning. Ideally, by pressing the two parts in each other, two channels with slits in between are formed. To clean the DFU, the two parts can be separated resulting in easy access to the plateaus. The idea is to fit precisely defined ‘large’ structures into or onto each other therewith defining the small structures, i.e. plateaus and oil and water channels, automatically.

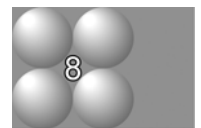


Regarding the choice of material, it is desirable to choose a material that is not wetted by the to-be-dispersed phase (Chapter 5). However, this may not always be compatible with the other requirements that need to be met for the production of the structure. Therefore, surface modification is an interesting tool to influence or stabilize the surface properties, and possibly, prevent fouling, although fouling has not been an issue in EDGE systems tested so far.

Naturally, the design of an up-scaled system is not limited to the options and ideas mentioned here; and several challenges remain for the (food) engineers and technologists working on improved emulsification procedures. Production and design of new devices is far from done, but it is our expectation that ultimately it will result in a commercially attractive alternative for the traditional devices.

Final remarks

Emulsification with microstructures has been an important research topic for the last twenty years, and given the recent developments, it is expected that this technology will become available for larger scale production of monodisperse single and double emulsions. For this, the advances in process understanding and design, as described in this thesis, in fabrication methods of microfluidic systems, and in surface modification research, need to come together in a large-scale production apparatus. Given the current speed at which developments are taking place, it should only be a matter of time before emulsions can be produced in a much more controlled and efficient way by microtechnological devices, even at the large throughputs required in food industry.



REFERENCES

- Abrahamse, A. J.; van der Padt, A.; Boom, R. M.; de Heij, W. B. C. *AIChE J.* **2001**, 47, 1285.
- Abrahamse, A. J.; van der Padt, A.; Boom, R. M. *J. Membr. Sci.* **2002**, 204, 125.
- Allen, M. P. and Tildesley, D. J. *Computer Simulation of Liquids* **1987** Oxford University Press, Oxford, United Kingdom.
- Anna, S. L.; Bontoux, N.; Stone, H. A. *Appl. Phys. Lett.* **2003**, 82, 364.
- Bals, A. and Kulozik, U. *J. Membr. Sci.* **2003**, 220, 5.
- Brackbill, J. U.; Kothe, D. B.; Zemach, C. *J. Comput. Phys.* **1992**, 100, 335.
- De Menech, M.; Garstecki, P.; Jousse, F.; Stone, H. A. *J. of Fluid Mechanics* **2008**, 595, 141.
- Garstecki, P.; Gitlin, I.; DiLuzio, W.; Whitesides, G. M.; Kumacheva, E.; Stone, H. A. *Applied Physics Letters* **2004**, 85, 2649.
- Garstecki, P.; Fuerstman, M. J.; Stone, H. A.; Whitesides, G. M. *Lab Chip* **2006**, 6, 437.
- Garti, N. and Bisperink, C. *Current Opinion in Colloid & Interface Science* **1998**, 3, 657.
- Gijsbertsen-Abrahamse, A. J.; van der Padt, A.; Boom, R. M. *AIChE J.* **2004**, 50, 1364.
- Hashimoto, M.; Shevkoplyas, S. S.; Zasonska, B.; Szymborski, T.; Garstecki, P.; Whitesides, G. M. *Small* **2008**, 4, 1795.
- Higashi, S.; Shimizu, M.; Nakashima, T.; Iwata, K.; Uchiyama, F.; Tateno, S.; Tamura, S.; Setoguchi, T. *Cancer* **1995**, 75, 1245.
- James, A. J. and Lowengrub, J. *J. of Computational Physics* **2004**, 201, 685.

References

- Kawakatsu, T.; Kikuchi, Y.; Nakajima, M. *J. Am. Oil Chem. Soc.* **1997**, 74, 317.
- Kawakatsu, T.; Trägårdh, G.; Kikuchi, Y.; Nakajima, M.; Komori, H.; Yonemoto, T. *J. Surfactants Deterg.* **2000**, 3, 295.
- Kawakatsu, T.; Trägårdh, G.; Trägårdh, C. *Colloids and Surfaces A - Physicochemical and Engineering Aspects*, **2001**, 189, 257.
- Kim, E. H.; Kim, S. Y.; Kim, S. S. *Molecular Crystals and Liquid Crystals* **2007**, 464, 799.
- Kobayashi, I.; Nakajima, M.; Nabetani, H.; Kikuchi, Y.; Shohno, A.; Satoh, K. *J. Am. Oil Chem. Soc.* **2001**, 78, 797.
- Kobayashi, I.; Nakajima, M.; Chun, K.; Kikuchi, Y.; Fujita, H. *AIChE J.* **2002a**, 48, 1639.
- Kobayashi, I.; Nakajima, M.; *Eur. J. Lipid Sci. Technol.* **2002b**, 104, 720.
- Kobayashi, I.; Mukataka, S.; Nakajima, M. *Langmuir* **2004**, 20, 9868.
- Kobayashi, I.; Mukataka, S.; Nakajima, M. *Langmuir* **2005a**, 21, 5722.
- Kobayashi, I.; Mukataka, S.; Nakajima, M. *Langmuir* **2005b**, 21, 7629.
- Kobayashi, I.; Mukataka, S.; Nakajima, M. *Ind. Eng. Chem. Res.* **2005c**, 44, 5852.
- Kobayashi, I.; Lou, X.; Mukataka, S.; Nakajima, M. *JAACS* **2005d**, 82, 65.
- Kobayashi, I.; Uemura, K.; Nakajima, M. *J. Chem. Eng. Jpn.* **2006**, 39, 855.
- Kobayashi, I.; Uemura, K.; Nakajima, M. *Colloids Surf. A* **2007**, 296, 285.
- Kobayashi, I.; Takayuki, T.; Meada, R.; Yoshihiro, W.; Uemura, K.; Nakajima, M. *Microfluid Nanofluid* **2008**, 4, 167.
- Lago, M.; Araujo, M. *Physica A* **2003**, 319, 175.
- Lambrich, U.; Van der Graaf, S.; Dekkers, K. S.; Boom, R. M.; Schubert, H. In *Proceedings ICEF 9*, **2004**, Montpellier, France.

-
- Link, D. R.; Anna, S. L.; Weitz, D. A.; Stone, H. A. *Phys. Rev. Lett.* **2004**, 92.
 - Lucassen-Reynders, E. H.; Kuijpers, K. A. *Colloids and Surfaces* **1992**, 65, 175.
 - McClements, D. J. *Food Emulsions: Principles, Practice, and Techniques* **1999** CRC Press: Boca Raton, United States.
 - Mine, Y.; Shimizu, M.; Nakashima, T. *Colloids and Surfaces B-Biointerfaces* **1996**, 6, 261.
 - Muller-Fischer, N.; Bleuler, H.; Windhab, E. J. *Chemical Engineering Science* **2007** 62, 4409.
 - Nakahara, H.; Shibata, O.; Rusdi, M.; Moroi, Y. *Journal of Physical Chemistry C* **2008**, 112, 6398.
 - Nakaya, K., Kohata, T., Doisaki, N., Ushio, H., Ohshima, T. *Journal Fisheries Science* **2006**, 72, 877.
 - Nakashima, T.; Shimizu, M.; Kukizaki, M. *Key Eng. Mater.* **1991**, 61/62, 513.
 - Nisisako, T.; Torii, T.; Higuchi, T. *Lab on a Chip* **2002**, 2, 24.
 - Nisisako, T. and Torii, T. *Lab on a Chip* **2008**, 8, 287.
 - Rayner, M.; Trägårdh, G.; Trägårdh, C.; Dejmek, P. *J. Colloid Interface Sci.* **2004**, 279, 175.
 - Sagis, L. M. C.; de Ruiter, R.; Miranda, F. J. R.; de Ruiter, J.; Schroën, K.; van Aelst, A. C.; Kieft, H.; Boom, R.; van der Linden, E. *Langmuir* **2008**, 24, 1608.
 - Saint-Jalmes, A.; Vera, M. U.; Durian, D. J. *European Physical Journal B* **1999**, 12, 67.
 - Saito, M.; Yin, L.-J.; Kobayashi, I.; Nakajima, M. *Food Hydrocolloids* **2005**, 19, 745.
 - Saito, M.; Yin, L.J.; Kobayashi, I.; Nakajima, M. *Food Hydrocolloids* **2006**, 20, 1020.

References

- Sasaki, M.; Yasunaga, T.; Tatsumoto, N. *Bull. Chem. Soc. Jpn.* **1977**, 50, 858.
- Schröder, V. and Schubert, H. *Colloids Surf. A* **1999**, 152, 103.
- Steegmans, M. L. J.; Schroën, K.; Boom, R. M. *Langmuir* **2009**, 25, 3396.
- Sugiura, S.; Nakajima, M.; Tong, J.; Nabetani, H.; Seki, M. *J. Colloid Interface Sci.* **2000**, 227, 95.
- Sugiura, S.; Nakajima, M.; Iwamoto, S.; Seki, M. *Langmuir* **2001** 17, 5562.
- Sugiura, S.; Nakajima, M.; Kumazawa, N.; Iwamoto, S.; Seki, M. *J. Phys. Chem. B* **2002a**, 106, 9405.
- Sugiura, S.; Nakajima, M.; Seki, M. *Langmuir* **2002b**, 18, 5708.
- Sugiura, S.; Nakajima, M.; Seki, M. *Langmuir* **2002c**, 18, 3854.
- Sugiura, S.; Nakajima, M.; Seki, M. *Ind. Eng. Chem. Res.* **2004a**, 43, 8233.
- Sugiura, S.; Nakajima, M.; Oda, T.; Satake, M.; Seki, M. *J. Colloid Interface Sci.* **2004b**, 269, 178.
- Tan, Y.-C. and Lee, A. P. *Lab on a Chip* **2005**, 5, 1178.
- Tan, Y.-C.; Cristini, V.; Lee, A. P. *Sensors and Actuators B – Chemical* **2006**, 114, 350.
- This, H. *EMBO reports* **2006**, 7, 1062.
- Tong, J.; Nakajima, M.; Nabetani, H.; Kikuchi, Y.; Maruta, Y. *J. Colloid Interface Sci.* **2001**, 237, 239.
- Umbanhowar, P. B.; Prasad, V.; Weitz, D. A. *Langmuir* **2000**, 16, 347.
- Unnikrishnan, S.; Jansen, H.; Berenschot, E.; Mogulkoc, B.; Elwenspoek, M. *Lab Chip* **2009**, 9, 1966.
- Utada, A. S.; Chu, L.-Y.; Fernandez-Nieves, A.; Link, D. R.; Holtze, C.; Weitz, D. A. *MRS Bulletin* **2007**, 32, 702.

-
- van der Graaf, S.; Steegmans, M. L. J.; van der Sman, R. G. M.; Schroën, C. G. P. H.; Boom, R.M. *Colloids Surf. A* **2005**, 266, 106.
 - van der Graaf, S.; Nisisako, T.; Schroën, C. G. P. H.; van der Sman, R. G. M.; Boom, R. M. *Langmuir* **2006**, 22, 4144.
 - van der Zwan, E.; van der Sman, R.; Schroën, K.; Boom, R.M. *J. Colloid Interface Sci.* **2009a**, 335, 112.
 - van der Zwan, E.; Schroën, K.; Boom, R. M. *Langmuir* **2009b**, 25, 7320.
 - van Dijke, K. C.; Schroën, K.; Boom, R. M. In: *Proceedings of the 8th World Congress of Chemical Engineering* **2009** Montréal, in press
 - Van Rijn, C. J. M. and Elwenspoek, M. C. In *Technical Proceedings of the International Conference on Micro Electro Mechanical Systems (MEMS)* **1995**, Amsterdam, The Netherlands.
 - Vladislavljević, G. T.; Kobayashi, I.; Nakajima, M. *Powder Techn.* **2008**, 183, 37.
 - Vlahovska, P. M.; Danov, K. D.; Mehreteab, A.; Broze, G. *J. Colloid Interface Sci.* **1997**, 192, 194.
 - Walstra, P. *Physical Chemistry of Foods.* **2003**, Marcel Dekker Inc., New York, United States.
 - Walstra, P.; Geurts, T. J.; Wouters, J. T. M. *Dairy Science and Technology* (2nd edition). **2006** CRC Press, Boca Raton, United States.
 - Wooster, T. J., Golding, M., Sanguansri, P. *Langmuir* **2008**, 24, 12758.
 - Wrangham, R. *Catching Fire How cooking made us human.* **2009** Basic Books, New York, United States.
 - Wu, W. D.; Patel, K. C.; Rogers, S.; Chen, X. D. *Drying Technology* **2007**, 25, 1907.
 - Xu, Q. and Nakajima, M. *Appl. Phys. Lett.* **2004**, 85, 3726.

References

- Yasuno, M.; Suguira, S.; Iwamoto, S.; Nakajima, M.; Shono, A.; Satoh, K. *AIChE J.* **2004**, 50, 3227.

Internet:

- www.elbulli.com
- www.nanomi.com
- www.micronit.com

SUMMARY

A dispersion is a multiphase product in which at least one phase is dispersed into another phase. In emulsions, those phases are immiscible liquids, for example oil and water. Many products which we use in everyday life are emulsions. One can think of ointments, paints, or sun protection cream, but the largest variety of emulsion-based products can be found in food: butter, mayonnaise, cream, milk, salad dressings (like vinaigrettes), soups, sauces, ice cream, and margarine are some examples. Emulsions are generally thermodynamically unstable and they tend to separate into the original phases in due time. The droplet size and the droplet size distribution are two important properties of an emulsion that have influence on the stability, but also the taste and appearance.

Traditional emulsification techniques are based on disrupting larger droplets in coarse pre-mix emulsions into smaller ones using intense force fields. A lot of energy is put into the product; almost all energy dissipates into heat and only a very small fraction is used to form the emulsion. In addition, the resulting emulsions have a wide droplet size distribution. New microtechnological emulsification techniques hold a large advantage over conventional techniques as they can produce narrowly dispersed emulsions, while using the energy much more efficiently for the formation of droplets. This implies that the process is much milder, therewith allowing production of shear and temperature sensitive products such as multiple emulsions, which have great potential for reduced calorie products or encapsulation of (healthy) components but cannot be produced with traditional methods.

With these microtechnological techniques, droplets of the desired size are directly generated with a device that is structured on the same scale as the droplets itself. In general, one can divide these emulsification techniques into two categories based on the driving force: shear-induced and spontaneous droplet generation. In the first category, cross- or co-flow of the continuous phase is used to snap off droplets. In the second category, interfacial tension forces cause droplet snap off without the need of a flow field. These latter devices show the highest potential for the production of monodisperse

emulsions. Given the potential of these emulsions for a variety of purposes, this thesis focuses on these microtechnological emulsification systems. The goal of this thesis was to gain a thorough understanding of the principles and dynamics of spontaneous droplet generation, and to use this understanding to design better devices, for improved product properties at reasonable throughput.

In Chapter 2, experimental observations and extensive Computational Fluid Dynamics simulations of a so-called terrace system are combined into an analytical predictive model, based on the analysis of local pressures in the device. This model was shown to have good predictive value and to give direct insight in the relevant process parameters. Based on that, the terrace structure itself could be evaluated, and various design rules could be derived. The analytical model was also used as a steppingstone to gain insight in complex phenomena such as dynamic interfacial tension effects and contact angle (surface properties) of the used microdevices.

In Chapter 3, the ratio of the viscosities of the dispersed and the continuous phases was found to be an important parameter for droplet formation in terrace-based systems. At high viscosity ratios, the droplet size is constant, but below a critical value droplet size increases, and below a minimum value no droplet formation is possible. These characteristic ratios were found to be dependent on the device geometry, both experimentally and through CFD simulation. The inflow of continuous phase is relatively difficult at low viscosity ratios, resulting in steep pressure gradients on the terrace structure which result in more oil supply during droplet formation, which in turn results in larger droplets.

Detailed understanding of the existing spontaneous droplet formation in microchannel systems resulted in a new design: Edge-based Droplet GEneration (EDGE), which is described in Chapter 4. In EDGE, droplets are formed simultaneously along the edge of a wide but shallow nozzle, in contrast to the terrace systems discussed in Chapters 2 and 3 where only one droplet is formed at a time. With EDGE, narrowly dispersed emulsion droplets were formed in a broad pressure range. The system seems self-regulating: a

disturbance in the flow pattern does not influence the droplet formation. The droplet size scales with the height of the droplet formation unit by a factor 5.5 – 6.5.

Fundamental aspects related to EDGE are discussed in Chapter 5; especially the filling of the plateau was found to be essential for multiple droplet formation. Crucial for this is the difference in pressure needed for the dispersed phase to invade the plateau and the pressure needed to flow over the edge at the other end. In addition, the nozzle needs to have a relatively high hydrodynamic resistance compared to the whole system, which ensures even oil supply to the plateau and complete filling. The droplet formation locations along the nozzle were found to be regularly distributed along the length of the nozzle, and to be dependent on plateau depth. The EDGE process was simulated with CFD, which revealed that the pressure distribution on the plateau is influenced only very locally by droplet formation, therewith explaining the robust behavior of EDGE systems. Also for EDGE, viscosity ratio was found to be an important parameter. Behavior similar to that described for terrace structures (Chapter 3) was found, therewith also explaining the differences in size between liquid droplets in emulsification and gas bubbles in foaming. The minimum droplet size that can be obtained with EDGE could be derived from a geometric model that includes contact angle effects.

EDGE has an advantage over microchannel systems mainly due to its simple structure, robustness, and parallelization possibilities as discussed in Chapter 6. An important design criterion when parallelizing droplet formation units is designing both oil supply and emulsion drainage channels properly, i.e. minimizing the pressure drops in these channels to obtain similar pressure conditions for each nozzle. The shape of the plateau may further be tuned to the properties of the phases (especially viscosity is important), to obtain a more stable process.

Many microfluidic droplet generation devices can generate equally sized droplets, but emulsions with droplets below 10 micrometer are not common. Similarly, many devices have limitations in the types of ingredients that can be used, due to their small dimensions. Unfortunately, food-grade ingredients often pose problems. We found in Chapter 7 that EDGE is rather tolerant in the type of ingredients used. Some examples of food-grade

Summary

dispersions are shown; for example, sunflower oil in whey protein concentrate gave an emulsion with an average droplet size of about 7 micron and very stable process operation. Furthermore, food-grade double emulsions (again 7 micron droplet size) were produced, and foams of whey protein (with a bubble size of 30 micron). This indicates the suitability of EDGE for products that otherwise cannot be made, and together with the sizes of scaled-up versions, this shows that EDGE could be a truly interesting new technology for the food industry.

The last chapter in this thesis discusses the research strategy followed in this project. The combination of experiments with computational modeling of fluid dynamics, and relatively simple analytical or geometric models is shown to be a very effective method for investigating complex systems, to obtain fast process understanding and for further development of the devices. EDGE has several possibilities to increase production capacity, and this together with the advances in precision engineering is expected to make large-scale application of emulsification with EDGE microstructures a possibility in the near future.

SAMENVATTING

Een dispersie is een product waarin minstens één fase is gedispergeerd in een andere fase. In emulsies zijn deze fasen niet mengbare vloeistoffen, bijvoorbeeld olie en water. Een heleboel producten die we dagelijks gebruiken zijn emulsies. Zalf, verf, zonnebrandcrème zijn bekende voorbeelden, maar de meeste emulsies vindt men terug in levensmiddelen: boter, mayonaise, room, melk, salade dressings (zoals vinaigrettes), soepen, sauzen, roomijs en margarine zijn enkele voorbeelden. Emulsies zijn over het algemeen thermodynamisch instabiel en hebben de neiging om na verloop van tijd te scheiden in de verschillende fasen waaruit de emulsie is gemaakt. De druppelgrootte en de druppelgrootteverdeling van emulsies zijn twee belangrijke eigenschappen die de stabiliteit beïnvloeden, evenals het uiterlijk en de smaak.

Traditionele technieken om emulsies te maken zijn gebaseerd op het gebruik van brute kracht waarmee een ruwe (zogenaamde premix) emulsie wordt verfijnd. Hierbij wordt erg veel energie gebruikt, die bijna allemaal wordt omgezet in (ongewenste) warmte en daarom is het erg lastig om druppels van gelijke grootte te verkrijgen; het produceren van emulsies verloopt zeker verre van optimaal. Nieuwe emulgeertechnieken met behulp van microstructuren hebben een belangrijk voordeel ten opzichte van de traditionele methoden. Hiermee kunnen namelijk wel op een energie-efficiënte manier nagenoeg gelijke druppels worden gemaakt. Bij deze technieken wordt weinig kracht op de druppels uitgeoefend waardoor het zelfs mogelijk wordt om producten die gevoelig zijn voor deze krachten en temperatuurseffecten, zoals dubbele emulsies, te maken terwijl dat met traditionele methoden niet mogelijk is. Dubbele emulsies hebben een enorme potentie omdat ze kunnen dienen als basis voor calorie arme producten of voor incapsulatie van (gezonde) ingrediënten.

Door moderne microtechnologische apparaatjes, is het mogelijk om druppels te fabriceren in dezelfde orde van grootte als de kleinste dimensie van de structuren. De emulgeerprocessen die zich afspelen in deze apparaatjes kunnen grofweg worden ingedeeld in twee categorieën, gebaseerd op de drijvende kracht: afschuiving gerelateerde

en spontane druppelvorming. Bij de eerstgenoemde categorie snoert een snel stromende continue fase druppels af van de andere fase die uit een kanaaltje stroomt. Bij spontane druppelvorming worden druppels gevormd door grensvlakspanningskrachten zonder dat daarbij stroming van de continue fase is vereist. De laatste categorie lijkt de meeste potentie voor het maken van gelijkgroter druppels te hebben en gezien het grote potentieel voor dit type emulsies focussen we in dit onderzoek op die systemen. Het doel van dit onderzoek was om grondige kennis te verzamelen over de principes van spontane druppelvorming, en deze kennis toe te passen om zo te komen tot betere processen voor verbeterde producten die op redelijke schaal geproduceerd kunnen worden.

In hoofdstuk 2 zijn experimentele waarnemingen en resultaten van uitgebreide vloeistofdynamica modellen van zogenaamde terras-systemen gecombineerd tot een analytisch voorspellend model op basis van lokale drukken. Het model heeft goede voorspellende waarde en geeft direct inzicht in procesparameters waardoor ontwerpregels kunnen worden afgeleid, ook voor de terrasstructuur. Deze relatief simpele beschrijving is gebruikt als springplank om inzicht te verkrijgen in complexer gedrag zoals dynamische grensvlakspanningseffecten en contacthoeken van de fasen met de gebruikte microstructuren.

In hoofdstuk 3 is gevonden dat de viscositeitsratio van beide fasen een belangrijke parameter is voor het druppelvormingsproces in de terrassystemen. Bij een hoge viscositeitsratio is de druppelgrootte constant, onder een kritische waarde worden echter grotere druppels gevormd en beneden de minimale ratio is er geen druppelvorming meer mogelijk. Uit zowel de experimenten als uit de computersimulaties bleek dat deze karakteristieke waarden afhankelijk zijn van het systeemontwerp. De instroom van continue fase in de microstructuur (terras) is relatief lastig bij lage ratio, waardoor steile drukgradiënten op het terras ontstaan die resulteren in grotere olie toevoer, en dus grotere druppels.

Gedetailleerde kennis over spontane druppelvorming in de eerder genoemde microkanaalsystemen resulteerde in een nieuw ontwerp: Edge-based Droplet GEneration (EDGE), welke in hoofdstuk 4 wordt geïntroduceerd. In EDGE worden meerdere druppels

tegelijkertijd aan de rand van een brede, ondiepe sleuf gevormd, dit in tegenstelling tot de terrassystemen uit hoofdstuk 2 en 3 waar altijd één druppel gelijktijdig gevormd wordt. Met EDGE, worden druppels van nagenoeg gelijke grootte over een breed drukgebied stabiel gegenereerd en het systeem lijkt zelfregulerend als er een verstoring van het stromingsprofiel optreedt. De druppelgrootte schaalt met een factor 5.5-6.5 met de hoogte van de druppelgenerator.

Fundamentele aspecten van het EDGE principe worden in hoofdstuk 5 beschreven; vooral het opvullen van de plateaus is essentieel in om deze systemen tot meerdere druppels tegelijkertijd te komen. Hiervoor is een voldoende groot verschil nodig tussen de druk die nodig is om over het plateau te stromen (spreiden) en om druppels te maken. Daarnaast dient de microstructuur de hoogste stromingsweerstand in het systeem te hebben om voldoende olietoevoer en volledig vullen van het plateau te garanderen. De locaties aan de rand waar druppels gevormd worden bleken regelmatig te zijn verdeeld over de beschikbare lengte en afhankelijk te zijn van de plateaudiepte. Het EDGE proces is met CFD software gesimuleerd, en daaruit volgde dat de drukgradiënten op het plateau beperkt zijn tot een klein gebied, wat ook de stabiliteit van het gehele systeem verklaart. Daarnaast bleek ook hier de viscositeitsratio een belangrijke procesparameter en het verschil in grootte tussen oliedruppel en luchtbel kon hiermee worden opgehelderd. Een minimale druppelgrootte die met EDGE kan worden verkregen kan worden afgeleid met een puur geometrisch model dat ook de invloed van de contacthoek meeneemt.

In hoofdstuk 6 is beschreven dat EDGE systemen een groot voordeel hebben ten opzichte van andere microtechnologische systemen doordat het relatief simpele structuren zijn, het een robuust proces is en het goed op te schalen is. Belangrijk is wel dat de toevoer- en afvoerkanalen goed worden ontworpen zodat grote drukgradiënten worden voorkomen en vergelijkbare condities bij elk plateau in het systeem opgelegd kunnen worden. De vorm van de plateaus kan worden aangepast aan de eigenschappen van de fasen (vooral viscositeit is van belang) om een stabiel proces te krijgen.

Veel micro druppelgenerators kunnen druppels van gelijke grootte produceren, maar slechts enkele systemen kunnen dit als het om druppels kleiner dan 10 micrometer gaat.

Daarbij is de keuze aan ingrediënten beperkt als gevolg van de schaal van de structuur; helaas geven ‘food-grade’ ingrediënten vaak problemen. In hoofdstuk 7 laten we zien dat EDGE weinig beperkingen kent wat betreft ingrediënten en stabiele procesvoering. Als voorbeeld is zonnebloemolie in een wei-eiwit oplossing geëmulgeerd, waarbij druppels van 7 micron werden verkregen. Verder is een ‘food-grade’ dubbele emulsie in magere melk gemaakt (ook hier waren de druppels 7 micrometer) en zijn schuimen gemaakt met melkeiwit (met een belgrootte van ongeveer 30 micron). Deze testen geven aan dat EDGE geschikt is om producten te maken die anders niet gemaakt kunnen worden. Samen met de dimensies van de opgeschaalde EDGE apparaten, geeft dit aan dat EDGE een waarlijk interessante nieuwe technologie is voor de levensmiddelenindustrie.

Het laatste hoofdstuk in dit proefschrift beschrijft de onderzoeksstrategie die gebruikt is tijdens dit project. De combinatie van experimenten, uitgebreide computersimulaties en analytische modellen bleek erg effectief om complexe systemen te onderzoeken en snel tot procesbegrip en ontwikkeling te komen. Voor EDGE bestaan verschillende opties voor opschaling om tot een hogere productiviteit te komen. Door deze opschalingstap, samen met de vooruitgang in de fijnmechanische productie mag worden verwacht dat emulgeren met EDGE microstructuren mogelijk wordt in de nabije toekomst.

DANKWOORD

Druppels maken, bekijken, berekenen, meten, beschrijven en wat je al niet meer met druppels kunt doen. Viereneenhalf jaar lang en er ook nog, naar mijn bescheiden mening, een mooi proefschrift over schrijven. Nu zit het promotietraject er voor mij op en kijk ik er met een tevreden gevoel op terug. Eindelijk mag ik dan ook het meest gelezen stuk van een proefschrift schrijven en is het tijd om de voor mij belangrijke personen te bedanken.

Karin, als directe begeleider wil ik graag jou als eerste bedanken. Ik denk dat we van het begin af aan op een lijn hebben gezeten qua manier van denken en doen. Je flexibiliteit, geduld en relativiseringsvermogen maken jou de ideale begeleider voor mij en ik ben dan ook erg blij dat ik toentertijd besloten heb om het voorgestelde promotieproject onder jouw supervisie te gaan doen. Jouw enorme kennis en ervaring op veel gebieden waar ik weinig tot niets van wist (of weet) hebben me vaak in de juiste richting gewezen. Uiteraard mag ik je gesleutel aan mijn manuscripten niet vergeten, ondanks dat je er vaak hele stukken uitsloopte. Ze zijn daardoor wel een stuk sterker en beter leesbaar geworden. Ik hoop ook dat we in de toekomst af en toe kunnen blijven 'buurten'. Ik zie dit proefschrift als een bekroning op onze samenwerking en ik ben je erg dankbaar hiervoor.

Remko, ik vind het een eer om bij jou te mogen promoveren. Tijdens de meetings die we hadden, maar ook daarbuiten, wist je altijd met nieuwe mogelijkheden op de proppen te komen. Niet alleen voor de aanpak van een bestaand probleem, maar ook voor de daarop volgende opties. Soms zoveel stappen vooruit dat het onmogelijk binnen een promotietraject uitgevoerd zou kunnen worden. Maar juist die ver vooruitziende blikken zijn volgens mij erg belangrijk om het enthousiasme in het huidige werk te behouden. Normaal kom je niet zoveel op het lab, maar bij mijn houtje-touwtje 'druppel-device met objectglaasjes, aluminiumfolie en Praxis-lijm' heb je ruim anderhalf uur naar de gevormde druppels staan kijken, met de mooiste speculaties over de mogelijkheden. Dat heeft me toen nog even een extra zetje gegeven! Ik heb erg veel van je geleerd, ook tijdens de gesprekken die we in Chili hadden onder het genot van een Pisco Sour. Bedankt.

Technische en administratieve ondersteuning is onmisbaar bij onderzoek. Gelukkig hebben Jos, Maurice, Joyce, Hedy, Miranda, Martin, Boudewijn (microscopiecentrum) en Hans (werkplaats) me hierbij altijd erg goed geholpen. Gerrit, dank voor hulp met mijn PC en het omzeilen van allerlei ICT restricties die vanwege mijn simulatiewerk simpelweg niet konden en voor het plunderen van het paaseibakje. Pieter, jou ben ik enorm veel dank verschuldigd. Ik was intensief computercluster gebruiker, had geen enkele sjoegie van een Linux omgeving en wilde altijd meer nodes, een uitgebreidere licentie en snellere machines. Daarbij pikte ik ook eigenlijk altijd wel een stuk boterkoek mee als je die bij je had. Je ijzersterke analyses van de man-vrouw relatie zal ik overigens ook zeer gaan missen! Jan, als mede CFD-er bedankt voor je hulp bij diverse STAR-CD fratsen, je flexibiliteit met licentie verdeling of gewoon het slap ouwehoeren.

Het project was een samenwerking met verschillende industriële partners. Regelmatig zijn we dan ook naar het oosten afgereisd voor overleg. Gert, Albert, Ramona en Dennis, met jullie heb ik het meeste te maken gehad. Gert, in het begin had ik moeite met je directe manier van communiceren, ondanks dat ik het wel vaak met je eens was. Ik heb waardering voor de manier waarop je Nanomi leidt en ik hoop dat je met zowel de originele als de nieuwe EDGE technologie succesvol zult blijven. Albert, Ramona en Dennis, ik vind het erg leuk dat mijn onderzoek zo gewaardeerd wordt door jullie. Ik ben blij dat ik uiteindelijk ook echt met food-grade ingrediënten heb gewerkt, iets wat jullie logischerwijze erg gestimuleerd hebben. Ik ben benieuwd naar de vervolgstappen met EDGE; ik hoop dat het octrooi erg waardevol zal blijken.

During my PhD project I was lucky enough to supervise 8 students with their BSc. or MSc. thesis: Linda, Siyu, Wei, Sophie, Peiheng, Jannes, Abid and Riëlle. With great pleasure I am looking back to the time we have worked together. I hope you did not develop a phobia about droplets and enjoyed your time in the process engineering group. You all contributed to this thesis in one way or another, thank you very much.

In the last stage of my PhD I had the opportunity to go to the ‘founding fathers’ of the microchannel emulsification in Japan. I would like to thank Nakajima-sensei, Kobayashi-san and Uemura-san very much for giving me this chance and for the wonderful time I

had during those two months. All the members of the Food Engineering division immediately did me feel comfortable and I have enjoyed the several parties and activities, *domo arigato gozaimasu!* I am very proud that chapter 3 in this thesis resulted in a joint publication of the National Food Research Institute, University of Tsukuba and Wageningen University. Kobayashi-san, it is an honour that you agreed to undertake the long trip from Japan to be a member of the thesis committee. Of course, I would like to thank Prof. Norde, Prof. Mugele and Prof. Van Straten for taking place in the committee as well and I hope you have enjoyed reading this thesis.

Kamergenoten, ik richt mij tot u. Mede 619-iconen, Marieke en Daniël, we hebben ruim 4 jaar bij elkaar op de kamer gezeten. Vreemd dat we nooit een enzymatische druppelspons hebben geconstrueerd, had vast en zeker een publicatie opgeleverd! Marieke, beide als Zeeuw geboren dus konne me mekaore verstaee zelfs at d'r naer uus hebeld wier omda je nog blommen most bestelle. Dank voor het introduceren van de onderwaterwereld, ook al was het zicht soms slecht, het water koud en schijnen de Snorkels niet te bestaan. We liepen parallel met ons onderzoek en dus konden we nogal eens sparren over waarom, hoe, wie en wat. Je bent een week eerder begonnen maar promoveert ruim een maand eerder, gefeliciteerd met je overwinning. Gelukkig won ik meestal met tennis. Daniël, uit het zeer hoge noorden, toch te verstaan en ook nog een Bourgondische instelling (ik ben stoofpotjes zeker meer gaan waarderen). De gedachte aan de legendarische BBQ waar jij het vlees had besteld (en ik je van deskundig advies had voorzien) tovert altijd een glimlach op m'n gezicht: Er was niet teveel vlees, er werd gewoon te weinig gegeten. The Wall of Science bevat ook enkele toppers. En ik dacht dat ik me niet snel druk maakte, maar volgens mij span jij hier de kroon. In het begin hield Martijn ons gezelschap, toen een tijdje Marzia, maar toen toch weer een meer bekende naam: Martijntje. Het was, om in kneuterige termen te blijven, altijd gezellig en vertrouwd. Allen erg bedankt daarvoor. Martijntje, de zorg voor de planten en de BBQ-folders wil ik graag aan jou overdragen.

Dorinde, Anja en Wouter, ik heb het erg leuk gevonden om met jullie de AIO-reis naar Japan te organiseren. Ik heb altijd geprobeerd om me regelmatig met nog iets totaal anders dan m'n druppels bezig te houden bij Proceskunde. De AIO-reis was daarvan het grootste

Dankwoord

project. Ik denk dat het een zeer geslaagde reis was, zowel op educatief als sociaal vlak. Wij vulden elkaar als commissie goed aan op punten of momenten als er om wat voor reden dan ook (ja Anja, ik weet het...) even iemand wat minder bij de les was. Ik stel voor om regelmatig een yakitori-sessie of een sushi-boot bij de Japanner te blijven doen. Dorinde, jou heb ik het beste leren kennen. Bij de bergen werk die jij verzet is de Fuji-san een heuveltje en stiekem ben ik nu ook meer bekend met de kuren van je algjes. Ik ben blij dat jij m'n paranimf wilt zijn.

Het is een komen en gaan van mensen op de vakgroep, ik wil iedereen bedanken voor de vele gezellige koffiepauzes, borrels, labuitjes, lunches en andere activiteiten. Klaske, Sina en Dorinde: Keep the borrelcie alive! (en plan eens een oud-AIO borrel)

Pa en ma, een goede basis is het begin van alles, dus dit proefschrift is ook van jullie. As stugge Zeeuw heboore kan je toch een 'wereldreiziger' oare, maar op Flupland kom ik oaltied tuus. Mark (ik hoop dat je me geen Dirrkoen gaat noemen in navolging van Droetker) en Saskia, Anja en Wim, Dennis en Chelly, vrienden uit Zeeland, Wageningen of waar dan ook, bedankt voor jullie interesse en gezelligheid. Jaap, ik zal je binnenkort overhoren met betrekking tot de inhoud van dit boekje. Bert (Brutus), als Zeeuwse vriend uit Wageningen vind ik het erg leuk dat je beide 'clubs' kan vertegenwoordigen als paranimf. Ook wil ik graag Hans apart bedanken voor de wekelijkse squashstrijd en voor het bewijzen dat barbecueën niet seizoensgebonden is.

Eén iemand zit nog met smart te wachten. Het is al een heel verhaal geworden, maar je schrijft ook maar één proefschrift-dankwoord in je leven. Een leven dat ik graag wil delen met mijn meisje, Bianca. Samen zijn we heel sterk en genieten we van de dingen die we leuk vinden. Ik ben ervan overtuigd dat we nog een fantastische tijd tegemoet gaan!

Koen

PUBLICATIONS

Peer reviewed journals

van Dijke, K. C.; Schroën, K.; Boom, R. M. Microchannel Emulsification: From Computational Fluid Dynamics to Predictive Analytical Model. *Langmuir* **2008** 24, 18, 10107-10115.

van Dijke, K. C.; Veldhuis, G.; Schroën, K.; Boom, R. M. Simultaneous formation of many droplets in a single microfluidic droplet formation unit. *AIChE J.* **2009** DOI: 10.1002/aic.11990.

van Dijke, K. C.; Veldhuis, G.; Schroën, K.; Boom, R. M. Parallelized Edge-based Droplet GEneration (EDGE) Devices. *Lab on a Chip* **2009** 9, 2824-2830.

van Dijke, K. C.; Schroën, K.; van der Padt, A.; Boom, R. M. EDGE emulsification for food-grade dispersions. Submitted.

van Dijke, K. C.; Kobayashi, I.; Schroën, K.; Uemura, K.; Nakajima, M.; Boom, R. M. Effect of viscosities of dispersed and continuous phases in microchannel oil-in-water emulsification. Accepted for publication in *Microfluidics and Nanofluidics* **2009** DOI: 10.1007/s10404-009-0521-7.

van Dijke, K. C.; de Ruiter, R.; Schroën, K.; Boom, R. M. The mechanism of droplet formation in microfluidic EDGE systems. Accepted for publication in *Soft Matter* **2009** DOI: 10.1039/b916141d.

van der Zwan, E.; Schroën, K.; van Dijke, K. C.; Boom, R. M. Visualization of droplet break-up in pre-mix membrane emulsification using microfluidic devices. *Colloids and Surfaces A* **2006**, 277, 223.

Patent

van Dijke, K. C.; Schroën, K.; Boom, R. M.; Veldhuis, G.; van der Padt, A. Microfluidic method and apparatus for generating a dispersion **2009** NL2002862

Conference proceedings

van Dijke, K. C. ; Schroën, K; Boom R. M. Pressure gradient criterion for microchannel emulsification processes. In *tenth international congress on engineering and food (ICEF)* **2008** 20-24 April, Viña del Mar, Chile.

van Dijke, K. C.; Schroën, K.; Boom, R. M. Microstructures for emulsification. In *fourteenth World Congress of Food Science and Technology (IUFOST)* **2008**, 19-23 October, Shanghai, China.

van Dijke, K. C.; Schroën, K.; Boom, R. M. In: *Proceedings of the 8th World Congress of Chemical Engineering* **2009** 23-27 August, Montréal, Canada

Oral presentations

Department of Food Technology at Lund University, PhD-trip **2006** Lund, Sweden.

Netherlands Process Technology Symposium. **2007**, Veldhoven, The Netherlands.

10th International Congress on Engineering and Food. **2008**, Viña del Mar, Chile

Lecture at National Food Research Institute. **2009**, Tsukuba, Japan.

8th World Congress of Chemical Engineering **2009** Montréal, Canada.

Poster presentations

Netherlands Process Technology Symposium. **2005**, Veldhoven, The Netherlands.

4th World Congress on Emulsions **2006**, Lyon, France

Netherlands Process Technology Symposium. **2007**, Veldhoven, The Netherlands.

10th International Congress on Engineering and Food. **2008**, Viña del Mar, Chile

Award

Best Poster during Netherlands Process Technology Symposium. **2007**

Documentary

Dijke, K.C. van, van der Zalm, E.; Boom, R.M.; amongst others De Toekomst van ons Voedsel. *VPRO Tegenlicht (on DVD)* **2008**

<http://www.vpro.nl/programma/tegenlicht/afleveringen/38243331/>

CURRICULUM VITAE

Koen Cornelis van Dijke was born in Sint Philipsland, The Netherlands, on September 16th, 1980. He went to primary school in this small village in the province of Zeeland and continued education at the Regionale Scholengemeenschap 't Rijks in Bergen op Zoom. After graduation in 1998, Koen started to study Mechanical Engineering at the Technical University in Eindhoven, but after the first year he switched to Food Technology at Wageningen University. During his study



he performed a minor thesis project at the Systems and Control group of Prof. Van Straten about the "*Optimization of cooling processes of pig carcasses.*" His major thesis project was about "*Pre-mix membrane emulsification*" in the Food Process Engineering group of Prof. Boom. Koen finalized his study with an internship about "*Intelligent decision systems in food industry*" at the Kaunas University of Technology in Lithuania and "*Modelling and optimizing the scalding process of chickens*" at Stork PMT in Boxmeer, The Netherlands. In February 2005 Koen started his PhD-project under supervision of Prof. Boom and Dr. Schroën at the Food Process Engineering group. This so-called "*Microdruppels*" project focused on emulsification with microstructures, in which the goal was to gain thorough understanding of spontaneous droplet formation processes that can occur in specially designed structures with very small characteristic dimensions. In the final stage of the PhD trajectory (April and May 2009) Koen joined the Advanced Food Technology Lab at the National Food Research Institute in Tsukuba, Japan for a collaborative project with Prof. Nakajima, Dr. Kobayashi and Dr. Uemura. The results of the research performed in the last 4 and a half years are described in this thesis, including a new and promising emulsification process. On October 5th 2009, Koen started working as Scientist Process Technology Powders at Danone Research in Wageningen.

Email: koenvdijke@hotmail.com

TRAINING ACTIVITIES



Discipline specific activities

Courses:

Unified Approach to Mass Transfer (OSPT, 2005, Enschede, The Netherlands)
Star-CD Basic Training Course (CD-Adapco, 2005, Nürnberg, Germany)
Numerical Methods in Chemical Engineering (OSPT, 2006, Eindhoven, The Netherlands)
Hochschulkurs Emulgiertechnik (TH Karlsruhe, 2006, Karlsruhe, Germany)
Modelling and Computation of Multiphase Flow (ETH, 2007, Zurich, Switzerland)

Congresses, symposia:

Netherlands Process Technology Symposium (2005 / 2007, Veldhoven, The Netherlands)
World Congress on Emulsions (2006, Lyon, France)
Euromech: Numerical Simulation of Multiphase flow (2006, Scheveningen, The Netherlands)
10th International Congress on Engineering and Food (2008, Viña del Mar, Chile)
Internship at National Food Research Institute (2009, Tsukuba, Japan)
8th World Congress on Chemical Engineering (2009, Montreal, Canada)

General courses

Supervising and Guiding BSc./MSc. Thesis Students (OWU, 2005, Wageningen, The Netherlands)
PhD Competence Assessment (WGS, 2005, Wageningen, The Netherlands)
Scientific Writing (Centa, 2006, Wageningen, The Netherlands)
Career Perspectives (WGS, 2008, Wageningen, The Netherlands)
Effective Behaviour in Professional Surroundings (WGS, 2008, Wageningen, The Netherlands)
Business Course Strategic & Innovation Management (Arthur. D. Little, 2008, Rotterdam, The Netherlands)
Entrepreneurial Bootcamp (DAFNE, 2008, Wageningen, The Netherlands)
Advanced Course: Guide to Scientific Artwork (WU Library, 2009, Wageningen, The Netherlands)

Optionals

Brainstorm Week Process Engineering 2005
PhD-trip Process Engineering 2006 (Denmark and Sweden)
PhD-trip Process Engineering 2008 (Japan)
Organization of PhD-trip to Japan (2007/2008)
Brain & Game Day Process Engineering 2008
Network Young Membrains
(2005, Enschede, The Netherlands; 2007, Thessaloniki, Greece; 2008, Berlin, Germany)

The research described in this thesis was part of the Microdruppels project, a collaboration between Wageningen University, Nanomi, FrieslandCampina, and Demcon amongst others. The project was financially supported by the Dutch Ministry of Economic Affairs and the Dutch provinces of Gelderland and Overijssel.

Printed by Ipskamp, Nijmegen.

Cover design: Koen van Dijke and Roy van Eck.